Ph.D. Dissertation of Engineering

Development of Spheroid-on-a-Chip for Evaluating the Apoptosis of Lung Cancer Cells Using Sericin Nanoparticles with SHMT1 siRNA

세리신 나노입자 유전자 전달체의 SHMT1 siRNA를 통한 폐암 세포의 세포사멸 유도 효과를 확인하기 위한 스페로이드 배양 플랫폼 개발

February 2023

Graduate School of
Seoul National University
Biosystems Engineering
Jae Woon Lim

Development of Spheroid-on-a-Chip for Evaluating the Apoptosis of Lung Cancer Cells using Sericin Nanoparticles with SHMT1 siRNA

Advisor: Prof. Jong Hoon Chung

Submitting a Ph.D. Dissertation of Public Administration

February 2023

Graduate School of Seoul National University

Biosystems Engineering

Jae Woon Lim

Confirming the Ph.D. Dissertation written by
Jae Woon Lim
December 2022

Chair	Ghiseok Kim	(Seal)
Vice Chair	Jong Hoon Chung	(Seal)
Examiner	Hoon Seonwoo	(Seal)
Examiner	Kyoung-Je Jang	(Seal)
Examiner	Pankaj Garg	(Seal)

Abstract

Lung cancer adenocarcinoma is one of the most aggressive type of cancer with low survival rate and treatment strategies are often marred by poor prognosis. Depending on the disease progression, the conventional therapies such as radiotherapy, chemotherapy and immunotherapy might not be able to completely cure the disease which necessitates the intervention of gene editing using gene therapy. However, delivery vectors used in gene therapy have their own limitations such as oncogenicity and toxicity in case of viral vectors and higher toxicity and low biocompatibility incase cationic polymers non-viral vectors. Thus, biodegradable non-viral vectors with low toxicity and high delivery efficiency could be a pragmatic approach for gene therapy. Silk derived natural polymer sericin can be used for vector fabricating as nanoparticle, which have many functional groups like other protein, and also can be used as wound dressing and supplement for serum-free media indicating its biocompatibility.

In therapeutic research, animal models have more reliable and better performance compared to *in vitro* assays on monolayer cells. The promising results obtained during invitro experiments often do not translate into the *in vivo* results using animal models. However, it is not easy to develop models even asides from ethical issues or high costs, and survival of animals can hinder the experimental process. 3D culture of cancer cells, which is also called spheroids could be solution to this when combined with microfluidic based biochip. The spheroids inside microfluidic device can mimic more precise microenvironment around the cells similar to *in vivo* tumors. Therefore, it is more relevant to use on-chip spheroids instead of monolayer culture for chemotherapy during *in vitro* experiments. But the operation of microfluidic device can be challenging, which requires special equipment design such as pumps and operational skilled enough to obtain desired results.

In this research, we developed microfluidic biochips that can culture cancer spheroid and evaluated the efficiency of sericin based nanoparticles to deliver therapeutic agents. Nanoparticles were successfully fabricated and showed better transfection of reporter genes compared to positive control, Polyethylenimine (PEI). Cancer spheroids cultured inside the biochip showed prominent cell viability and

transfection using sericin/siRNA-based nanoparticles on the spheroid inside biochip showed apoptotic events. The experimental finding could be promising in the field of 3D culture-based cancer gene therapy research.

Keyword : Biochip, Cancer, Sericin, Gene delivery, Nanoparticle, Spheroid
Student Number : 2018-32443

Table of Contents

List of Tables

List of Figures

Chapter 1. Introduction
1.1. General introduction

Lung cancer is still one of the cancer types with poor prognosis in 2019, and this is also an ongoing problem. About 85% of lung cancer patients are diagnosed as non-small cell lung cancer (NSCLC), which includes lung adenocarcinoma and many other types. While considered less rapid and progressive than small cell lung cancer (SCLC), yet NSCLC is still important topic. This is because NSCLC occurs in non-smokers, keeping the mortality rate of lung cancer high even smoking population decreased by time [1]. NSCLC is known for developing resistance to radiotherapy, chemotherapy drugs in advanced stages. This leads to metastasis, recurrence, and low survival rates in patients. Considering recent outbreak of COVID-19, the medical resource shortage may affect the survival of these patients even worse considering circumstances.

Such properties of NSCLC are available to be explained by cancer stem cell (CSC) theory. CSCs are small rare fraction of cells [148] suspected of having potential to differentiate into specificized, mature tumor cells, as stem cells differentiate to predestined cells [149]. Many researchers suspected that CSCs have tumor inducing ability when injected to animal models, also evading immune system [150, 151]. Nature of CSC makes it difficult to indicate and target due to low population in tumor mass and rather quiescent behavior. Thus, it is difficult to eradicate the CSC completely within the tumor by conventional therapeutic methods such as surgery, chemotherapy. Such therapies can only remove large mass of tumor, or target rapidly proliferating cells, resulting in resistance development toward therapeutic drugs or relapse, metastasis due to remaining CSCs [152, 153]. Thus, various reports are suggesting more precise, specific method should be selected to inhibit cancer stem cell population in NSCLC, by tracking signaling pathways associated with maintaining stemness, proliferation, and renewal of the tumor [151, 154, 155]. There are previous reports of targeting the cancer stem cells, presenting promising results which could be applicated in future studies [18, 156] . Various signaling pathways are possible as targets to prevent metastasis and relapse of tumor [2, 158-160] Wnt, Notch, Shh signaling pathway are the examples. The pathways regulate development and stemness of human cells, provoke phenotype

switching in cells, eventually leading to cancer formation in common [2]. Disorder in Wnt signaling pathway is suspected to be related with colorectal cancer, breast cancer, melanoma, and many other cancer types. It is also considered closely related with self-renewal mechanism of cancer stem cells [2, 161, 162]. Notch signaling pathway provoke small-cell lung cancer (SCLC), Basal cell carcinoma, neuroblastoma, and Shh pathway malfunction which leads to oncogenicity of leukemia, breast, and colon cancers [3, 163]. Understanding the key function and mechanism of these pathways can attribute to more effective CSC targeted therapy.

Among the therapy to target cancer stem cells, gene therapy can be prominent solution. Gene therapy have many advantages, such as more specific targeting of genetical defects which cause the disease [164], being more flexible in application and have many alternatives. Most of these benefits can be also applied in targeting cancer stem cells, where they can knock-out or neutralize the self-renewal pathways regardless of their quiescent behavior. For application of gene therapy, the first step should be identification of the appropriate therapeutic target. Previously mentioned signal pathways like Wnt, Shh, Notch can be targeted. Next, selection of gene editing method is required. In early times in the field, Zinc finger editing, Transcription activator-like effector nuclease (TALE), Meganuclease editing were popular as gene editing methods. Later, the previously scribed gene editing methods were replaced by CRISPR-Cas9, due to limitations including complicated steps, consuming excessive labor and expense [5]. Although CRISPR-Cas9 is robust and precise gene editing method, RNAi by siRNA is also available as an option with high specificity, with simple structure and process for silencing genetic defects. Finally, the vector to transport gene editing systems or nucleic acids to the site is needed. Most of living organisms are prepared with defense systems against post-script gene editing [165, 166]. Therefore, gene delivery vector is needed for protection and precise delivery of therapeutic genes. The vector binds and form nano-sized complex with genes or loaded with genes by the variation, resulting in more stable and appropriate structure for delivery. However, viral vectors are known to be cytotoxic or oncogenic despite of their advantages in transfection capability [167, 168]. Non-viral vectors are relatively free from virus related issues [169, 170], but the transfection capability is poor compared to viral vectors. Polycations such as polyethyleneimine have relatively high transfection

capability compared to other non-viral vectors, but also cytotoxic [171, 172]. Therefore, adjusted non-viral gene delivery vector with enhanced gene delivery capacity and less adverse effects is needed to be fabricated for more safe and effective gene therapy in future.

In addition to selecting right therapy and delivery vector, the therapies should undergo experimental and clinical certification before the actual application. The very first step for such certification is *in vitro* study. Target cells are cultured in 2D surface, and therapy is evaluated by molecular biologic assays after treatment. The growth of cell line is almost infinite and stable when the culture conditions are adequate, and protocols are well established and verified through decades [173].

However, *in vitro* studies have clear limitations besides its convenience and reliability. Even when the application results of *in vitro* studies seem to be promising, the results can be different from *in vivo* studies in animal models or actual clinical cases [174, 175]. The major difference that is shown between *in vitro* and *in vivo* study is drug sensitivity. This is because actual organs and biologic systems of living organism, which is ultimate target of therapy, is composed of various cells and extracellular matrix in 3D structure [176-178]. These structures closely interact with each other, giving the unique features when compared to *in vitro* cultured cells. Even tumors have previously explained features, which is very distinct from *in vitro* cultured cell lines. When compared to actual tumors in animal model or therapeutic targets, *in vitro* cultured cells have at maximum of three to two cells co-cultured, absent of 3D structures since the cell lines are usually cultured in monolayers.

While *in vivo* evaluation on animal models have less of concern in previously mentioned issues, it is expensive and labor consuming, have ethical issues, and even successful models can fail due to death of animals. Thus, novel platform which is available to assist *in vivo* animal models while maintaining the advantages of the *in vitro* process is required.

1.2. Objectives

The fundamental hypothesis for this study was i) By 3D culture, *in vitro* cultured lung cancer cells can be induced properties more similar to *in vivo*. ii) Nanoparticle

vectors can be robust delivery vehicle for anticancer gene therapy, and sericin, which is natural polymer derived from silk, would be suitable for fabricating the nanoparticle vector. iii) The nanoparticles would show different results on the biochip platform compared to *in vitro* experiment.

For this purpose, i) A passive pumping microfluidics-based biochip with concaved well was fabricated by casting polydimethyloxane (PDMS) on 3D printed mold, for culture of cancer spheroid. ii) Sericin based nanoparticles were fabricated for gene delivery vector. iii) Sericin nanoparticles were applied to the spheroid cultured on microfluidics platform.

The aims of this study are as following:

Aim 1. To fabricate microfluidics-based passive pumping spheroid-on-a-chip and culture cancer cell spheroid preserving *in vivo* properties on the platform.

Aim 2. To fabricate nanoparticle for drug and gene delivery with silk originated natural polymer sericin.

Aim 3. To determine gene delivery effect of sericin nanoparticle (SNP) on cancer spheroid cultured by the spheroid-on-a-chip platform.

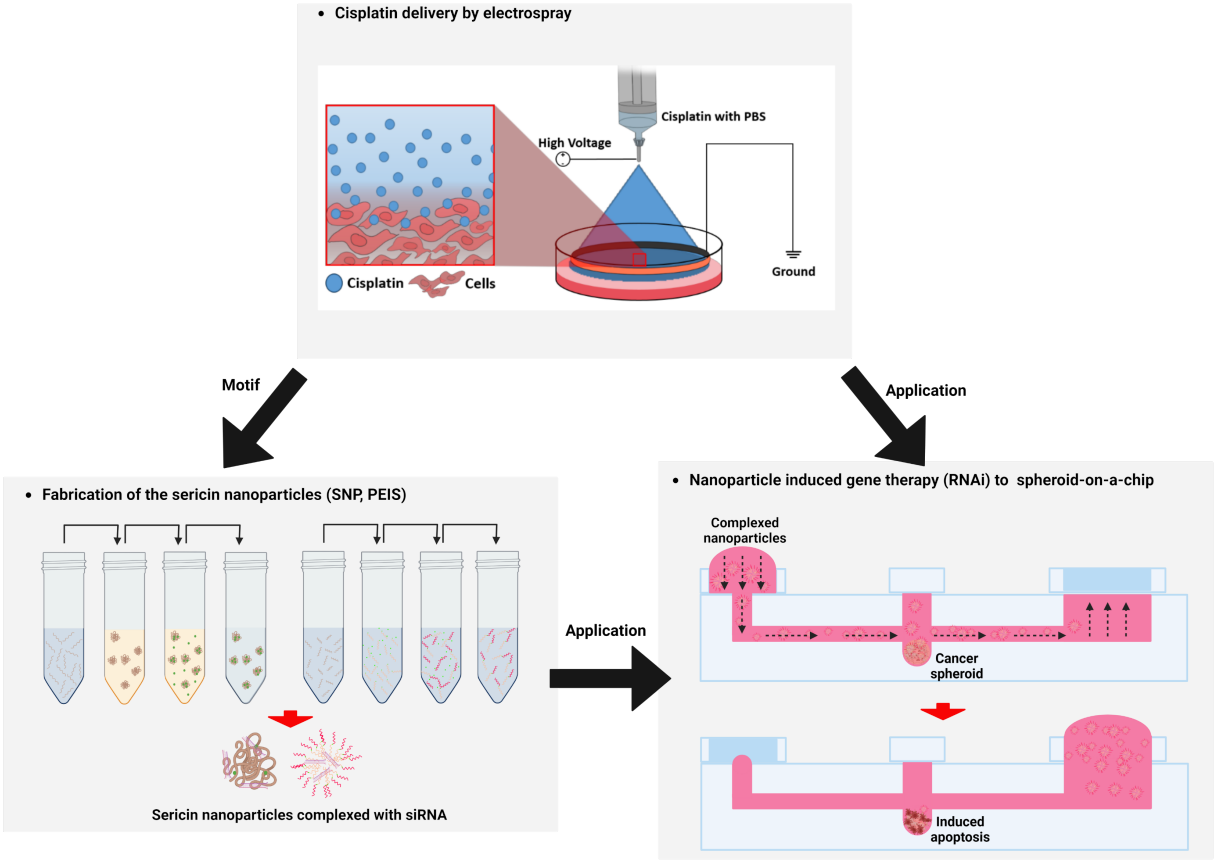

Figure 1.1. Overall schematic presentation of the study. Images were fabricated on Biorender (Biorender.com).

Chapter 2. Literature Review

2.1 Lung Cancer and Current Anticancer Therapies

Lung cancer or lung carcinoma is disease that can be identified by outbreak of uncontrolled, malignant tumor tissues in lung and bronchia. The tumor progress and proliferate in the lung, then gradually transfer to lymph nodes or other organs in late stages [179, 180]. lung cancer is particularly fatal among the cancer, responsible for 25% of total cancer deaths as shown in 2019 cancer statistics of the USA even when total cancer rate steadily decreased by year [1, 181, 182, 183]. This is because lung cancer progress rapidly, and lung is complicated in structure and function. This presents the reason of high mortality from lung cancer and importance of appropriate treatment as well. This is still significant problem even in recent era, which cancer treatment have advanced, and interest toward cancer diagnosis is high from past. Lung cancer is classified by two large categories, non-small cell lung cancer (NSCLC) and small cell lung cancer. It is nomenclated after the morphology and size of the cancer cells. Non-small cell lung cancer consist over 80% of the lung cancer diagnosis [6].

Lung cancer can be diagnosed by computed tomography (CT) or tissue analysis. Molecular mutations in EGFR, KRAS, BRAF, HER2, MET can lead to adenocarcinoma and small cell cancer. Rearrangements in genes such as ALK, ROS1, RET can provoke non-small cell lung cancer while some researchers suggest overexpression of exosome microRNA can also act as diagnostic marker for lung cancer [2, 5, 7].

Smoking is major cause of lung cancer, especially rapidly growing and proliferating small cell lung cancer in most cases [8] while influence to non-small lung cancer still cannot be ignored. The relation between lung cancer and smoking is clearly present in the case studies, as decrease in smoking population resulted in decrease of lung cancer diagnosis.

However, there are still other causes for lung cancer. Genetical defect in family history can be the problem, while asbestos can cause cancer when inhaled or ingested [9]. Exposure to fine particulate air pollution can also be the cause [10], including fumes from kitchen or incinerator.

Previous explained causes of lung cancer may provoke malfunction in expression

of certain component in the cell. Such components can be part of certain signaling pathway, or receptor for certain ligand. It may be associated with enhancing cellular activity such as retaining proliferation, stemness, or transformation of cell morphology, leading to survival and maintenance of cancer stem cells. Such proteins are called cancer stem cell markers [129, 151, 154, 155]. Cancer stem cell marker can be classified into four groups: First, there are proteins which promote growth and proliferation of cancer or pre-tumor cells. Secondly, there are proteins which inhibit apoptosis, anti-angiogenesis, immune response, and other anti-tumor activity. Finally, there are proteins that degrade cohesive molecule or matrices of tissue, leading to tumor invasion or metastasis [11]. The cancer marker can be categorized by the expression site. some cancer markers are overexpressed on the surface because they are receptor or membrane proteins, such as CD44 and CD133 [184, 185]. Other markers are associated with Wnt, Shh, Notch signaling pathway, which leads to maintenance of genetically defected cells, cell phenotype transformation, and other malfunctions [2, 3, 161-163]. Markers which are expressed on cell surface would be targets to guide therapeutic vehicles, and proteins that are associated with function of cancer activity would be actual targets to be inhibited by therapeutic molecules.

There are several cellular components which are suspected as lung cancer stem cell specific marker. Epidermal growth factor receptor (EGFR) is known to be mutated in advanced stages of lung cancer. Chemotherapeutic reagents such as gefitinib, erlotinib, afatinib are approved and treated to target tumor causing mutation in non-small cell lung cancer. Ubiquitin-like with PHD and ring finger domains 1 (UHRFI) is also one of the lung cancer stem cell marker candidates as it is overexpressed in lung cancer, also found in proliferating cells, and associated with S stage of the cell cycle [12]. Another marker, Ubiquitin-specific peptidase 17 (USP17) regulate formation of TRAF2/TRAF3 complex and overexpress macrophage-promoted inflammation, promote stemness and transformation. Therefore, it is also a possible target for therapeutics which have fundamental on lung cancer stem cell theory [13]. CD44 as described before also function in lung cancer metastasis of non-small cell lung cancer with KRAS, N-Ras. While markers introduced above is mainly about non-small cell lung cancer, MYC, MYCN, MYCL1 can cause or make conditions for small cell lung cancer.

Also, there are functional proteins that maintain homeostasis in normal cells, but highly expressed in cancer cells, such as Aldehyde dehydrogenase 1 and 2 (ALDH1 and ALDH2). High levels of ALDH1 and ALDH2 indicate normal or early stage of cancer [14] while cancer stem cells and resulting cancer cells develop resistance toward chemotherapy by overexpressing ALDH1. Repressing ALDH1 had effect of increasing tumor chemosensitivity to therapeutic drugs in the report of Visus et al. [15], yet the outcome of the inhibition should be carefully studied considering function of the protein in normal cells.

Meanwhile, Treatments for lung cancer used to be surgery, radiation, and chemical therapies, which are also available as combined therapy. For chemotherapy, pacilitaxel, cisplatin, doxorubicin, and some other post-treatment drug such as erlotinib are used. However even after the treatment, tumor may relapse or begin to develop some resistance, becoming difficult to eradicate which eventually leads to bad prognosis.

As bimolecular analysis in cancer research advanced by time, the origin of lung cancer is available to be examined down to single protein level. Also new targeted anti-cancer strategies are intended for complete eradication of cancer and cancer stem cells. For example, Shh signaling including Smoothened, SHMT1 and p53 signal pathway are constantly reported as targets for chemical and genomic therapies as well as other cancers [16-18].

2.2 Gene Therapy for Cancer Treatment

Often considered as fundamental and effective way to treat incurable disease, gene therapy alters or edit defected sequence of genes to function as in normal state. Gene therapy can be applicated to disease which are hard to be treated by traditional methods [186]. Especially in case of inherited diseases, where conventional treatment was merely management of apparent symptoms.

Before applying gene therapy, it is important to identify defected genes associated with the disorder. After the analysis, normal gene sequence which would substitute defected gene, or siRNA programmed to knockdown the malfunctioning genes are cloned. Afterwards the nucleic acid is loaded on vector, reaches to the target cell and deliver therapeutic gene into the nucleus, leading to transfection and function of induced normal genes. The most important part of gene therapy is gene delivery,

which is involved with developing the right vector within strategy to overcome internal barriers of the body. Moreover, vectors should be safe, and have no harmful effects to body, such as strong immune response or oncogenic function. And finally, targeting ability intended cell and organ without any off-target gene editing is required for gene delivery vector, in ideal [19].

First approved gene therapy procedure was done on a four-year-old girl born with severe combined immunodeficiency, in 1990. The practice was done by infusing autologous T cells inserted with normal functioning genes [187]. As the procedure suggests, the idea of inserting the nucleic acid directly to patient was already considered ineffective even on the very first application of the therapy. Also, the DNA itself is unavailable to target intended cells or organs.

To overcome these limitations, viral vectors were introduced because of their natural mechanism to transfect other organisms. To prevent cytotoxicity and pathogenicity of vectors, researchers altered some sequences of the vector to remove the recombination ability by self-inactivation. While gene transfection by viral vectors was successful, there were still some technical problems were left, such as transient expression of transfected genes, or recombination of vectors which led to vectors with wild type like cloning ability. This led to development of gut less virus and other viral vectors, such as adenovirus associated vector (AAV), lentivirus vectors. Also, non-viral vectors were improved with transfection ability and safety issues, although there are some doubts that non-viral vectors would have sufficient transfection ability compared to viral vectors. Current main applications for gene therapy are: hematopoietic stem cell gene therapy, AAV gene therapy for hemophilia, and chimeric antigen receptor T-cell (CAR-T cell). Some AAV based gene therapy products are even approved in FDA, in case of liver, retinal, and spinal muscular atrophy, although there are still many obstacles to overcome [19-21].

For contents with vectors, various options can be considered, starting from gene editing systems. Within introduction of CRISPR-Cas9 in 2010s, the field of gene therapy is predicted to advance even further. CRISPR is abbreviation of clustered regularly interspaced short palindromic repeats, and Cas9 is RNA guided endonuclease which indicate the CRISPR and ‘cut’ the sequence including it. CRISPR has drawn interest of many researchers since its first discovery in 1987,

because the sequence has robust potential as gene editing tool in various fields. It was originally RNA-guided endonuclease, which was defensive sequence in bacteria or archaea toward viral gene insertion. CRISPR-Cas9 functions by following mechanisms: First virus or plasmid origin spacer is received in CRISPR location. And CRISRP RNA which have unique repeat sequence is expressed and interfere in alien genome [22, 24, 25].

It is available to insert desired gene in desired site with CRISPR-Cas9 by short RNA guide. Before CRISPR-Cas9, Zinc finger, Transcription activator-like effector nuclease (TALE), Macronuclease were such techniques to indicate certain sequence and edit genes [22], but there were limitations such as lack in specificity [23] or convenience, and high in cost, time consuming [24] to be directly applied in the research. However, by discovery of CRISPR-Cas9 system, topics that were theoretically available with previously scribed methods but hard to accomplish due to limitations became visible targets for researchers.

By CRISPR-Cas9, animal model in on various polygenic disease became available. Diabetes, heart disease, schizophrenia, autism for example, which needed great deal of time and money became easier and available target recently. Also, gene-edited products, gene screening, transcription modifying process which was produced with tradition gene editing method became more effective in production [25].

Beside of CRISPR-Cas9, there exists another robust gene editing method, RNAi, which silence certain sequence of gene by siRNA. RNAi or post-transcriptional gene silencing is originally part of cellular immune system which prevents gene editing by virus or parasites. It works by trigger DNA or double-stranded RNA (dsRNA) introduced into the cells. By intracellular mechanism, dsRNA is processed into short interfering RNA (siRNA). Afterwards, siRNA is bind to RNA-induced silencing complex, and triggers nucleolytic degradation of target mRNA by the RNase H enzyme Argonaute, or Slicer.

The RNAi was first reported by Napoli and colleagues in 1990, which they reported RNAi in petunia petals [26]. Fire et al. discovered that RNAi is also available to be applicated in animal, C. elegans, in 1998 [27]. After the discovery, Kamath et al knocked out specific gene in C. elegans by feeding E. Coli expressing double-stranded RNA induced RNAi in 2001, first indicating the potential of RNAi,

which is capable of artificially induced gene editing [28]. In addition, Sledz et al. first introduced activation of specific system by siRNA in 2003 that indicating the RNAi can also induce certain editing of the sequence, in addition to selective gene sequence silencing [29]. On the same year, Rubinson et al. induced gene silencing also in mouse [30], and Konnikova et al. first reported the application of RNAi as anticancer purpose, by inducing knockdown of STAT3 in astrocytoma [31].

As previously described, RNAi can be triggered by introducing dsRNAs or constructs expressing shRNAs. There are two variations of RNAi, which directly treat siRNA unit to the cells or treat dsRNA to be processed with innate cell mechanisms. In most of the study, effect of first is rather transient and latter is more stable.

The advantage of RNAi is that it is theoretically applicable to any genetical disease, including cancer. Also, it is more effective than using other antisense oligo or ribozyme for knockout because it does not require a lot of doses. Finally, RNAi can be very specific to the target gene itself. However, it may provoke immune response when long siRNA is treated with Dicer substrates. Also, it is in fact not very specific since siRNA itself cannot recognize the normal cell and diseased cells. It is important to consider thermodynamic end stability, target mRNA accessibility, structural features, and additional position specific determinants when applying siRNA for RNAi treatment. To deal with the problems mentioned before, use of modified siRNAs or nanoparticles are expected as solutions [32. 33]. Recently, using nanoparticles for the delivery of siRNA is proven to be legitimate, as some of the nanoparticles are approved to be used for the purpose by FDA [34].

2.3 Gene delivery vectors

As explained before, gene delivery vectors are essential in delivering gene editing toolbox into the cells. This is because foreign nucleic acids are difficult to be introduced into the cell nuclear, as it is neutralized by various innate immune system of cells. Gene delivery vectors protect nucleic acid or gene editing reagent from degradation by forming compact nanoparticles or binding with the nucleic acid [191-193].

To begin with, there are two types of vectors: viral and non-viral. Viral vectors refer to using virus originated materials or virus itself with suppressed nature, such

as self-replication ability. While viral vectors are proven with their effective nature over time, there always have been concerns about the safety of viral vectors when applied *in vitro*. It may induce strong immune response, severely harming the patient. Also, there is awareness for viral genes incorporated in the target genes may trigger or act as oncogene [188-190]. Considering such disadvantages, non-viral vectors have been proposed as alternatives of viral vectors.

Non-viral vectors are usually constructed with materials other than viral particle. Inorganic particles such as calcium phosphate, silica, gold can be used as gene carriers. Degradable materials such as cationic lipid, lipid nano emulsions, peptide, or polymer are adapted as vectors, considering potential dangers of nanoparticles accumulating in tissue. Physical methods are also applied for relatively simple procedure. Gene gun (Ballistic DNA), electroporation, sonoporation, photoporation, magnetofection are also examples of physical methods to deliver gene into the cells [19, 35].

Advantages of non-viral vector or delivery method is that it is free from side effects of viral vector such as immunogenicity, oncogene activation. However, there are still some limitations for non-viral vectors. Although the transfection efficiency has improved, non-viral vectors still have low transfection efficiency compared to viral vectors. Also, although non-viral vectors are much safer than viral vectors, they still can cause negative response such as cytotoxicity or immunogenicity. In case of physical delivery methods, tissue damage by electricity or inability of penetrating into deeper layers of body can be limitations. Novel non-viral vector for gene delivery should be able to overcome previously described limitations, by effective vector design or combined application of the methods [19].

2.4. 3D cell culture method for cancer research

Considering mortality and bad prognosis, and aggressive progress in some cancers, it is important to develop research platform which is more accessible and reliable. Nowadays *in vitro* cultured cell lines and *in vivo* animal model are used in cancer research, but both have problems. *In vitro* experiments show adverse reactions to therapeutic assay. Animal models are at least more like actual human body but requires quite a cost to develop certain model for the case and the results still could be different from actual clinical study to humans. Also, public attention on ethical

aspect of animal test is growing nowadays, making it hard to prepare.

Three-dimensional (3D) culture can be a solution to this. 3D cultured tumors, or spheroids can be prepared by well-developed *in vitro* culture methods and have many common properties with tumors in living organism when compared to traditional *in vitro* culture. Though it would not be able to completely replace *in vivo* models, 3D culture have huge potential in the cancer research field.

The first device that probably can be called as lab-on-a-chip device was proposed by S.C Terry and colleagues in 1979 [36], which constructed miniature gas chromatic air analyzer on silicon wafer. By building sub-millimeter structure in the chip, the study pioneered new field for ambitious researchers. development of microvalves [37], micropumps [38], and HPLC [39] on chip, lab-on-a-chip research slowly turned to its modern form. In 1992, Harrison et al proposed first concept of 'laboratories-on-a-chip', by introducing capillary electrophoresis and sample injection systems on glass chip [40].

Before adapting PDMS, there was early research that can be so-called ancestors in biology field. Using soft lithography, Singhvi et al [41] fabricated platform that can engineer hepatocyte shape and function by varying surface environment in 1994. The lab-on-a-chip field came to a turning point in 1998. Duffy and colleagues introduced poly(dimethylsiloxane) (PDMS) into fabrication of LOCs, which is flexible and biocompatible, inert polymer material. In the study, master mold was fabricated by rapid prototyping, then PDMS was cast onto the mold to create microfluidic device. By this method, instead of using fragile silicon wafer for the LOCs, PDMS and other 'soft' materials became available in the field [42], even cell biology field [43].

Based on previous advances, LOCs reached a milestone of first 'organ-on-a-chip' in 2010, by D. Huh et al. The researchers reconstituted lung on a chip, which showed lung-like behavior such as response to bacteria and inflammatory cytokines, and uptake of nanoparticles just like actual *in vivo* experiments [44]. Afterwards intestine and kidney glomerular structure was fabricated on LOC platform, and recently the trend moved to construction of body-on-a-chip [45, 46]. Recently researchers are mainly focusing on vascularized organoids and tissues, blood cell associated disease screening, and tumor infiltration and migration on LOC. As the present research suggest, lab-on-a-chip is old but still popular and studied in

various research fields [48-51].

While previous section focused on reproducing organoids *in vitro* by LOCs, there is also an important use of the device. It is, to culture multicellular spheroid. Multicellular spheroid, or spheroid in short is mostly cultured in microfluidic biochips. Not like the nomenclature, spheroids are not exactly 'round'. But they have relatively dense and compact structure consisted of aggregated cells, which give them unique properties away from 2D cultured, *in vitro* cells. First, they have three layers from the surface: Proliferating layer, inactive layer, and necrotic core [51]. This is because it is harder for material exchange as they go deep inside, where cells become more compacted [52-55]. Secondly, spheroids have different cell to ECM structure or cell to cell adhesion since it has less surface contact to rigid materials like polystyrene [51, 56-59]. Thirdly, they tend to grow exponential, which is like the growth behavior of *in vivo* tumors [60, 61]. These features make spheroid excellent platform for drug screening *in vitro*.

Spheroids can be prepared by various methods. First there is hanging drop culture, which is performed by placing small drop of cell suspension on non-adhesive surface. It is considered relatively old but still used even in recent studies with modification [47]. Secondly, it can be prepared by suspension culture. Suspension culture is rather a concept close to bioreactors, in which Cells are suspended in media and shaken to induce aggregation with other cells. Multiple spheroids are cultured in this method. Thirdly, spheroids are also available to be cultured on microfluidic biochips. It is able to give spheroids *in vivo* like environment such as constant shear stress and substrate exchange, which previous two methods does not have or less effective in cost.

The history of spheroid culture began when Sutherland et al. at 1971 first cultured cancer stem cell for therapy study by suspension culture. They proposed the term 'multicellular spheroid' first in the research [62]. Afterwards, Yuhas et al. cultured spheroid on agar mixed media in 1977, and Fukuda et al. cultured spheroid on multiple wells of microarray in 2005 [63, 64].

And in 2008, Wu and colleagues cultured spheroid on microfluidic device. The research designed U shaped traps that are directed to opposite of the media flow, so cells in suspension could be trapped and aggregated, finally into spheroids [65]. From the research, culture of multicellular cancer spheroid in various lab-on-a-chip

platform were customized for their own therapeutic target for even now. Torisawa et al. fabricated lab-on-a-chip co-culture platform to control the cell composition of the spheroid in 2009, suggesting that spheroids with various shapes and cell composition is possible by their platform [66]. In 2010, Liu et al fabricated salivary gland adenoid cystic carcinoma spheroid on hydrogel embedded biochip, to examine tumor infiltration behavior [67]. From research of Ziółkowska et al., colon carcinoma tumor spheroids were cultured on lab-on-a-chip platform to study long term culture of the spheroids *in vitro* [68], and in 2017 Zuchowska et al. Fabricated A549 and MRC-5 spheroids to determine *in vitro* lung cancer spheroid fabrication on microchambers of lab-on-a-chip as in Figure [69], and Alexander and colleagues in 2018 fabricated HepG2 Spheroids on chip [70].

Most recently the biochips are combined with complicated systems or procedures that can introduce desired features in spheroids, which can be seen in 2021 study of Petreus et al. in which they fabricated SW620 colorectal cancer spheroid and induced *in vivo* like pharmacokinetic profile for drug screening [71]. Or as in research of Yildiz-Ozturk in same year, culturing the lung cancer spheroid in agar micro-tissue wells and then transferring it to perfusion system which is like *in vivo* [72].

2.5 Nanoparticles as gene delivery vector

Nanoparticles are particles in size of submicron to nano scale, and nano means ‘dwarf’ in Greek word. The word nano nowadays designates 10^{-9} unit in scientific fields. The size of nanoparticles has wide variety depending on purpose and material but are practically under 500 nm in diameter. Due to the small size, it has large surface to volume area when compared to same mass of material in larger scales, thus enabling its unique property and behaviors. When dissolved to solvent, it is in ultra-dispersed, solid supramolecular structure. Nanoparticles can be fabricated from various materials, such as metals, minerals, and polymers depending on the purpose [73].

Application of nanoparticles itself or concept have existed from long time ago. Concept about ‘nanoparticle’ itself was at least from early 1900s, which predicted very small particles exists, which would behave on their own principles. In 1902, nanoparticle was first detected, and when 1931 first transmission electron

microscope was developed, visual confirmation of nano-sized materials became available [74]. Since then, nanoparticles were widely studied and applied in various fields, including chemistry, energy, electronics, environmental engineering, and bioscience and bioengineering [75-78].

One of the first studies that applied nanoparticles in bioengineering field was by Birrenbach and Speiser in 1975, which proposed concept of 'polymerised micelle. In the research authors fabricated nanoparticle by mixing and polymerising bis(2-ethylhexyl) sodium sulfosuccinate (I) and polyoxyethylene 4 lauryl ether into nanoparticles for adjuvant to enhance vaccine effeciency [79]. Afterwards, nanoparticles were applied in biological fields for other purpose than adjuvant, such as drug delivery vehicle, imaging agent, phototherapy, and as gene delivery vehicle [79, 80-82].

When nanoparticles are applicated as bioengineering tool such as drug delivery or gene transfection vehicle, it will be eventually adsorbed to cells by active process called endocytosis. There are two types of endocytosis mechanism, which are phagocytosis and pinocytosis. They are endosome meditated endocytosis process, first takes solid particle that reacted with surface receptor, while latter reacts with specific ligand and absorb liquid phase into cell.

In uptake process, Various factors are involved. Chithrani and chan suggested in their study of transferrin-coated gold nanoparticles, that shape can influence cellular uptake of nanoparticles. According to the study, spheric shaped nanoparticles had large adsorption rate compared to rod shaped nanoparticle (Nanorods), while uptake rates were even lower when aspect ratio of nanorods increased. They explained this phenomenon as wrapping time difference by clathrin-mediated endocytosis [83].

While morphology of the nanoparticle can affect uptake of nanoparticles, Harush-Frenkel and colleagues suggested that surface charge can modify uptake behavior of nanoparticles. In the study, they prepared poly (DL-lactide-co-glycolide) coated (PEGylated) nanoparticles of various charge and treated it to HELA cells. In the result, positively charged nanoparticles were absorbed more rapidly to the HELA cells, possibly by activating clathrin-mediated endocytosis [84].

Functional groups present on nanoparticles also affect the uptake of nanoparticles. Hail and colleagues discovered anticancer synthetic retinoid N-(4-

hydroxyphenyl)retinamide (4HPR) was more effective in promoting conspicuous cellular ROS production, mitochondrial disruption, or DNA fragmentation of the transformed cells when compared to both N-(4-methoxyphenyl)retinamide (4MPR) and N-(4-trifluoromethylphenyl)retinamid(4TPR) due to hydroxyl functional group enhanced the cellular uptake of 4HPR [146]. Additionally, in study of Wang *et al*., the researchers investigated endocytosis of hydrophilic endocytosis-promoting peptide (EPP6) rich in hydroxyl groups with no positive charge. EPP6 transported a wide array of small-molecule cargos into a diverse panel of animal cells, even without positive charge, suggesting hydroxyl groups can play critical role in cellular uptake of substrates [147].

2.6 Drug delivery systems (DDS)

Drug delivery systems (DDSs) control the transmission and release of pharmacologically active substances to cells, tissues, and organs for optimum effectiveness using various physical and chemical techniques [85]. Examples of chemical delivery systems can use carriers consisting of a wide variety of materials and structures, such as lipid micelles and nanoparticles that can transfer target molecules into cells; physical delivery systems include stimulations by electricity, ultrasonication, heat, and magnetism to penetrate the cell membrane [86-89].

In particular, many studies related to cancer treatment have been conducted. Depending on the target cancer and type of medicine, the delivery system is applied differently. DDS has facilitated the treatment of cancer and pain management associated with cancer progression and chemotherapy [88, 89]. Thus, many patients have experienced DDS cancer therapeutics, and many researchers are working to discover superior methods to the existing systems [86,90]. However, anticancer drugs can cause many side effects, such as resistance and various toxicities, including cardiotoxicity, hepatotoxicity, cardiotoxicity, ototoxicity, and neurotoxicity, and secondary malignancy [91].

Thus if anticancer drugs can be used to treat locally at a tumor site, the side effects could be minimized, and the treatment effectiveness could be increased [92–98]. Cisplatin, which contains two chlorine atoms and ammonia in platinum atoms, is the most representative anticancer drug used to treat a number of cancers [99]. Cisplatin, which binds DNA, can inhibit the replication of cancer cells. Generally,

this drug is ad- ministered via an injection. Thus, there are many side effects, such as a large impact on the kidneys [100,101]. Many researchers continue to study cisplatin or other drug delivery systems to improve efficiency and thus reduce these side effects. For example, by decorating biomarkers and magnetic materials to nanocarriers, loaded drugs were delivered to only the cancer site [102–106]. Additionally, the drug was injected directly into the tumor mass [107], hyperthermia was applied in the target area to induce rapid movement of the drug [108,109], or electroporation was used to accelerate the absorption of the drug into the cancer tissue [110–112]. Electrospray (ES) techniques provide micro- or nano-sized and charged droplets. This approach is generally used to manufacture nanoparticles and to encapsulate drugs or cells in polymers [113-117]. However, Ikemoto et al. proposed that an electrospray method can be used to introduce genes into cells [118]. Subsequently, several research teams used this technique to transfer external materials into cells [119,120]. These studies showed that applying an electrical field by electrospraying can facilitate the delivery of exogenous materials, making the ES technique a novel physical drug delivery system without severe damage, similar to traditional electroporation methods, because the delivery is mainly done by the impact of droplets on the cell surface [121].

2.7. Passive pump systems on microfluidics

Although spheroid culture by microfluidics device had many successes as previously described, However, operation of cancer spheroid culture platform can be frustrating the adaption. Current microfluidics devices require extensive training on operating and complicated equipment, which are specifically designed for the purpose, such as micropumps or tubes. Also, the bubble in the device should be extensively examined because it may detach cells in the channel, cause leakage to the tubes, or damage the platform itself.

With rapid prototyping technology and passive pump powered by surface tension, microfluidics platform without any external equipment is available. There are many methods to drive fluid from the inlet to output. Evaporation [122], permeation [123], osmosis [124] are such methods, and fluid transport by surface tension gradient is also one of the methods. Walker and Beebe introduced surface tension driven micropump to the field. Size of the droplet at reservoir drop (“outlet”) is

large enough to cause pressure gradient to pump drop (“inlet”), thus resulting flow in the device [125]. Based on the discovery, Meyvantsson and colleagues fabricated automated, microfluidic cell culture device that does not require any tubes or motors, only powered by surface tension of the fluid [126]. This was first fabricated to do mass screening on the microfluidics platform, and the cells are intended to be grown inside channel of the device.

However, it would be a different problem if it comes to culturing spheroids. As previously described, passive pumping culture systems are intended to culture cells on the walls of the channel. It would be available to culture the spheroid by filling the channel with hydrogel, but it is not the fundamental solution to culturing spheroid in the system. Therefore, reference from other culture devices, such as microwell or U-shaped traps should be considered to fabricate the right system. Also, structure of the device would be important to induce right flow acquired for the culture environment.

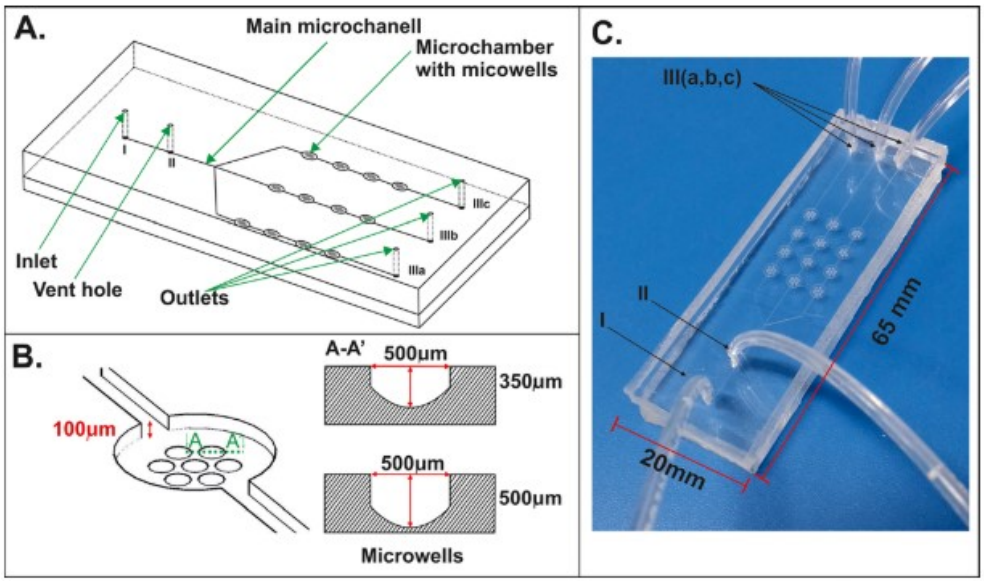

Figure 2.1 Spheroid-on-a-chip for culture of A549 and MRC-5 device design. A. The Scheme of the microfluidic system. B. Microchamber with cross-sections of two different wells. C. The fabricated microchip system (I: inlet, II: Vent hole, III: Outlets) [69].

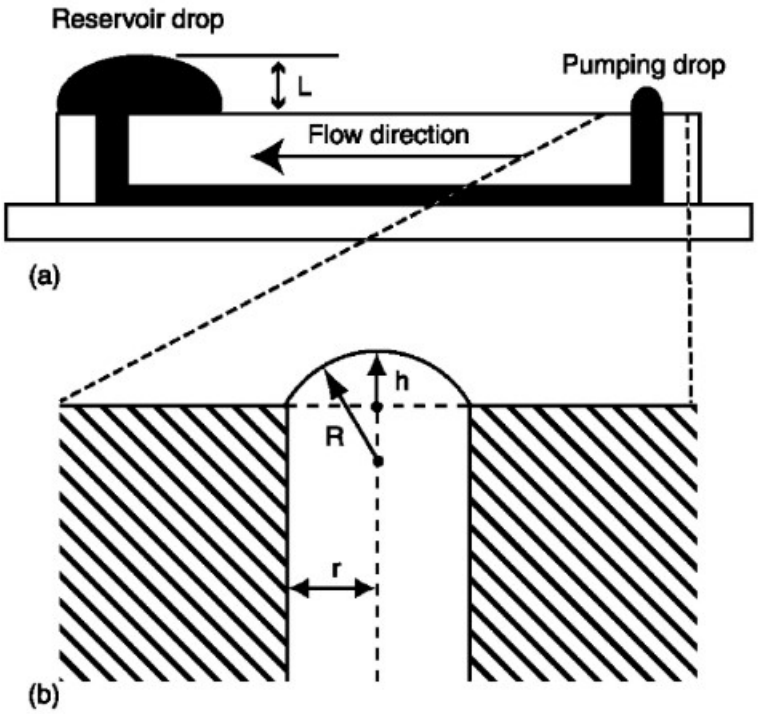

Figure 2.2 The schematic of the microchannel with passive pump system. A. Side view of the microchannel. B. Schematic of drop on the device. Drop of volume *V* will form a spherical cap of radius *R* on a port radius r, and the cap will rise above the surface of the device a distance *h*. If the drop volume is less than that for a hemisphere of radius *r*, then the drop radius *R* will be larger than *h* [125].

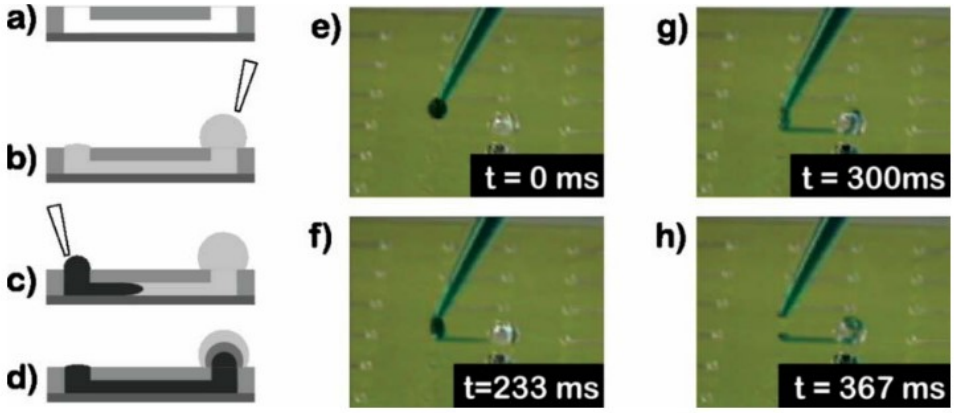

Figure 2.3 Schematic and image of passive pumping system. A-D. Schematic of empty system filled by first fluid, then second fluid introduced filling the system, resulting in outflow of first fluid. E-F. Actual image of passive pumping in action, by time lapse [126].

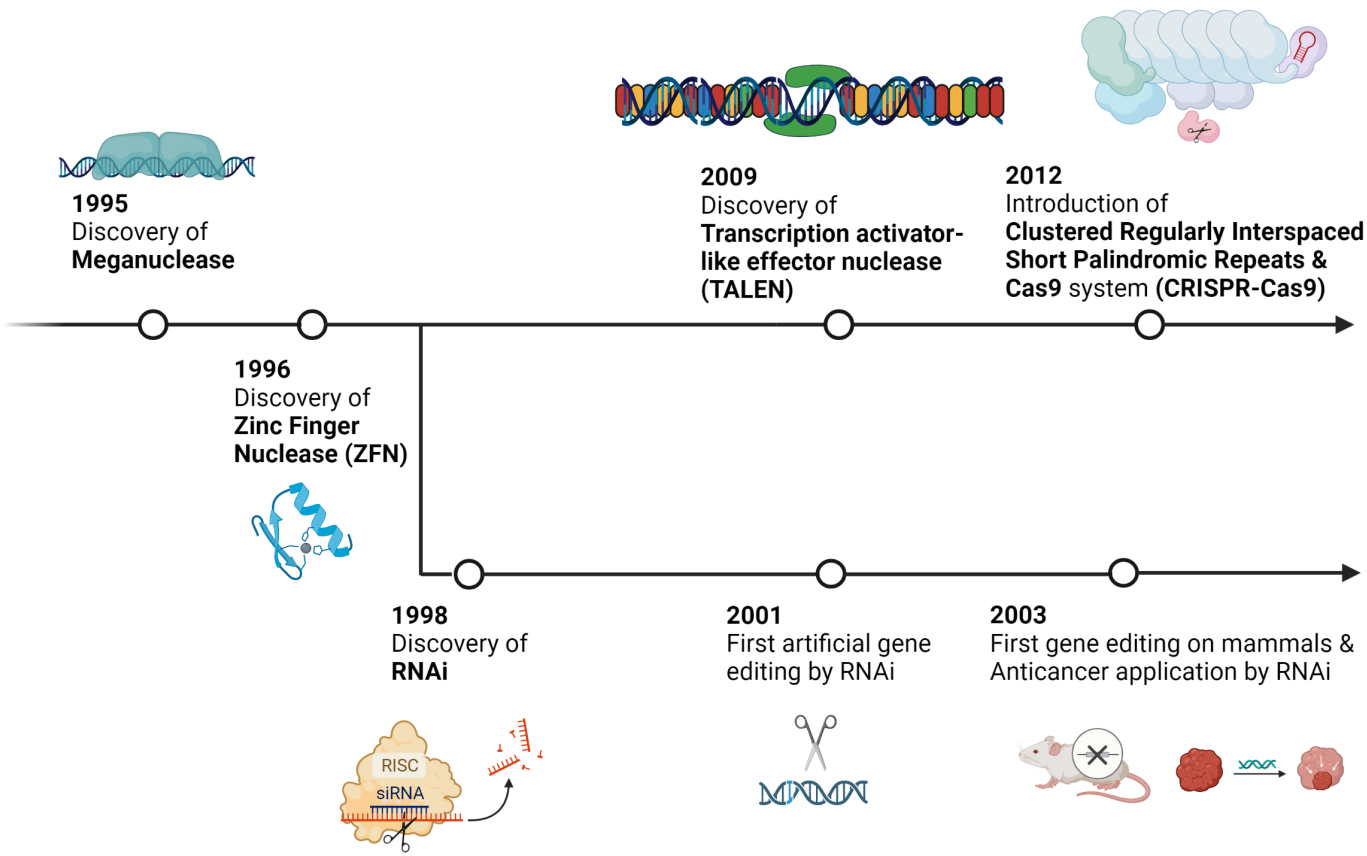

Figure 2.4 Schematic of gene therapy method discovery by years. Images were fabricated on Biorender (Biorender.com).

Table 2.1. Brief history of microfluidic systems and organ-on-a-chip system.

Year	Researcher	Content	Ref.
1979	Terry et al.	Miniature gas chromatic air analyzer on silicon wafer	[36]
1988	Esashi et al.	First development of microvalves	[37]
	Van Lintel et al.	First development of micropumps	[38]
1992	Manz et al.	Proposal of first 'Lab-on-a-chip' term	[39]
1994	Singhvi et al.	Culture of hepatocyte on modified gold surface	[41]
1998	Duffy et al.	First concept of microfluidics system on PDMS	[42]
2010	Huh et al.	Construction of lung organ-on-a-chip model	[44]
2012	Kim et al.	Construction of intestine organ-on-a-chip model	[45]
2017	Musah et al.	Glomerular capillary model construction on organ-on-a-chip	[46]
2022	Goreke et al.	Diagnosis and analysis on sickle red blood cells	[50]
	Kameda et al.	Vascularized tissue model	[49]
	Li et al.	Aryl hydrocarbon receptor analysis on cancer cell invasion	[48]

Table 2.2. Brief history of spheroid culture.

Year	Researcher	Content	Method	Ref.
1971	Sutherland et al.	First culture of spheroid for cancer therapy study	Suspension culture	[62]
1977	Yuhas et al.	Spheroid on agar media	Suspension culture	[63]
2005	Fukuda et al.	Spheroid on microarray	Multiple wells	[64]
2008	Wu et al.	Spheroid on microfluidic device	Biochip/ U shaped trap	[65]
2009	Torisawa et al.	Co-cultured spheroid	Biochip/ Microchambers/hydrogel embedded	[66]
2010	Liu et al.	Salivary gland adenoid cystic carcinoma spheroid to examine tumor infiltration	Biochip/ hydrogel embedded	[67]
2011	Tung et al.	Human epithelial carcinoma spheroids on multiple hanging drop array	Hanging drop	[144]
2012	Ziółkowska et al.	Colon carcinoma tumor spheroids on long term culture	Biochip/ Microchambers/hydrogel embedded	[68]
2017	Zuchowska et al.	A549 and MRC-5 spheroids	Biochip/ Microwells	[69]
2018	Alexander et al.	HepG2 spheroids on lab-on-a-chip	Biochip/ Chamber	[70]
2021	Petreus et al.	SW620 colorectal cancer spheroids on lab-on-a-chip	Biochip/ Chamber	[71]
2021	Yildiz-Ozturk et al.	Lung carcinoma spheroid on agar well to biochip	Micro-molded agar to microchip	[72]

Chapter 3. Induction of apoptosis of cancer cells using the cisplatin-based electrospray (CDES) system

3.1 Summary

Cisplatin, a representative anticancer drug used to treat cancer, has many adverse effects. In particular, it causes significant damage to the kidneys. Thus, many researchers have studied the delivery of drugs, such as cisplatin, to cancer areas using targeted drug-delivery systems. Here, we propose a new way to treat cancer by delivering anticancer drugs directly to the tumor site using the electrospray (ES) technique. We determined the optimal conditions for ES to promote the introduction of cisplatin into cancer cells. In our results, the group with cisplatin delivery-based electrospray (CDES) at 6 kV had an apoptosis of cancer cells approximately two times more than the group treated with cisplatin alone. We also confirmed that ES alone did not affect the survival of cells up to a voltage of 6 kV, but increased the permeability of the cell plasma membrane instantaneously, facilitating the influx of the drug.

3.2 Introduction

We reported previous studies that applied this technique to transfer genes into cells [120]. By applying an appropriate voltage, this technology can promote the influx of external substances while minimizing the impact on cells. In this study, we endeavored to develop a novel cisplatin delivery-based electrospray (CDES) system for cancer cell lines, proposed a new method for inducing apoptosis of cancer cells by delivering cisplatin using an electrospray method and indirectly proved the mechanism. Figure 3.1. shows a schematic of the CDES system. All the system facilities were installed on a clean bench. The syringe tip and the ground of the ring shape were connected to a high-voltage generator. Phosphate-buffered saline (PBS) was used as the electrospray solution, as was done in our previous study. Initially, to confirm how much damage was caused to cells by ES, cell viability was measured after treatment with ES at various voltages. Subsequently, the live and dead assay and WST-1 assay were used to confirm the optimal voltage to deliver cisplatin to the cancer cells. Additionally, to compare how apoptosis and necrosis are induced after CDES treatment, an Annexin V analysis was performed.

Finally, to analyze the drug delivery mechanism of CDES, changes in plasma membrane permeability were confirmed by propidium iodide (PI) analysis.

3.3 Materials and Methods

3.3.1 Materials

Roswell Park Memorial Institute (RPMI)-1640 medium and fetal bovine serum (FBS) were purchased from Welgene (Gyeongsan, Korea). A water-soluble tetrazolium salt (WST-1), to measure cytotoxicity, was purchased from Daeil Lab Service Co. (Seoul, Re- public of Korea), and a Live/Dead Viability/Cytotoxicity assay kit (Invitrogen (Thermo Fisher Scientific), Waltham, MA, USA) to investigate cytotoxicity, was purchased from Mi- toSciences (Eugene, OR, USA). For the apoptosis analysis, the FITC Annexin V Apoptosis Detection Kit was purchased from BD Biosciences (San Jose, CA, USA). A propidium iodide solution (PI, Sigma-Aldrich, St. Louis, MO, USA) was used to observe membrane permeability. A syringe pump (KdScientific, Holliston, MA, USA) and a DC high-voltage generator (TEKKAM, Seoul, Republic of Korea) were also used. Cisplatin (50 mg lyophilized powder) was purchased from Donga ST (Cisplan, Donga ST, Seoul, Korea).

3.3.2 Cell Preparation

HeLa (ATCC, Manassas, VA, USA) cells were cultured in a 100 mm dish (NUNC) for 2 days in 15 mL complete medium containing RPMI-1640 and antibiotics (Welgene Inc., Gyeongsan, Korea) supplemented with 10% FBS. HeLa cells were seeded at a density of 2×10^6 cells on the plate. After 2 days, the cells were harvested and seeded according to the manufacturer's instructions.

3.3.3 The Cisplatin Delivery-Based Electrospray (CDES)

The ES system was placed on a clean bench. The system consisted of two main components: the syringe pump and a high-voltage generator (Figure 3.5.). Cisplatin was dissolved in PBS and loaded into a 10 mL syringe, which was then fixed to the syringe pump. A 24-well plate was placed on the support. Subsequently, the syringe tip and the ground of the ring shape with a diameter and thickness of 12 mm and 1 mm, respectively, were connected to the high-voltage generator. The cisplatin solution was sprayed through the needle of the syringe at a constant flow rate of 1.8 mL h^{-1} and applied to a target in each well filled with media. The distance between the syringe tip and the grounded ring was 10 mm, the distance of the ground to the

media surface was 1 mm, and the distance of the grounded ring and plate well bottom was 3 mm. The solution was treated at the half maximal inhibitory concentration (IC50, 4 μg/mL) [121] of cisplatin for HeLa cells for one minute. The IC50 value means the drug concentration that inhibits certain biological processes by half. When electrospray was applied to the target, the electrospray voltage was varied (0, 2, 4, 6, and 8 kV).

3.3.4 Live/Dead Assay

To investigate cell cytotoxicity after CDES, a live/dead cell assay kit was used 1 day and 3 days after the treatment. For the live/dead assay, calcein and ethidium homodimer (EthD-1) were used as in the kit information sheet. Calcein is retained within live cells and produces green fluorescence at ex/em 495 nm/515 nm, while EthD-1 enters dead or damaged cells and produces red fluorescence at 495 nm/635 nm as stated in the data sheet of the kit. When ES was run on a 24-well plate, cells were seeded at a density of 3×10^4 cells per well, and the electrospray voltage was varied (0, 2, 4, and 6 kV). When dye was used for the assay, the live/dead dye was diluted by 5X in PBS. The cells were stained according to the kit instructions and incubated for 20 min at room temperature. The treated cells were observed by fluorescence microscopy (Nikon N-Storm, Nikon, Tokyo, Japan). The cell density in this section was 3×10^4 because the live/dead assay was part of the optimization process of the assays below. Additionally, considering the existence of the control group and the proliferation rate of HeLa cells, the cell number between day 1 and day 3 was assumed to not make any difference in the results. 400 μL of 1X binding buffer was added to the samples and analyzed by FACS within 1 h (FACS Aria II from BD Biosciences, USA).

3.3.5. Cell Membrane Permeability Analysis

Using PI Staining Simultaneously, after the Annexin V assay, PI staining was performed to determine the permeability of ES, using their nature of exhibiting red fluorescence upon binding to DNA inside the cell. HeLa cells were seeded in 24-well plates at a density of 5×10^4 cells per well. After 1 day, the cells were treated with 6 kV ES. Afterward, at various time periods (after 0, 30, 60, and 120 min), PI solution at a concentration of 3 μM was added, and the cells were incubated for 5

min. After washing the wells with PBS one-time, red fluorescence was observed using a fluorescence microscope (Ti-E, Nikon, Tokyo, Japan).

3.3.7. Statistical Data Analysis

A statistical analysis was performed using R v3.2.1 software (The R Project for Statistical Computing. Available Online: http://www.r-project.org (accessed on 02 October 2020). The least significant difference (LSD) method, Duncan's test, and one-way ANOVA were used to compare the means of the properties of the samples. The level of significance was set at $p < 0.05$. The data are reported as the mean ± standard deviation, with $n = 3$ or 5.

3.4. Results

3.4.1 Cell Viability

Analysis after ES at Each Voltage To use the electrospray system as a tool for drug delivery to cells, it is necessary to check how much cell damage is done by the high voltage of the process. Thus, we measured cell viability after treating ES at various voltages. Figure 3.6. shows the results of the WST-1 assay after ES at various concentrations (2, 4, 6, 8 and 10 kV). In the ES treatment group below 6 kV, no significant cytotoxicity was measured. However, the ES treatment group with 8 kV or more showed more red fluorescence in the live/dead assay and significantly lower viability in the WST-1 assay than the control. These results showed that ES above a specific high voltage caused significant damage to the cells, and up to 6 kV allowed the delivery of a drug using ES. Thus, we decided to use a voltage of 6 kV or less for the ES drug delivery system.

3.4.2 The Induction of Apoptosis by CDES

We hypothesized that treatment with a higher voltage ES would promote the delivery of cisplatin. However, CDES was performed with a voltage of 6 kV or less since ES alone at more than 6 kV impacted cells. To determine the optimal voltage, CDES was performed at various voltages. One day after treatment, cell proliferation was investigated by live/dead analysis (Figure 3.7. A, B). Living cells (green fluorescence) were classified according to intracellular esterase activity, which involved the release of red dye (ethidium homodimer-1). In contrast, the dead cells (red fluorescence) degraded esterase activity and did not release red dye. As a result, there was no significant difference between the cisplatin-only, 2 kV CDES, and 4 kV CDES treatment groups. The fewest live cells were found in the 6 kV CDES treatment group. The analysis showed that the ratio of dead to live cells was almost twice that of the group treated with cisplatin alone. In the WST-1 analysis, it was found that the cell viability was the lowest in the 6 kV CDES treatment group, similar to the live and dead results (Figure 3.7. C). Based on these results, we confirmed that the optimal voltage of CDES for inducing apoptosis in cancer cells is 6 kV. Figure 3.2. shows the cell viability of the 6 kV CDES and cisplatin treatment groups 3 days after treatment. Interestingly, in the group treated with only 6 kV ES, most of the cells were alive, similar to the control group.

However, it was confirmed that the 6 kV CDES treatment group had significantly lower proliferation than the group treated with cisplatin alone. After the fluorescence image analysis for the live and dead assays, it could be seen that the ratio of dead/live cells in the 6 kV CDES treatment group was approximately 7 times higher than that of the cisplatin-treated group (Figure 3.2. B). Cell viability using the WST-1 assay also showed similar results to the live and dead assays (Figure 3.2. C). Based on these results, we expected that cisplatin would be delivered to the cells with higher efficiency through the CDES method, and accordingly, apoptosis of cells was better induced. To determine accurately whether apoptosis was caused by CDES, FACS analysis was performed using the Annexin V assay (Figure 3.3.). Apoptotic cells were detected by staining with phosphatidylserine with green fluorescence (FITC), and necrotic cells were detected by PI through red fluorescence. Early apoptotic cells showed only green fluorescence, while late apoptotic cells showed both green and red fluorescence. Surprisingly, it was confirmed that more than 85% of the cells were in the process of apoptosis in the 6 kV CDES treatment group. In the group treated with cisplatin alone, approximately 40% of the cells were undergoing apoptosis. Few cells were apoptotic in the 6 kV ES treatment group. This means that the ES method promoted the delivery of cisplatin, dramatically increasing the induction of apoptosis, even though it did not cause much damage to the cells by itself.

3.5. Discussion

PI staining analysis was performed to confirm indirectly the mechanism of how drugs are forcibly injected into the cells by ES. PI is a substance that exhibits red fluorescence upon binding to DNA inside the cell. PI is generally used to detect dying or dead cells because the cell membranes of healthy cells do not allow PI to pass. On the other hand, it is also used as a tool to detect the opening of the plasma membrane when a specific stimulus is applied to a cell [127,128]. We hypothesized that the ES method temporarily increased the permeability of the cell plasma membrane, thereby increasing the influx of drugs into the cells, so PI was administered at increasing time intervals (0, 30, 60, and 120 min) after ES treatment. In our results, numerous red spots resulting from PI, which indicates dying or dead cells, appeared in the group treated with 6 kV ES at 0 min. However,

as time passed, the expression of red fluorescence rapidly decreased, and there were almost no red spots at 60 min (Figure 3.4. A). Compared with the control, the amount of red fluorescence in the 6 kV ES treatment group was approximately 20 times higher at 0 min (Figure 3.4. B). After ES treatment, the red fluorescence derived from DNA-bound PI was different at each time interval, indicating that the opening of the plasma membrane was changed. Thus, we indirectly indicated that when a specific substance is delivered to cells using ES, it can facilitate substance transfer by increasing the permeability of the cell plasma membranes. Figure 3.4. C shows the proposed CDES mechanism. The charged droplets generated by ES increase the plasma membrane permeability of the cells and greatly increase the influx of cisplatin.

In this study, we proposed a new method for inducing apoptosis of cancer cells by delivering cisplatin using an ES method and indirectly proved its mechanism. Several studies have reported the transfer of genes and proteins to cells using ES, but our study is the first to induce apoptosis by delivering anticancer drugs to cancer cells using ES. Recently, a study on the delivery of genes using a miniaturized ES device was reported [120]. If an anticancer drug can be delivered using such a miniaturized ES device, it is expected that a new anticancer treatment method can effectively deliver the drug to a limited target area. In the future, we plan to use technology to reduce the size of skin cancers and *in vivo* tumors.

3.6 Conclusions

In summary, we have confirmed that electrospray technology facilitates the introduction of cisplatin, an anticancer drug, into cancer cells and discovered that electrospray at 6 kV is the proper voltage for delivery of the drug to the target. Compared with the group treated only with cisplatin, the 6 kV CDES-treated group effectively inhibited cell proliferation and induced apoptosis of cancer cells. Additionally, after ES treatment, the plasma membrane permeability was measured at regular intervals. This result indirectly showed that CDES increased the influx of the drug by increasing the permeability of the cell membrane. If this technology is further improved with additional *in vivo* studies, we expect it could be advanced to local anticancer treatment to apply the drugs selectively to tumor sites only. With our research, another anticancer delivery system fundamental for local treatment

has been established.

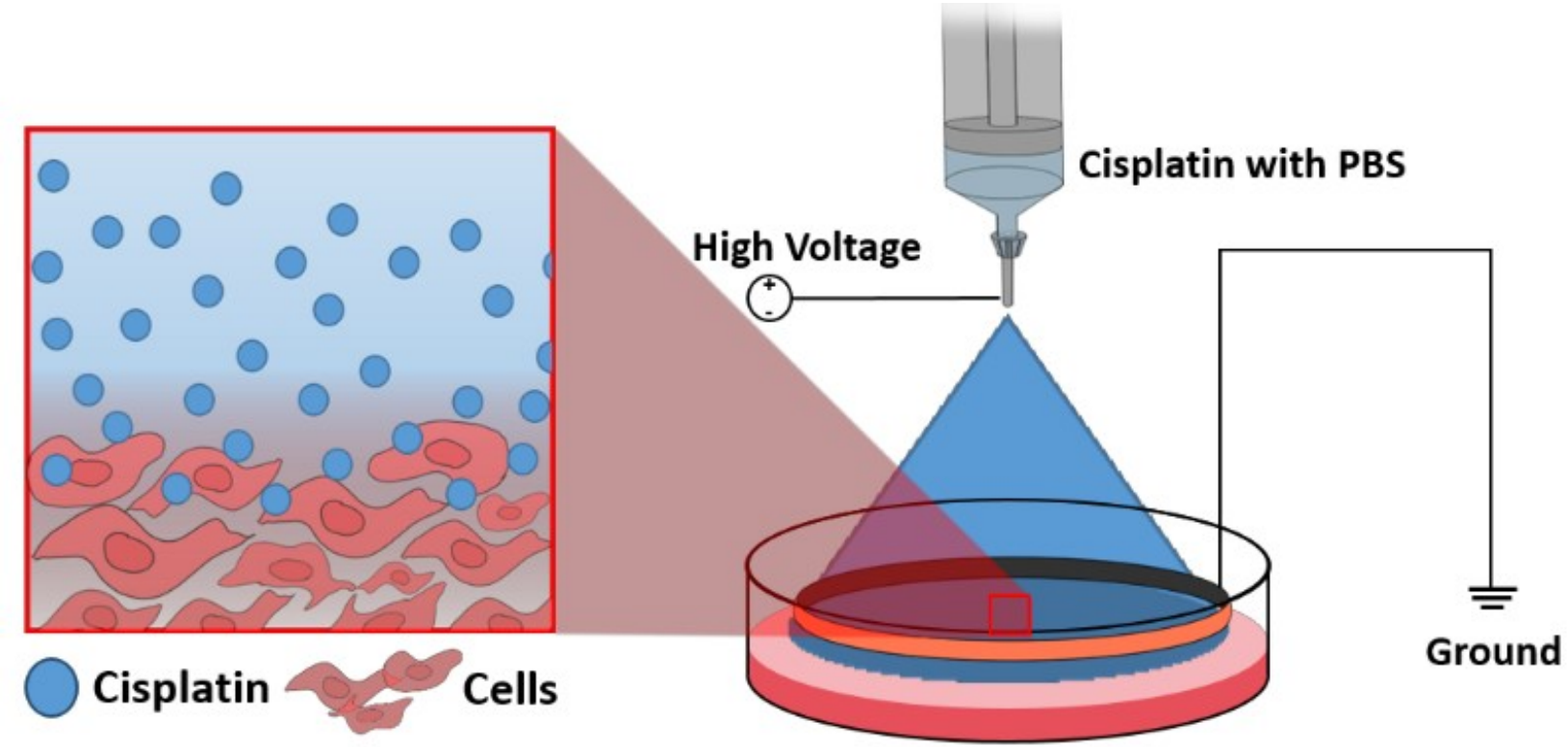

Figure 3.1. Schematic diagram of the cisplatin delivery-based electrospray (CDES) system. The CDES system facilitated the delivery of cisplatin to cancer cells. This method suggested a way to kill cancer cells by treating drugs locally into the tumor tissue [145].

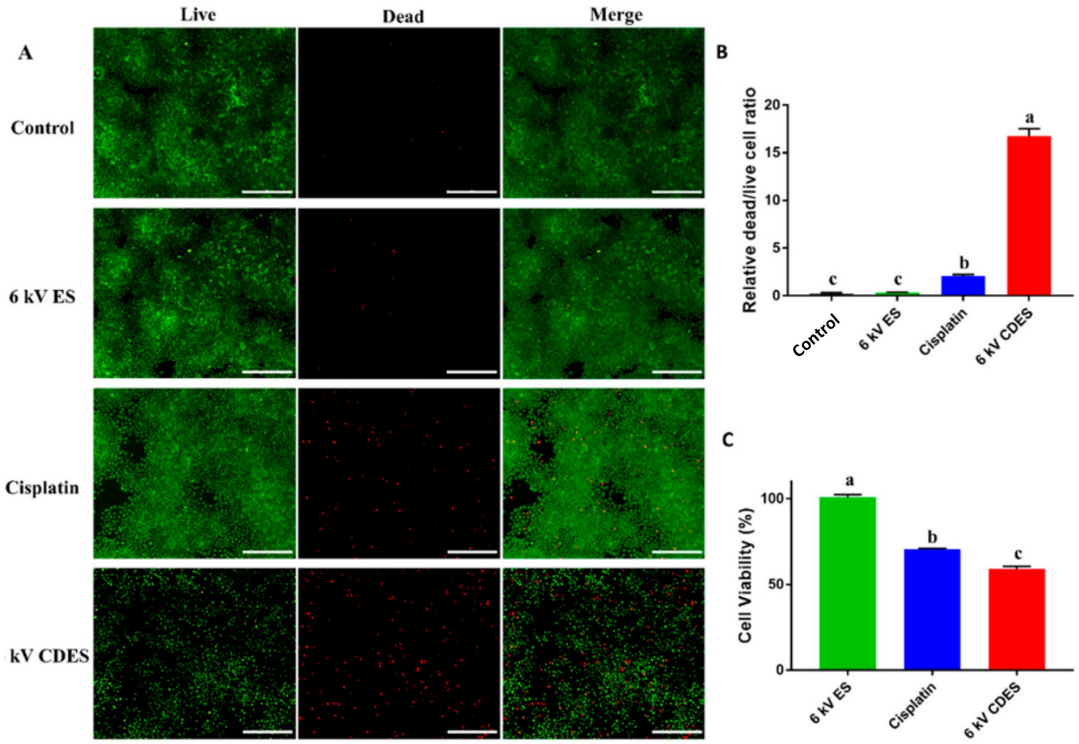

Figure 3.2. Comparison of cell viability of 6 kV CDES and cisplatin, (A) live and dead assay of 6 kV electrospray with cisplatin (Control, 6 kV ES, Cisplatin and 6 kV CDES), (B) the bar graph of the dead/live ratio, (C) water-soluble tetrazolium salt (WST) assay of 6 kV CDES (scale bar: 1 mm, n = 3, $p < 0.05$. Columns with different letters are significantly different according to the Duncan test). The ratio of dead/live cells in the CDES-treated group was approximately 7 times larger than that in the cisplatin-treated group 3 days after treatment [145].

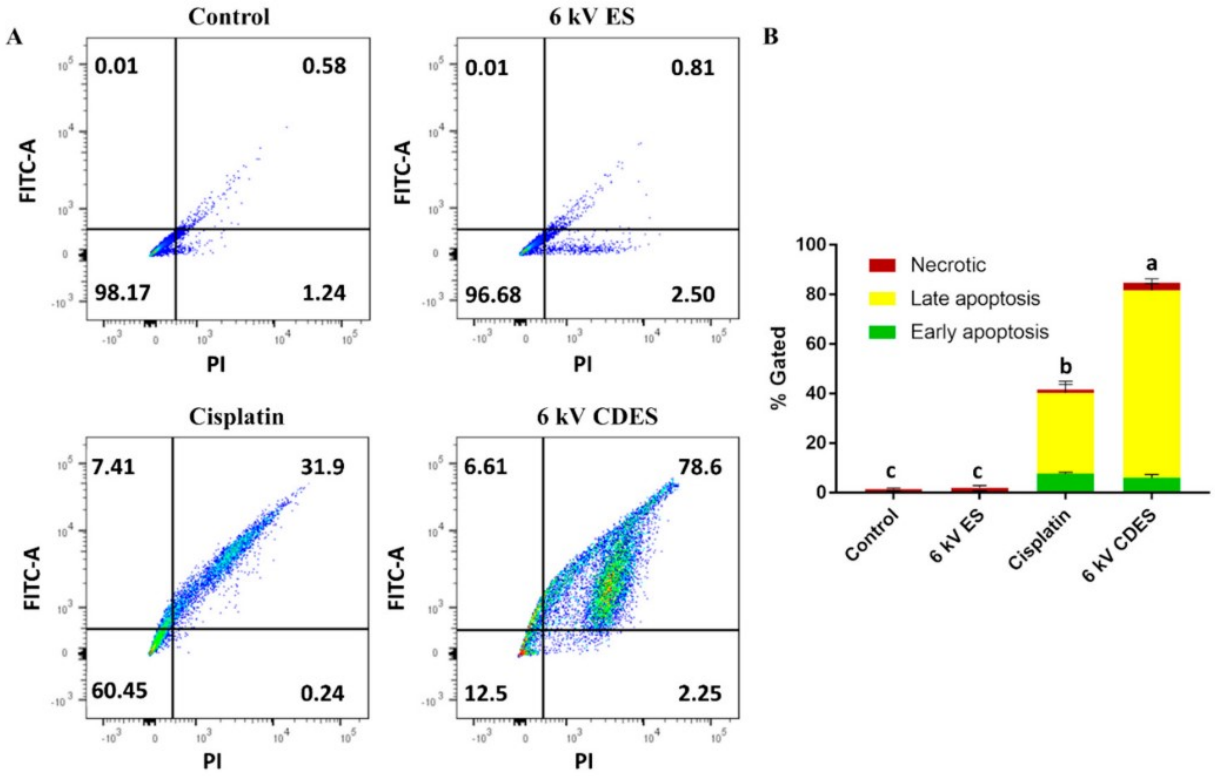

Figure 3.3. (A) The results of fluorescence-activated cell sorting (FACS) for Annexin V staining after 6 kV CDES (Control, 6 kV ES, Cisplatin, and 6 kV CDES). (B) FACS analysis showed more than 80% cell death in the 6 kV CDES group. Approximately 80% of apoptotic cells were shown in the 6 kV CDES treatment group ($n = 3$, $p < 0.05$. Columns with different letters are significantly different) [145].

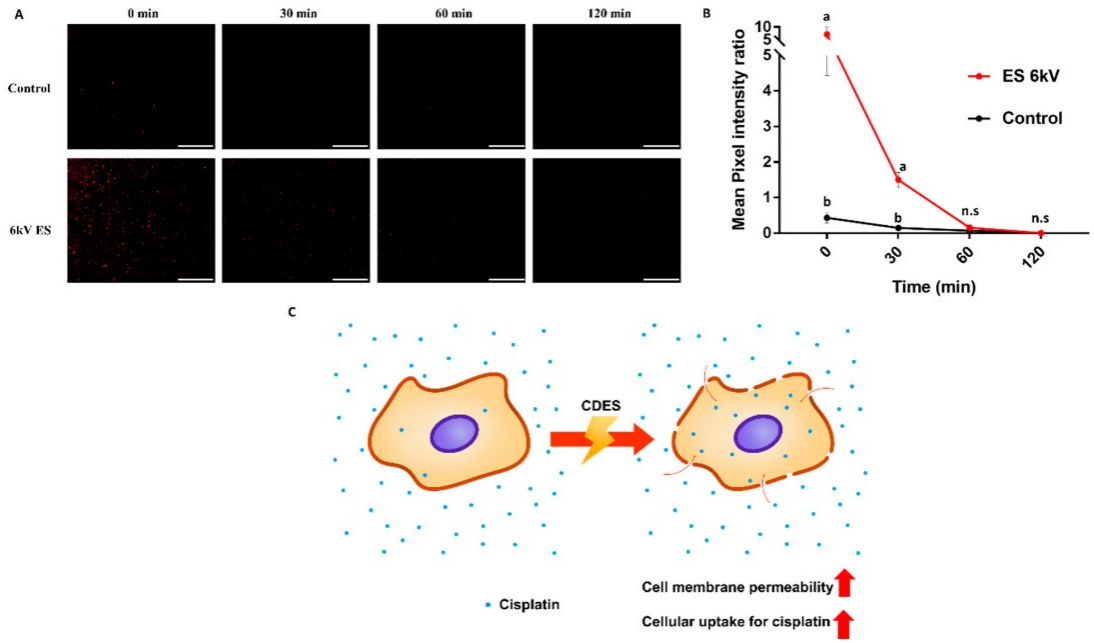

Figure 3.4. Proposed CDES mechanism. (A) Comparison of plasma membrane permeability after electrospray (ES) using propidium iodide (PI) staining (scale bar: 1 mm). (B) PI staining analysis over time. Compared to the control, when treated with 6 kV ES, red fluorescence derived from DNA-bound PI was significantly higher, but over time, the expression of PI decreased to a similar level ($n = 3$, $p < 0.05$. Columns with different letters are significantly different according to one-way ANOVA and Duncan's test). (C) Proposed CDES mechanism. The charged droplets generated by ES increase the permeability of the plasma cell membrane. Then, it increases the influx of cisplatin [145].

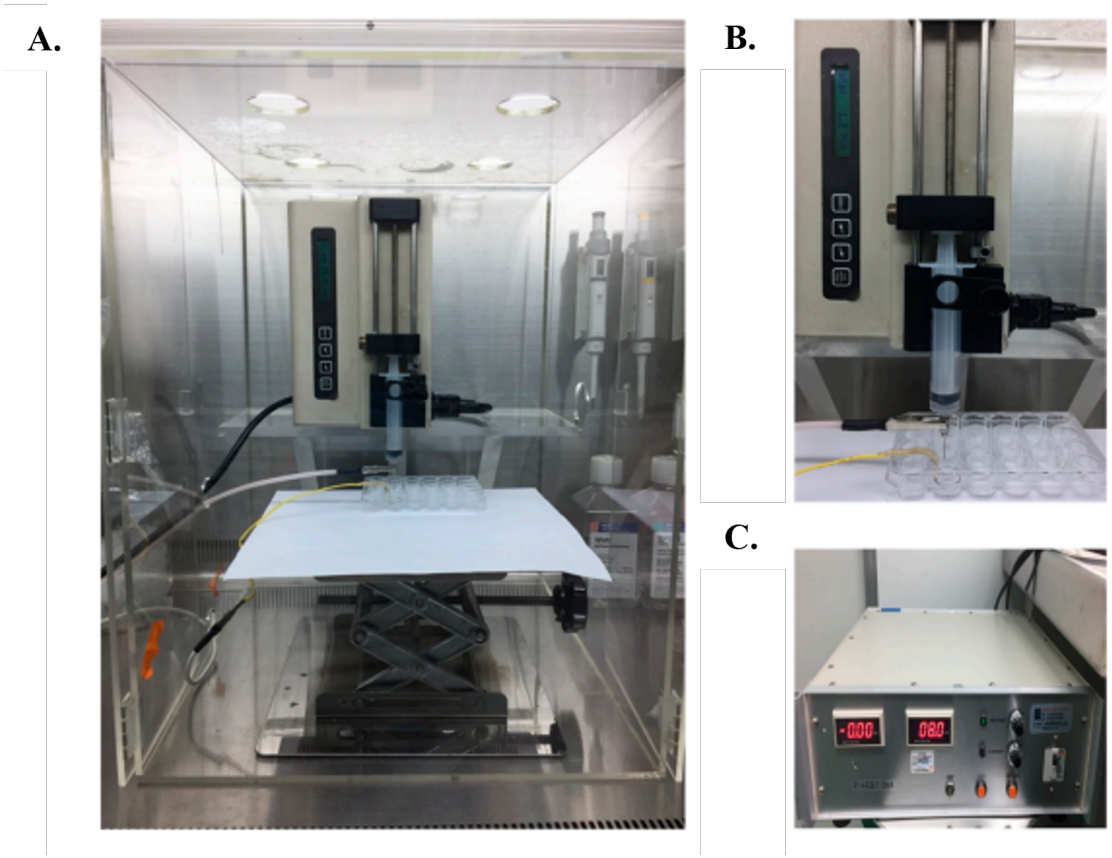

Figure 3.5. Components of CDES system [145]**.**

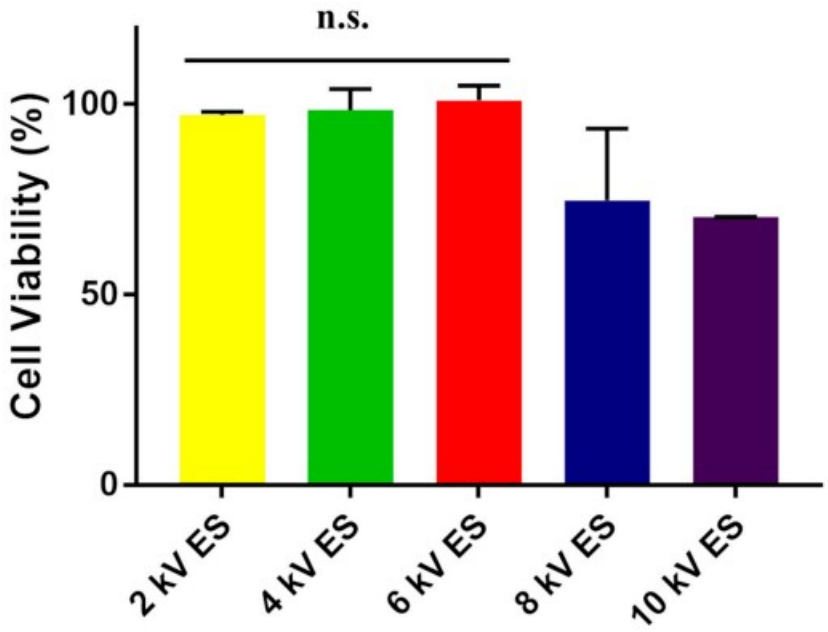

Figure 3.6. Cell viability after electrospray (ES) at various voltage. When the ES was treated with a voltage of 6kV or less, no toxicity to the cells was observed, but the damage to the cells was found to be large from the ES of 8kV [145].

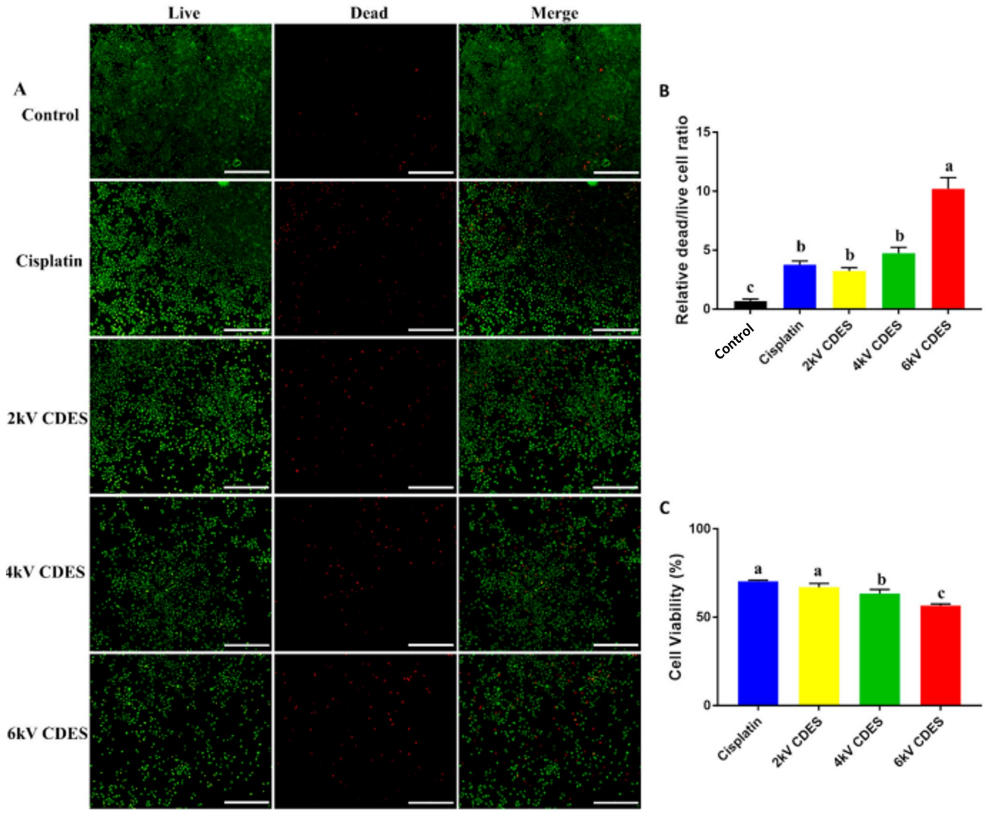

Figure 3.7. Comparison of cell viability at various voltage CDES. A. Live and dead assay of electrospray with cisplatin at various voltages (Control, Cisplatin, 2kV CDES, 4kV CDES, 6kV CDES), B. The bar graph of dead/live ratio C. WST assay of CDES (scale bar: 1 mm, n=5, $p < 0.05$. Columns with different letters are significantly different according to one-way ANOVA and Duncan's test) CDES at 6kV induced the largest number of cancer cell deaths 1 day after treatments [145].

Chapter 4. Fabrication of 3D-printing assisted Spheroid-on-a-chip platform

4.1. Summary

We fabricated a 3D cell culture platform with a channel and well that could culture a cancer spheroid inside the cells, which had a well size of 1,000 μm and 500 μm in diameter. The platform was built as intended, transporting fluids from the inlet to outlet without any external forces except for initial fluid feeding, as well as no leaking.

The culture conditions were optimized by varying the cell density and well size, which was narrowed down to a cell density of 3×10^6 cells/ml and well size of 500 μm, which showed fewer necrotic areas or clustered morphology in the early stages. Under the optimized conditions, A549 cells successfully formed spheroids and showed increasing viability to 1 week, when the viability of the spheroids increased significantly compared to the start of culture.

When doxorubicin was used to determine the cell death ratio and drug resistance induced by platform culture and cocultured cell variations, most of the cells showed almost half decreased viability *in vitro,* while there was no significant cell death in the platform when compared with untreated groups; however, variation of cells did not significantly affect the chemotherapy resistance. The effect of platform culture and cocultured cell variation on stemness gene expression, which could contribute to drug resistance, was determined by qPCR, and the A549 with CSC groups showed the largest increase; therefore, it is best to culture A549 and CSCs in the platform to culture spheroids that express stemness and drug resistance as natural tumors.

4.2. Introduction

As described in the previous chapter, cancers such as lung cancer progress rapidly and have a poor prognosis, thus making animal model construction and overall research difficult. Thus, a more suitable platform that could be studied *in vitro*, which has *in vivo* tumor-resembling features, is needed. Multicellular spheroids, or spheroids in short, can be a solution to this problem. Spheroids are compact and dense masses of cells growing without adhesion to the surface. Due to different

growth behavior compared to 2D culture, it shows more *in vivo*-like properties. Previous studies cultured spheroids on various platforms and harvested or moved them to biochips to fulfill research purposes. These studies reported that spheroids have *in vivo* tumor-like drug sensitivity or gene expression levels. Additionally, there is already research that focuses on culturing spheroids consisting of lung cancer cells, such as A549 cells, on lab-on-a-chip platforms [69, 72].

Additionally, spheroid cultured cancer cells are abundant with stemness-expressing cells, which are called cancer stem cells. These cells influence the therapeutic drug resistance or long-term survival of spheroids [129]. There is some evidence that spheroids cultured in microfluidic platforms can be enhanced with stemness gene expression levels [130, 131].

However, previous research still has some room for improvements and new discoveries. First, current spheroid culture methods have no such midpoints between spheroid function maintenance and convenience. Spheroids can be grown in microwell arrays, but spheroids may not be induced with sufficient shear stress or hypoxia resulting from media flow. Spheroids grown in LOC systems equipped with micropumps and tubes can be provided with the desired shear stress to the cells, but training and experience are needed to operate such equipment. This makes the culture of spheroids in such devices complicated.

Second, the effect of the nonactive pumping system on the behavior of spheroids is not well defined currently, which includes stemness gene expression. There was research that enriched stemness-like features to spheroids cultured on a microfluidic system, but it used an active device to induce flow to the system. Similar to the nonactive pumping system, the effect of CSC-like cells on the expression of stemness genes in cultured spheroids is also not yet well defined.

Considering the issues above, surface tension-based passive pumping can be combined with microwells. It was first used for high-speed drug screening, which transports droplets from the inlet to the outlet by the surface tension of the fluid. This method can induce shear stress in spheroids while eliminating the need for complicated equipment or skills. Within the device, the effects of CSC-like cells on stemness gene expression of spheroids can also be defined.

In this research, a microfluidic cancer spheroid culture platform with surface tension-induced passive pumping was fabricated, and A549 lung adenocarcinoma

cells and cancer stem cells were used together to culture spheroids inside the platform.

4.3 Material and Methods

4.3.1. Chip fabrication

The spheroid-on-a-chip platform (SOC) was fabricated by casting PDMS on the mold. First, the mold was designed by Fusion360 (Fusion360, Autodesk, California, USA), and the file was converted into an STL file. The mold of the upper part included an inlet and outlet and an air vent for the spheroid culture well. The mold of the bottom part included the overall channel, inlet, outlet, and well. The inlet size was 1.5 mm, and the outlet size was 6 mm in diameter. The channel was 750 μm in height, 500 μm in width, and 16.25 mm in total length. The spheroid well was in the midst of the channel. The diameters of the hemispheric bottom were 1,000 μm and 500 μm, and the depths were 1.35 mm (1,000 μm) and 0.95 mm (500 μm).

To print the design into a mold, rapid prototyping was used. A digital light projector Printer (Photon Mono X, Anycube, Shenzhen, China) was used to fabricate small features in the mold. The resulting mold was washed with isopropyl alcohol (5035-4410, Daejung chemistry, Gyeonggi-do, Korea), cured by UV rays to remove the remaining resin, and then additionally cured on a 60 °C hot plate (SMHS-3 Multi-Hotplate Stirrers, Daihan Scientific, Incheon, Korea) to prevent distortion.

After the mold was ready, polydimethylsiloxane (Sylgard 184 silicone elastomer kit, Dow Corning, Michigan, USA) was cast onto the mold, prepared as instructed by the manufacturer, and cured on a 60 °C hot plate. Within 3 hours of heat curing, the SOC structure was peeled off from the mold and additionally cured at 75 °C. Cured PDMS was then tailored, and the inlet, outlet, and air vent were punched into the upper part using 1.5 mm, 2 mm, and 6 mm biopsy punches (Disposable Biopsy Punch, Miltex, Texas, United States). Contaminants were removed from the surface using Kimtech wipes (Kimwipes, Kimberly Clark, Wisconsin, USA) and 70% ethanol (4204-4410, Daejung chemistry, Gyeonggi-do, Korea) and masked with adhesive tape. Finally, masking of the upper part and bottom part was removed, then assembled by treating O2 plasma by a vacuum plasma system (ACUTE, Femto Science, Hwaseong, Korea) for 90 seconds and bonding. After fabrication, the completed SOC was sterilized by autoclaving for further use.

4.3.2. Cell culture in the spheroid-on-a-chip platform

The A549 adenocarcinoma cell line, human umbilical vein endothelial cell (HUVEC) passage 4, and sorted cancer stem cell (CSC) passages 8 to 10 were used for the experiment. Cells were cultured to the desired density and passage until the seeding day. HUVECs were purchased from ATCC (CRL-1730, ATCC, Virginia, USA), A549 cells were purchased from Korea Cell Line Bank (10185, Korea Cell Line Bank, Seoul, Korea), and CSCs were sorted by a magnet-activated cell sorting (MACS) Tumor Cell Isolation Kit (130-108-339, Miltenyi Biotec, Maryland, USA) from glioblastoma cells according to the manufacturer's instructions.

On the seeding day, the internal channel and well of the SOC were washed with 70% ethanol and then with phosphate buffered saline (DPBS, Medicago, Chicago, USA) 2 times to remove contaminants while removing bubbles carefully. Channels and wells were coated with 5% polyethylene glycol (PEG) (88276, Sigma–Aldrich, Massachusetts, USA)-PBS solution for 90 minutes at room temperature to prevent adhesion of the cells on the channel and promote spheroid formation in the well.

After 90 minutes, the PEG solution was exchanged with RPMI growth media (LM011-60, RPMI growth media, Welgene, Korea) supplied with 10% fetal bovine serum (FBS) (S-101-01, Welgene, Korea) and 5% antibiotics (LS-203-01, Welgene, Korea). Prepared cells were washed with DPBS, treated with trypsin-EDTA (Trypsin-EDTA, Welgene, Korea) and then suspended in 1 ml growth media. Afterward, 10 μl of 200 μg/ml fibronectin solution was added to a 1 ml cell suspension. This was to help spheroid formation by adding extracellular matrix component. After the cell suspension filled the channel of the SOC platform, it was cultured in a 37 °C CO2 incubator. During the culture, DPBS washing and media change were performed daily.

4.3.3. Culture Optimization

This section was prepared to determine more suitable cell density and well size and long-term cell viability of spheroid formation. For the experiment, each chip was cultured with different well sizes and cell densities. The SOC platform and cell suspension were prepared as previously described.

To determine optimal well size for the culture, we prepared 500 μm and 1,000 μm well. 3×10^6 cells/ml of A549 cells were seeded in the device, then cultured for day3,

Day 5, and Day 7. After well size determination, optimal cell density for the culture was discussed. 3×10^6, 3×10^5, 3×10^4 A549 cells/ml of cell suspension was seeded in 500 μm well, then cultured for Day 3, Day 5, and Day 7.

On the day of analysis, LIVE/DEAD kit (L3224 LIVE/DEAD™ Viability/Cytotoxicity Kit, for mammalian cells, Thermofisher, Massachusetts, USA) was used to visualize the viability of the cells growing in the SOC device. LIVE & DEAD kit can show results fast, and easy to apply even on microfluidic devices like the one used in this experiment. Previous on analysis, SOC was washed with PBS to remove any FBS in the media to prevent any interference. Afterward, LIVE & DEAD working solution which have 5 μl calcein AM, 20 μl ethidium homodimer-1 in 10 ml was prepared, then added to the wells and cultured for 10 minutes. Afterward, SOC were moved to fluorescence microscope (Eclipse Ni-E, Nikon, Tokyo, Japan) stage and imaged in FITC, Texas Red wavelength for further analysis.

After optimization of well size and cell density, WST-1 assay was used to observe growth of spheroids in the platform. 3×10^6 cells/ml of A549 cell suspension was seeded in 500 μm well, and cultured for Day 3, Day 5, and Day 7 (n=5). After preset period, spheroids were washed, harvested, and made into cell suspension with culture media. The cell suspension of each well was then added to 96 well to total volume of each well is 100 μl. After one hour of stabilization, 10 μl of 10 × EZ-CYTOX (Ez-3000P, DoGen Bio, Seoul, Korea) solution was added to each well. After one hour incubation at 37 ºC, the plate was read at 450 nm wavelength at ELISA plate reader system (Sunrise absorbance microplate reader, TECAN, Männedorf, Switzerland).

4.3.4. Immunocytochemistry staining (ICC)

To determine and image cancer cell specific marker CD133 on the spheroid surface, expression on the spheroid surface immunohistochemistry analysis was prepared. First, Spheroid in the biochip was fixed by 4% Paraformaldehyde, then extracted on the slide glass. Fixed spheroids were blocked with bovine serum albumin (BSA) for an hour. Afterward, the samples were treated with anti-CD133 antibody (ab19818, Abcam, Boston, USA), FITC-conjugated secondary antibody, DAPI and vinculin. Afterward, the samples were mounted on slide glass, then moved to

fluorescence microscope (Eclipse Ni-E, Nikon, Tokyo, Japan) stage for further analysis.

4.3.5. Quantitative real time PCR (qPCR)

To determine effects of HUVEC and CSC on stemness gene expression of A549 cells in spheroid culture, eight experimental groups were set: A549, A549 and HUVEC, A549 and CSC, A549, HUVEC and CSC, and same variation of cells cultured in 96 well plate (n=3). Cells were seeded, cultured until Day 3, Day 7 as previously described.

For RNA extraction and cDNA synthesis, TRIzol (15596026, Thermofisher, Massachusetts, USA) and Omniscript RT Kit (205113, Qiagen, Venlo, Netherlands) and oligo DT primer (18418012, Thermofisher, Massachusetts, USA) was used as manufacturer's instruction. On the day of harvest, cells were harvested from biochip and wells, and treated with TRIzol. After RNA extraction and cDNA synthesis was done, total cDNA concentration of each group was adjusted to 25 ng/ml, then stored in -70 ºC for further use.

The expression of the stemness genes Oct4 and Nanog and the housekeeping gene GAPDH was analyzed using quantitative PCR (qPCR) with a Rotor-Gene Q real-time PCR system (Qiagen, Venlo, Netherlands), Ampigene® qPCR Green Mix Lo-ROX (ENZ-NUC103, Enzo, New York, USA), and Bioneer qPCR primer (20-S-1001, Bioneer, Daejeon, Korea). The forward and backward primer sequences for the genes are shown in Table 1. Each sample was prepared as follows: 10 µl of master mix, 0.8 µl each of 10 pmol/ml forward and backward primers, and 10 µl of 25 ng/µl DNA.

4.3.6. Cytotoxicity assay

To determine the effects of cell variation and biochip culture on the chemotherapy resistance of the cells, doxorubicin was used as a cancer chemotherapeutic drug. Four groups were set (A549, A549+HUVEC, A549+CSC, and A549+HUVEC+CSC, which are abbreviated as A, AH, AC, and AHC, respectively), which were divided into two groups: doxorubicin-treated and nontreated groups (control). Additionally, *in vitro* groups with the same variation of cells seeded in the biochip were also prepared.

In vitro groups were seeded at a density of 1×10^4 cells per well, and biochip groups were seeded as previously described. Then, doxorubicin solution in growth medium (10 µg/ml) was added to each experimental group.

After 24 hours of treatment, each sample was washed with PBS and subjected to the WST-1 assay as previously described. *In vitro* samples were added to 110 µl of 1× WST-1 working solution, and each sample was read after 1 hour of incubation at 37 °C. The LIVE & DEAD assay was also performed as described in 4.3.3. for both groups.

4.3.7. Doxorubicin ES on *In vitro*/Biochip

To investigate the effect of doxorubicin treatment by electrospray on *in vitro* and biochip, Electrospray settings were set as in Section 3.3.3., and the concentration of doxorubicin was set as 1.11 µg/ml, considering the electrospray rate. *In vitro* samples were treated as described in Section 3.3.3. Biochip samples were treated by placing ground above the vent, considering the nozzle-to-ground distance.

4.3.8. Statistical analysis

Viability assay results are given as the mean ± SD for the indicated number of wells. Statistical analysis and one-way ANOVA were performed using OriginPro 2018 software (Originlab Corporation, Massachusetts, USA). A minimum of three samples were analyzed. Differences were considered statistically significant at $P < 0.05$.

4.4 Results

4.4.1. Chip fabrication

A spheroid-on-a-chip platform was successfully fabricated. The size and morphology of the channels were equivalent to the initial design, while passive pumping successfully functioned as seen in Figure 4.1.

4.4.2. Culture Optimization

Initially, both wells formed spheroids successfully, showing bright green fluorescence to Day 3, indicating that no apparent cell death occurred in the spheroids. As shown in Figure 4.2, spheroids were successfully formed at a 1,000 μm diameter without showing any sign of clustering, but regions with red fluorescence were observed in the center after Day 5. This indicates necrosis in spheroids cultured in 1,000 μm diameter wells, possibly induced by hypoxia caused by excessive size. While the 1,000 μm wells showed red fluorescence after 5 days, the 500 μm diameter well also showed a red region. However, there was a relatively small area of red fluorescence, even considering the overall size difference.

In the cell density determination, there was a visually apparent difference between each group from the early stage. While the 3×10^6 cells/ml group showed complete spheroid formation from Day 3, the 3×10^5 and 3×10^4 cells/ml groups showed rather clustered, smaller sized spheroids distributed in the well. After several days, both groups also formed one agglomerate. However, we determined that it would be more suitable to culture cells at a density of 3×10^6 cells/ml further in the study. This was because the density was more uniform in morphology from the early stage. The even shape and size of spheroids would minimize standard deviations for therapeutic assays considering the total surface area, thus producing more stable data.

After confirming that the 500 μm diameter well and density of 3×10^6 cells/ml were the optimized culture conditions in the platform, spheroids were cultured to Day 7. The spheroids on Day 7 showed a significant viability increase when compared to Day 1 and Day 3 data, indicating that the spheroids in the platform were grown successfully.

4.4.3. Immunocytochemistry staining (ICC)

CD133 expression on spheroids was most prominent in the A549 and CSC cocultured group as green fluorescence. However, the expression of CD133 was more prominent in the A549, HUVEC and CSC culture groups. From the results, the expression of CD133 was more prominent when A549 spheroids were cultured with HUVECs and CD133.

4.4.4. Quantitative real time PCR (qPCR)

On Day 3, Nanog expression in the biochip-cultured groups except for the A549-only groups showed higher -ΔΔCt, indicating that the expression was higher than that in the other groups. Additionally, Oct-4 expression, except for the A549 only group, showed a higher -ΔΔCt value than the *in vitro* cultured groups. Although not statistically significant, the expression of the biochip-cultured AC group was highest among the others, showing that CSCs cultured with A549 cells promoted more stemness gene expression than the others.

On Day 5, all the -ΔΔCt values for Nanog expression were higher than those in the *in vitro* cultured groups, except for the A549 only group. The -ΔΔCt value for Oct-4 expression was lowest on BAC, while all biochip culture groups except for the A549 only group had higher expression than the *in vitro* groups. While Biochip-cultured AC showed the highest -ΔΔCt value for both Nanog and Oct-4 expression, AHC showed the second highest -ΔΔCt value for Nanog expression but lower expression than Biochip-cultured AH. Coculture of HUVECs and CSCs with A549 cells in the biochip platform induced higher expression of both stemness genes, although the difference was not significant.

4.4.5. Cytotoxicity assay

The cytotoxicity results on the biochip and *in vitro* samples showed remarkable changes. After doxorubicin treatment, *in vitro* cultured cells showed up to a 40% decrease in viability, as described in 4.3.A. However, biochip samples showed up to 90% viability even after doxorubicin treatment, as shown in 4.3.B. Live/Dead images also showed no significant cell death in the biochips, while the cell number decreased and red fluorescence increased, which indicates dead cells.

Among the doxorubicin-treated *in vitro* groups, the AHC group showed a

significant decrease compared to the other treated groups. When there was no significant difference between biochip cultured groups, the A group showed a tendency of decreasing viability when treated compared to the other groups.

4.4.6. Doxorubicin ES on *In vitro*/Biochip

The cytotoxicity results of doxorubicin delivered by electrospray on chip showed similar results to doxorubicin treatment without electrospray, while the AHC group showed no significant change *in vitro* after treatment. Additionally, percentage comparison showed no significant change between the *in vitro* and biochip groups, except for the AHC group.

4.5 Discussion

In regard to the formation of spheroids, the major critical factor for spheroid formation is cell number. When cell numbers decreased, cell aggregation in early spheroid development was small and formed in clusters. At very low density, the spheroids were barely formed or not formed. Although the clustered spheroids formed one aggregate in the wells, it would be better to inoculate a biochip with a cell density over 3×10^6 cells/ml. This is because clustered spheroids show less uniform surface area when compared to whole spheroids, affecting the experimental results in devices such as gene therapy and drug screening.

Meanwhile, the factor that influences the long-term survival of cells that are forming spheroids is suspected to be well size. The diameter of the well directly changes the size of the spheroid, and both the 500 and 1,000 μm diameter wells showed normal aggregation and growth of the cells. However, after Day 5 from the start of culture of the 1,000 μm diameter well, spheroids began to show necrotic areas from the center. This is due to the lack of surface area, which causes hypoxia, inferior nutrients, and waste exchange in the core region. In contrast, the 500 μm well did not show prominent signs of necrosis even on Day 7, which indicated that spheroids grown in the 500 μm well were more advantageous in material exchange. Live & Dead and WST assays on long-term culture also showed the spheroids cultured on optimized condition (500 μm diameter well, 3×10^6 cells/ml) maintained viability, and exponential growth throughout the culture, proving the condition is preferable in the device.

A cytotoxicity assay using doxorubicin indicated that spheroids had more resistance to chemotherapy than spheroids *in vitro*. When cultured *in vitro*, the AHC groups showed poor survival of the cells compared to other groups *in vitro*. However, the A group in the biochip showed a tendency of decreasing viability when compared to the other groups cultured in the biochip. This indicates that the features given by coculture of HUVECs and CSCs are not very effective in the *in vitro* groups, but they may increase the drug resistance features when compared to A549 only cultured groups. The surface area may explain the survival rate difference between the *in vitro* and biochip groups, and stemness expression may explain the viability difference between the biochip groups.

The qPCR data support the viability data, supporting the hypothesis that resistance to chemotherapy was promoted by the increase in stemness in spheroids. The expression of the stemness genes Nanog and Oct-4 was higher in the biochip-cultured groups than in the *in vitro groups on* both days except for the A549 only group. From the results, we can predict that A549 cell only groups cultured in biochip may have better resistance compared to *in vitro* groups but would show less tumor-like behavior when compared to same biochip cultured groups, especially cultured relatively long term like in qPCR samples. This is remarkable when compared to doxorubicin treatment results on biochip cultured groups, where A549 only group showed larger drop of viability compared to other groups. Although it is not significant in viability, it could be evidence that stemness induced by coculturing CSCs and HUVECs may also influence the survivability of cells when exposed to therapeutic drugs. Additionally, when the cell line is cultured in a well plate for over 3 days, the overgrown cells become detached from the surface and influence other cells on the plate. However, as shown in the results, cells cultured on the spheroid culture platform showed increased viability and maintained morphology even for 7 days, as mentioned in the results, even presenting live tumor-like characteristics on Day 5. When comparing the coculture effect of HUVECs and CSCs, CSCs showed more stemness gene expression than other groups, including the A549/HUVEC/CSC groups, but HUVECs showed stronger expression of Nanog on Day 5. Although the A549/HUVEC/CSC coculture did not show a very promising effect in *in vitro* culture, it showed the highest expression on Day 5 when inducing both Nanog and Oct-4 expression,

suggesting that coculturing both HUVECs and CSCs would be more promising to induce more live tumor-like properties after Day 3.

As mentioned in other research, the major factor that influenced formation of the spheroids in this well was constant shear stress by flow and 3D structure. Although it is possible to make the fluids circulate endlessly by adapting conventional microfluidic pumps or other passive pump systems, spheroids were formed successfully even without such equipment. Moreover, drug resistance and stemness expression increased in biochips *in vitro* by combining biochip culture and coculturing HUVECs and CSCs. The results suggest that even without complicated machinery, the *in vitro* culture platform can fabricate more *in vivo* spheroids expressing drug resistance and improved stemness gene expression.

4.6 Conclusion

Overall research in this study fabricated and operated the cancer spheroid culture platform with basic cell culture equipment such as micropipettes. Even with a simple procedure, the spheroids expressed better drug resistance and stemness gene expression. The resulting platform from this research will provide new insight into how it is possible to maintain cancer spheroids with a relatively simple structure and operating method for a long time, even without micropumps or tubes. When applied to the biochip platform developed in Chapter 4, SHMT1 siRNA applied with SNP 20 showed a significant decrease *in vitro* in most groups after treatment and no significant difference in the percentage of viability compared to the control. However, there was no significant difference after the same treatment by electrospray. This may be because the nucleic acid binds with the nanoparticle to form a complex, and the voltage applied in electrospray may have disrupted these interactions. SNP alone showed different results than doxorubicin applied to chips in Chapter 4, showing that the application of siRNA by SNP 20 to biochips had a rather similar effect *in vitro* when considering the percentage data.

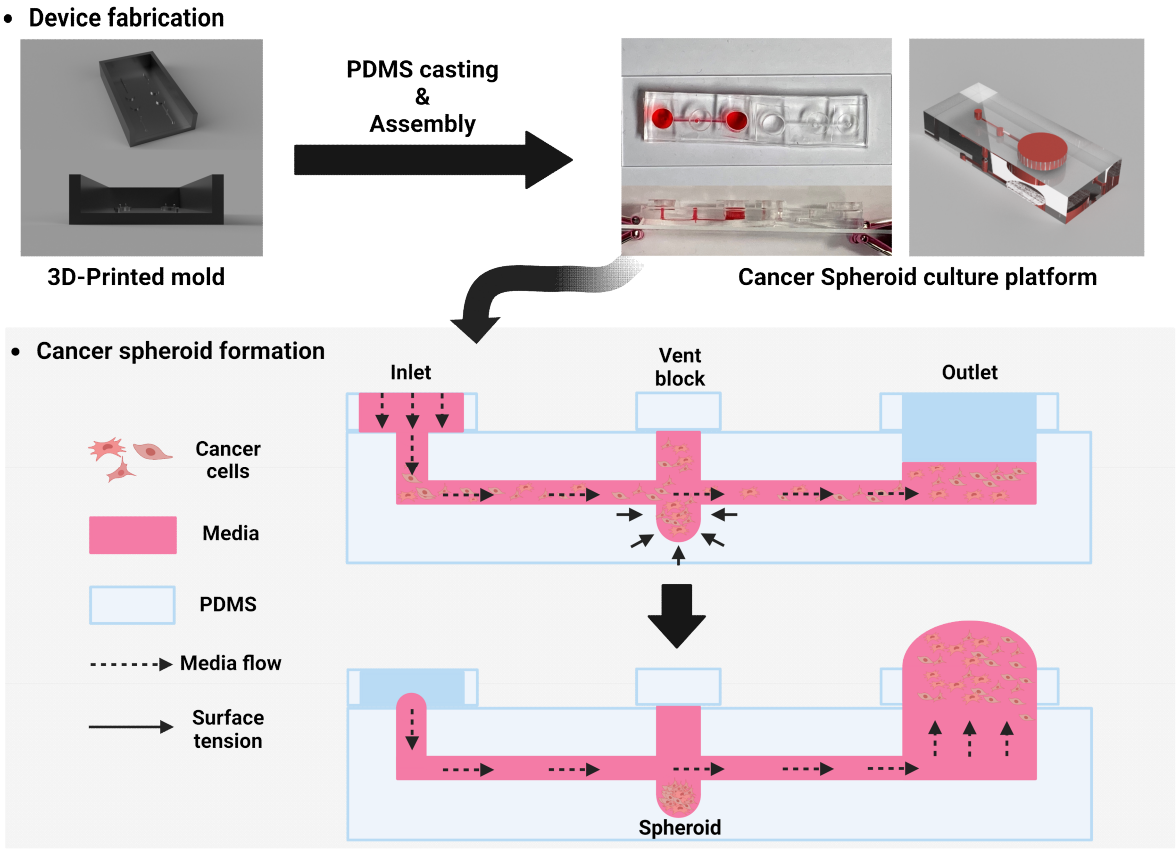

Figure 4.1. Schematic of the spheroid-on-a-chip platform and its application. Images were fabricated on Biorender (Biorender.com).

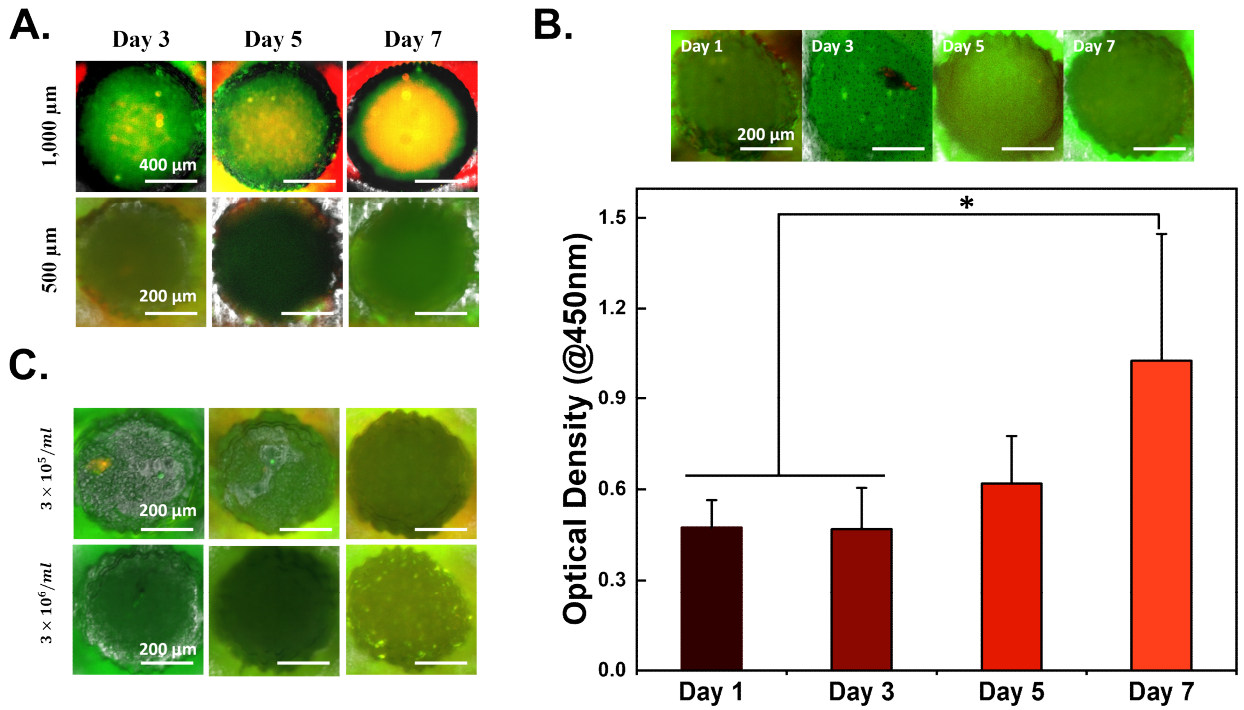

Figure 4.2. Cell culture conditioning on the biochip. a, c. Live/Dead images of Day 3 to Day 7 cultures of A549 cells in 1,000 and 500 µm wells at cell densities of 3×10^5 and 3×10^6 cells/ml. b. Culture of A549 cells at a density of 3×10^6 cells/ml in 500 µm wells from Day 1 to Day 7. (* indicates a significantly different value at $p<0.05$ (n=5))

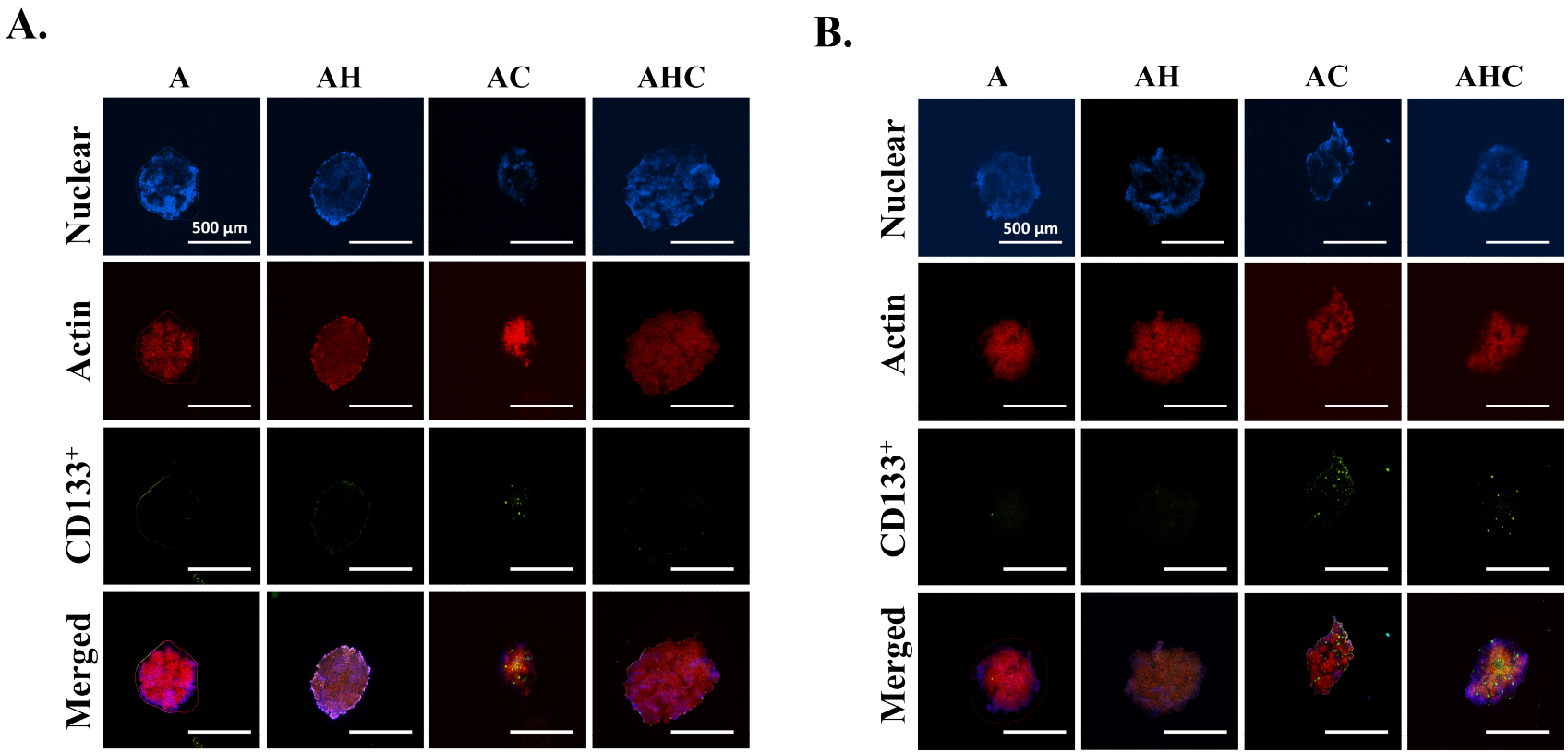

Figure 4.3. Day 3 and day 5 ICC results of CD133 expression. A. Day 3 images of spheroids. B. Day 5 images of spheroids. (Abbreviations: A: A549 only, AH: A549+HUVEC, AC: A549+CSC, AHC: A549+HUVEC+AHC).

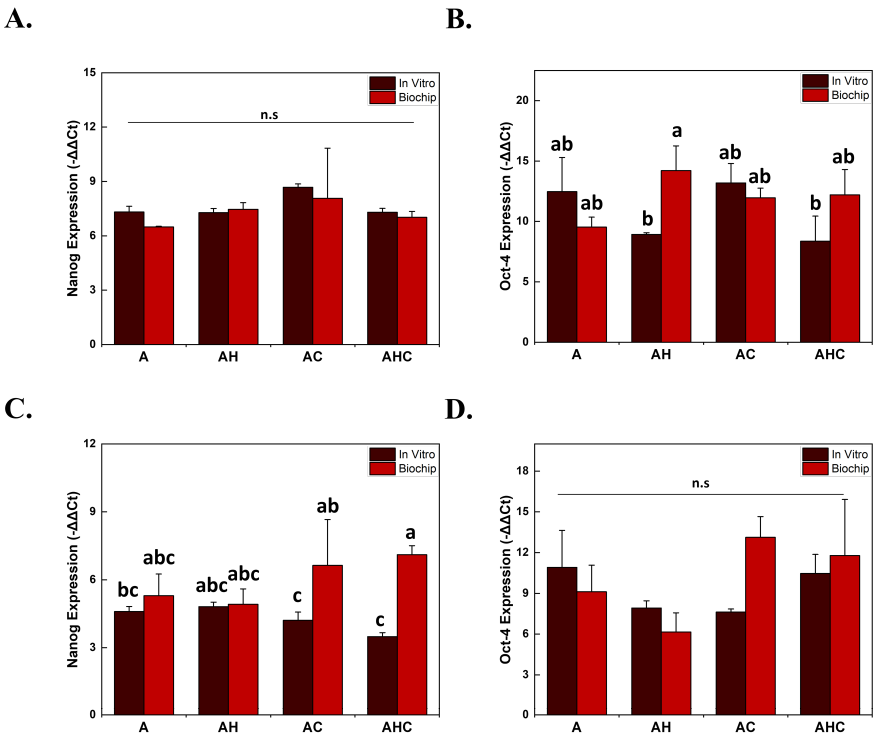

Figure 4.4. Day 3 and Day 5 qPCR results of stemness marker expression compared with *in vitro results*. A. Nanog expression by -ΔΔCt, Day 3. B. Oct4 expression by -ΔΔCt, Day 3. C. Nanog expression by -ΔΔCt, Day 5. D. Nanog expression by -ΔΔCt, Day 5. (Abbreviations: A: A549 only, AH: A549+HUVEC, AC: A549+CSC, AHC: A549+HUVEC+AHC. Different letters indicate significantly different values at $p<0.05$ (n=3)).

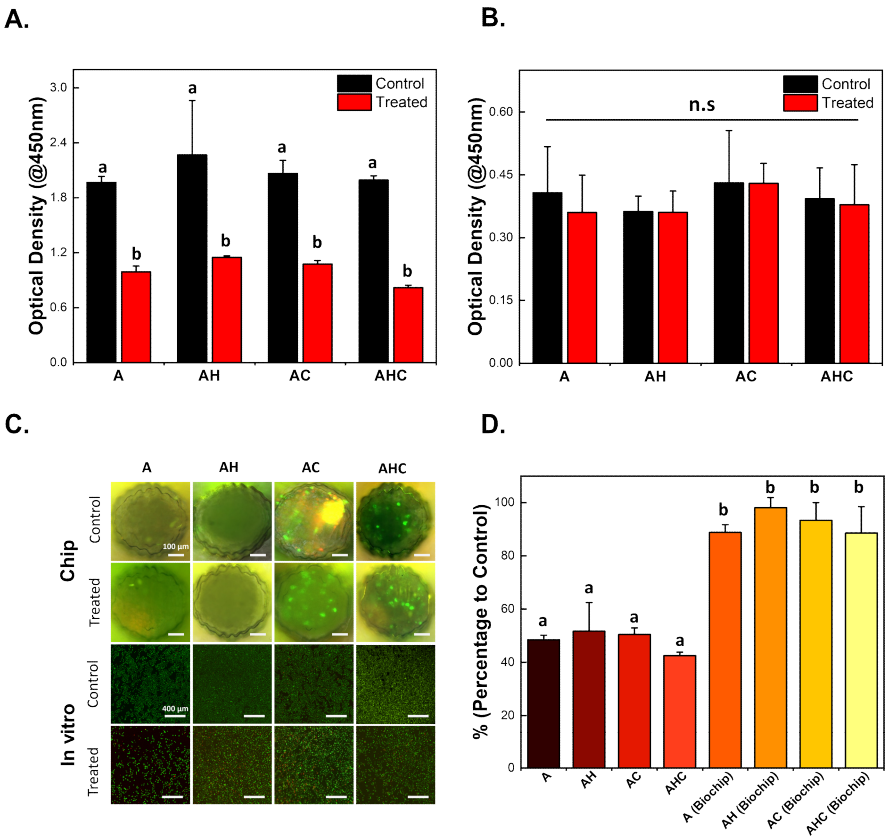

Figure 4.5. Drug resistance assay on biochips compared with *in vitro results*. a. WST-1 results of *in vitro* cultured cells treated with doxorubicin. b. WST-1 results of biochip-cultured cells treated with doxorubicin. c. LIVE/DEAD assay images of *in vitro* and biochip-cultured cells with control (nontreated groups). d. Percentage of control to doxorubicin-treated groups in each sample (Abbreviations: A: A549 only, AH: A549+HUVEC, AC: A549+CSC, AHC: A549+HUVEC+AHC. Different letters indicate significantly different values at $p<0.05$ (n=5)).

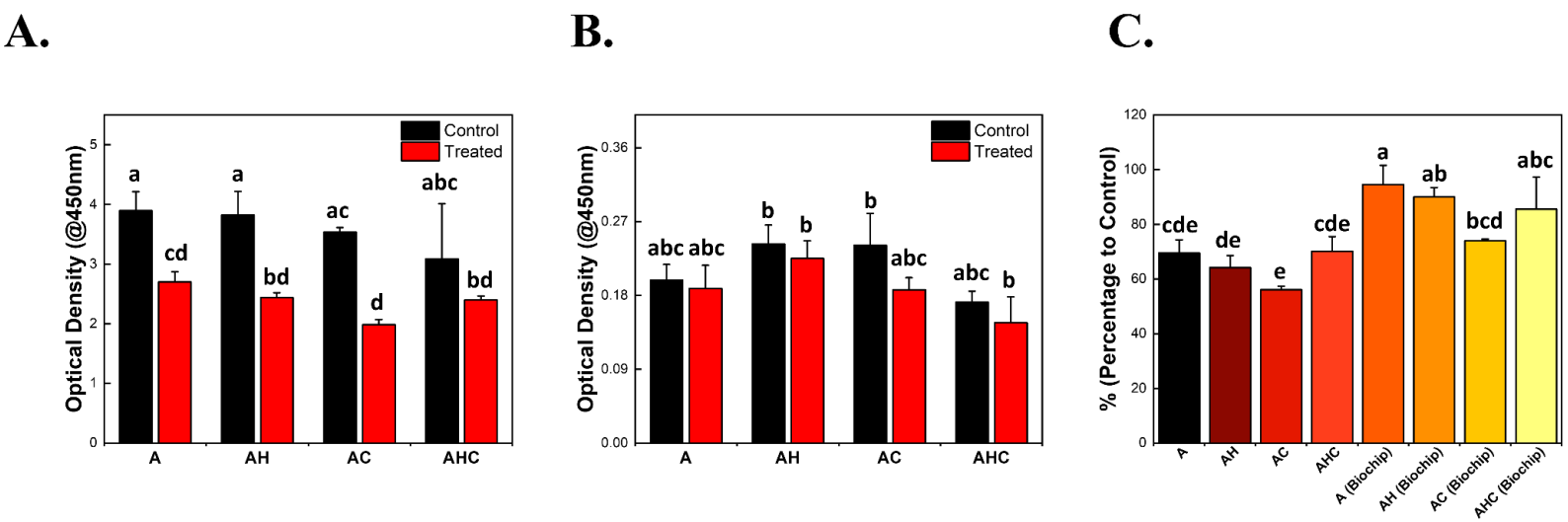

Figure 4.6. Comparison of cell viability at *in vitro* and biochip before and after 6 kV doxorubicin ES. A. WST-1 results of *in vitro* cultured cells treated with 6 kV doxorubicin ES. B. WST-1 results of biochip-cultured cells treated with 6 kV doxorubicin ES. C. Percentage of control to 6 kV doxorubicin ES treated groups in each sample (Abbreviations: A: A549 only, AH: A549+HUVEC, AC: A549+CSC, AHC: A549+HUVEC+AHC. Different letters indicate significantly different values at $p<0.05$ (n=5).

Table 4.1. Primer sequence used in qPCR.

Gene	Primer sequence (5'→ 3')	Size (bp)
GAPDH	F: ATGAGAAGTATGACAACAGCCT	113
(Housekeeping gene)	R: AGTCCTTCCACGAACCAAAGT	
Oct-4	F: GTGGACAGCAACTCCGATG	121
	R: TGCAGAGCTTTGATGTCCTG	
Nanog	F: AGCTACAAACAGGTCAAGAC	145
	R: GGTGGTAGGAAGAGTAAAGG	

Chapter 5. Design and fabrication of sericin nanoparticle for gene therapy

5.1. Summary

To overcome the limitations of electrospray in a previous experiment, we fabricated sericin nanoparticles for gene delivery. The nanoparticles were fabricated by two methods: one was fabricated by emulsifying the sericin solution in saline with ethanol and then crosslinking with glutaraldehyde, while the other was fabricated by grafting sericin with polyethyleneimine (PEI), making it easy to induce polymeric nanomicelle formation in aqueous conditions. The sizes of SNPs and PEIS were determined by DLS, which indicated that they successfully formed nanosized particles, while the surface zeta potential was slightly negative.

The viability of the nanoparticles was determined by WST-1 assay, which indicated that the SNPs were slightly cytotoxic at high concentrations. The RNAi and apoptosis-inducing effects of the nanoparticles were determined by WST-1, TUNEL assay, and qPCR. WST-1 assays showed that groups treated with SNPs showed a significant decrease compared to the PEI and control groups, while the group treated with PEIS also showed decreasing viability, although there was no significant difference. TUNEL assays showed induced apoptosis, which agreed with the result of the WST-1 assays. Finally, qPCR results on SHMT1 and P53 genes showed that expression of SHMT1 decreased significantly, and P53 expression increased indicating that the WST-1 and TUNEL assay results were due to RNAi delivery of nanoparticles in the cells, proving the feasibility of SNPs and PEIS for gene delivery drug in the future.

5.2. Introduction

In our former experiment, electrospray was used to deliver cisplatin to cancer cells. The electrospray method is available to generate nanosized structures by a relatively simple method. In this study, the viability of cancer cells was largely decreased by cisplatin. This was mainly caused by the function of the electric field, which enabled the particles to be more advantaged to invade into the cells by temporal electroporation.

However, electrospray is less attractive in regard to cancer therapy and applications

in vivo or in closed systems. This is because it is difficult to apply electrospray to the target area since most of the tumor is located deep in the body, unlike *in vitro* culture. Additionally, naked DNA solution is not very effective in gene transfection because the natural defense system of the cell easily degrades therapeutic nucleic acids. Thus, new delivery methods for genes are needed. Cationic liposomes are one of the most widely used gene transfection reagents, but cationic liposomes are cytotoxic and cause inflammation when excessive doses are administered [132]. On the other hand, nanoparticles have attractive features as gene delivery vehicles. Although it has been reported that the ideal particle size to increase uptake rate varies by the material and target organ or cell, in the case of drug delivery and gene transfection, studies suggest that polymer nanoparticle sizes over 100 nm are advantageous for cellular uptake [133, 134]. Therefore, to design and apply novel nanoparticles, the previously mentioned factors should be carefully considered for efficient experimental design and optimized outputs.

There are a variety of materials used for fabricating nanoparticles, such as metal, carbon, and synthetic and natural polymers. This may depend on the purpose, but in the biological field, natural polymers, particularly proteins, are preferred. This is because proteins are abundant in functional groups, which means that the properties of protein products can be easily modified for various purposes. Additionally, proteins used for biological and tissue engineering fields are amphiphilic, biocompatible, and biodegradable.

Sericin is a natural protein that is a byproduct of the silk industry. Silk fiber consists of fibroin fiber in the core and wax-like protein sericin surrounding the fibroin fiber. Although silk itself has been adopted in the medical biological field for a long time, its use is almost entirely limited to fibroin. This was mainly because sericin was considered to provoke immunogenic effects in humans, resulting in asthma [135-137], making it less popular than fibroin. However, years after research data on sericin were accumulated, it turned out that in fact sericin does not provoke immunogenic effects. Moreover, it was shown to be biocompatible [138-140] and have beneficial effects, such as enhancing wound healing [141, 142] and growth support of cell lines cultured in serum-free media [143].

From these aspects, sericin can also be adapted in fabricating nanoparticles. First,

sericin was adapted in the same way as its counterpart fibroin, mixed with water and crosslinked. Formaldehyde is often used as a crosslinker, but glutaraldehyde was used in this study because it is less cytotoxic and allergenic. While these types of fabrication methods are targeted to make stable nanoparticles, some researchers have focused on the functionality of the nanoparticle itself, such as targeted delivery and the capacity to deliver both hydrophobic and hydrophilic drugs. The functionality of sericin nanoparticles was achieved by grafting individual sericin units with desired materials to form nanosized polymeric micelles or blending sericin with other polymers, such as poloxamer, when fabricating the nanoparticles. Verification of sericin nanoparticles mainly focuses on proving cell uptake behavior by grafting florescent markers on the particles and on the actual effect of drug delivery. In most cases, *in vitro* studies, such as hemolysis assays, are conducted.

Although the above studies mainly discussed the drug delivery vehicle aspects of sericin nanoparticles, drug delivery and gene delivery are not much different in their fundamental principles. First, the drug/gene should be specifically and effectively delivered to target cells or tissue and then released into the desired cell organelles. For example, sericin nanoparticles developed for gene delivery and drug delivery are not very different in terms of their fabrication steps. This allows for further possibilities for applying drug delivery vehicle techniques to gene delivery and RNAi.

Fabrication of nanoparticles for this purpose can be a solution that maintains nanosize, binds well to the desired nucleic acid, and does not have any negative side effects after transfection, such as cytotoxicity.

Sericin can be an alternative. It has low cytotoxicity and excellent biocompatibility and can be modified easily because of its functional groups. While sericin can be fabricated into nanoparticles alone, other reagents can be conjugated to the structure. For example, polyethyleneimine is a good candidate for conjugation. When used alone, PEI has good transfection ability but is cytotoxic, which limits its use. If PEI is conjugated to sericin, the transfection rate will be increased, while the cytotoxicity of PEI will be repressed.

In this study, we fabricated sericin nanoparticles and sericin-PEI nanoparticles for the transfection of siRNA into cancer cells and examined the effects.

5.3 Material and Methods

5.3.1. Preparation of sericin nanoparticles (SNPs)

Sericin powder from mulberry silk was kindly provided by the Rural Development Administration and Sunchon National University. To prepare sericin nanoparticles, a desolvation method was used. Two hundred milligrams of sericin was completely dissolved into 2 ml of 10 mM NaCl (0241-1KG, Amresco Inc., Ohio, US) (pH 8.2) aqueous solution. Afterward, 8 ml of 99.9% ethanol (Daejung Chemical, Goryeong, Republic of Korea) was added dropwise at a rate of 1 ml/hr while stirring at 500 rpm and room temperature on a magnetic stirrer (SMHS-3 Multi-Hotplate Stirrers, Daihan Scientific, Incheon, Korea). After the sericin nanoparticles were dissolved as a turbid solution, 125 µl of 8% glutaraldehyde solution (4133-1405, Daejung Chemical, Goryeong, Republic of Korea) was added and then stirred at 500 rpm overnight to induce more stable nanoparticles by crosslinking. The next day, the solution containing crosslinked sericin nanoparticles was purified by centrifuging five times at 15,000 xG for 10 minutes, discarding and dispersing the same initial volume of 10 mM NaCl (pH 8.2) solution. After purification, sericin nanoparticles were lyophilized in a freeze dryer (FD 8508, Ilshin Biobase, Gyeonggi-do, Korea) for 48 hours for further analysis and use.

Sericin was also conjugated with PEI to form PEI-conjugated sericin nanoparticles (PEIS) to improve its gene transfection ability. The conjugation was performed by the EDC-NHS conjugation method. First, 100 mg of sericin was dissolved into 10 ml of 1 M NaCl in DW solution. Then, 50 mg each of EDC and NHS (E7750 and 56485, Sigma Aldrich, Massachusetts, USA) was added to the solution and reacted for 30 minutes at room temperature to activate. Afterward, 15 mg of PEI (Branched PEI 1,200, 06088, mw 1,200 kDa, Polyscience, Philadelphia, USA) was added to the solution and then conjugated with sericin for 12 hours with stirring at room temperature. The resulting substrate was dialyzed against 1 M NaCl for 6 hours and then against DW for 18 hours with a 12 kDa Spectra-POR dialysis membrane (132645, Repligen, Massachusetts, USA) and lyophilized with a freeze dryer for 48 hours.

5.3.2. Direct Laser Scattering (DLS)

The size, surface zeta potential, and polydispersity index (PDI) of SNPs and PEIS were determined by using a direct light scattering system (DLS; Zetasizer Nano-ZS60; Malvern Panalytical Ltd., Malvern, Worcestershire, UK) operated in size measuring mode and zeta potential measuring mode; water was set as the dispersant and protein was set as the material in the standard operation procedure (SOP) in the Zetasizer software with a folded capillary zeta potential cell (DTS1070, Malvern Panalytical Ltd., Malvern, Worcestershire, UK).

Size and PDI were analyzed in automatic mode with the following conditions: 173' Backscatter (NIBS default) setting, measured three times, 11 runs within a run duration of 10 seconds. The zeta potential was analyzed at an equilibration time of 120 seconds, Smoluchowski model, three-time measurement, and 10 to 100 runs.

Before the analysis, SNPs and PEIS were complexed/mixed with DNA to determine the exact size and surface charge before and after DNA complexation. SNPs was mixed with DW and DNA and complexed for 30 minutes before measurement. The PEIS were incorporated into a 3 mg/ml solution in DW and then mixed with the same volume of DNA. After mixing, the PEIS-DNA solution was vortexed for 20 minutes to induce DNA-polymer micelle formation without unnecessary aggregation.

5.3.3. Energy-filtered transmission electron microscopy (EF-TEM)

The morphology and particle size of each sample were determined at a high magnification by EF-TEM (LIBRA 120, Carl Zeiss, Baden-Württemberg, Germany). For sample preparation, the nanoparticle/DNA complexed DNA-PEIS solution was prepared as described in Section 5.3.2. Afterward, each sample was loaded and dried on a formvar-coated EM grid for 1 min for the nanoparticle to settle and then blotted with filter paper to remove excessive fluid. Afterward, samples were imaged under the microscope at 20,000× magnification.

5.3.4. Nuclear magnetic resonance (NMR) spectroscopy

To determine the chemical composition of the nanoparticles, NMR spectra of lyophilized SNPs and PEIS were obtained using an Avance 600 MHz high-resolution NMR spectrometer (AVANCE III, BRUKER, Massachusetts, USA) with 1H and 1D settings using D2O as the solvent.

5.3.5. Fourier transform-infra red (FT-IR) spectroscopy

To determine the chemical composition and structure of the nanoparticles, FT-IR spectra of lyophilized SNPs and PEIS were obtained using a vacuum FT-IR/microscope spectrometer (Vertex-80 V/Hyperion2000, BRUKER, Massachusetts, USA) with a resolution of 0.06 cm^{-1}, resolving power of 300,000:1, and spectral range of 8,000-370 cm^{-1} by a DLATGS detector.

5.3.6. Gel shift assay

To determine the optimal nuclear acid to polymer ratio based on NMR results, an electrophoretic mobility shift assay (EMSA) or gel shift assay was used. SeaKem LE agarose (50001, Lonza, Switzerland) gel was fabricated by dissolving 1% agarose in 1× TAE buffer (TR2026, Biosesang, Gyonggi-Do, Korea). After complete dissolution and cooling, 5 μl of EtBr (E1510, Sigma Aldrich, Massachusetts, USA) stock solution was added per 100 ml of agarose before the gel completely hardened. EtBr gel was cast on a mold with combs and then cooled for at least 1 hour to remove bubbles. For use, the gel was placed in a Mupid-2plus electrophoresis device (AD110, Takara, Shiga, Japan). Each group of nanoparticles was complexed with tGFP DNA for 30 minutes or made into nanomicelles by mixing and vortexing with a Wisemix Vortex mixer (VM-10, Daihan Scientific, Incheon, Korea) for 20 minutes. Afterward, the DNA-complexed nanoparticles were loaded in each well. Electrophoresis was performed for 45 minutes, and then the gels were removed and imaged by Chemidoc XRS+ (1708265, Bio-Rad, California, USA) in DNA gel mode in Chemidoc software.

5.3.7. Viability assay

To determine the cytotoxicity of the nanoparticles, a WST-1 assay was performed. A549 cells were prepared at a density of 1×10^4 cells/well in 96-well plates. The A549 adenocarcinoma cell line was purchased (10185, Korea Cell Line Bank, Seoul, Korea) and mainly used for the experiment. This was because A549 cell lines are the most widely used for cancer studies and gene transfections.

Four experimental groups were set: SNP 10, SNP 20, PEIS 10, and PEIS 20, with numbers indicating μg of nanoparticle/50 μl, which is the total complexation

volume for 1 × 10^5 cells. As a positive control, the commercial gene transfection reagent Fugene (E2311, Promega, Wisconsin, USA) and 1,200 kDa PEI (Branched PEI 1200, 06088, mw 1,200 kDa, Polyscience, Philadelphia, USA) was used. Each group was complexed with tGFP DNA and then treated for a certain period in the protocol. After treatment, the medium was replaced with fresh medium. After 48 hours, the growth medium was removed, 110 µl of 1:10 WST-1 assay reagent was added for an hour, and then the plate was read on an ELISA plate reader (Sunrise absorbance microplate reader, TECAN, Männedorf, Switzerland).

5.3.8 Reporter gene transfection

To determine the gene transfection ability of the nanoparticles, tGFP transfection was performed. Four experimental groups were set: SNP 20, PEIS, PEI, and blank, with numbers in each group indicating µg of nanoparticle/50 µl, which is the total complexation volume for 1×10^5 cells. A549 cells were prepared at a density of 1×10^5 cells/well in 24-well plates. tGFP DNA was complexed for 30 minutes at the determined concentrations of nanoparticles and deionized water up to a total volume of 50 µl per well was then added to wells with 500 µl of serum-free media. After 3 hours, the medium in each well was replaced with fresh medium with FBS. Beginning 2 days after transfection, the plate was removed, and images were taken with a fluorescence microscope (Eclipse Ni-E, Nikon, Tokyo, Japan) in FITC mode.

5.3.9. Quantitative real time PCR (qPCR)

To determine whether the viability change in RNAi-treated groups was caused by knockdown of genes, eight experimental groups were set: SNPs 20, PEIS 20, PEI, control (nontreated) and the same *in vitro* cultured A549 cells treated with SNP 20, PEIS 20, PEI, and control. (n=3). After RNAi transfection as previously described, each group was harvested for cDNA synthesis.

For RNA extraction and cDNA synthesis, TRIzol (15596026, Thermo Fisher, Massachusetts, USA), the Omniscript RT Kit (205113, Qiagen, Venlo, Netherlands) and oligo DT primer (18418012, Thermo Fisher, Massachusetts, USA) were used according to the manufacturer's instructions. After RNA extraction and cDNA synthesis were performed, the total cDNA concentration of each group was adjusted to 25 ng/µl and then stored at -70 °C for further use.

The expression of SHMT1, p53 and the housekeeping gene GAPDH was analyzed using quantitative PCR (qPCR) with a Rotor-Gene Q real-time PCR system (Qiagen, Venlo, Netherlands), Ampigene® qPCR Green Mix Lo-ROX (ENZ-NUC103, Enzo, New York, USA), and Bioneer qPCR primer (20-S-1001, Bioneer, Daejeon, Korea). The forward and backward primer sequences for the genes are shown in Table 1. Each sample was prepared as follows: 10 μl of master mix, 0.8 μl each of 10 pmol/ml forward and backward primers, and 10 μl of 25 ng/μl DNA.

5.3.10. RNA interference (RNAi) assay

To determine the RNA interference-inducing ability of the nanoparticles, a WST-1 assay was performed. A549 cells were prepared at a density of 1×10^5 cells/well in 24-well plates. The experimental groups were the same as 5.3.6., and then each group was complexed with anti-SHMT1 siRNA (Thermo Fisher, Massachusetts, USA). After complexation and transfection, each group was subjected to the WST-1 assay ($n=3$, $P<0.05$).

5.3.11. Terminal deoxynucleotidyl transferase dUTP nick end labeling assay (TUNEL)

To visualize apoptosis induced by RNAi, a TUNEL assay was performed using a DeadEnd Colorimetric TUNEL system kit (G7130, Promega, Wisconsin, USA). A549 cells were prepared at a density of 5×10^4 cells/well in 8-well chamber slides. On the day of transfection, cells were treated with SNP, PEIS, and PEI to induce RNAi. After 36 hours, the cells were fixed with 4% paraformaldehyde for 25 minutes, and then the TUNEL assay was performed according to the manufacturer's instructions.

Each well was treated serially with 100 μl of 0.2% Triton-X 100 for 5 minutes, TUNEL assay equilibration buffer for 5 minutes, TdT reaction mix for 60 minutes, 2× SSC for 15 minutes, 0.3% hydrogen peroxide for 5 minutes, streptavidin HRP for 30 minutes, and DAB solution until the background was light brownish.

Each treatment was followed by 5 minutes of washing with PBS twice, except for equilibration buffer and SSC treatment, which had no washing, and steps after hydrogen peroxide, which had 5 minutes of PBS washing trice. Images were obtained by fluorescence microscopy (Eclipse Ni-E, Nikon, Tokyo, Japan) in

optical mode at 40 × magnification.

5.3.12. SHMT1 RNAi on biochip cultured cells

To investigate the RNA transfection ability of nanoparticles on the biochip developed in Chapter 4, a WST-1 assay was performed after transfection. The experimental groups were the same as 4.3.2., and then each group was treated with anti-SHMT1 siRNA (Thermo Fisher, Massachusetts, USA), which was complexed with 20 μg SNP for 20 minutes. After complexation and transfection, each group was subjected to the WST-1 assay two days after transfection ($n=3$, $P<0.05$).

5.3.13. SHMT1 RNAi on biochip-cultured cells by electrospray

To investigate the RNA transfection ability of nanoparticles on the biochip developed in Chapter 4, a WST-1 assay was performed after transfection. The experimental groups were the same as 4.3.2., and then each group was treated with anti-SHMT1 siRNA (Thermo Fisher, Massachusetts, USA), which was complexed with 20 μg SNP for 30 minutes. After complexation, each group was treated by electrospray as in 4.3.7., while the parameter was adjusted to 0.3 ml/h, 10 minutes of treatment for *in vitro*, and 2 minutes of treatment for biochip groups considering the total volume of complexed nanoparticle solution. Three hours after transfection, the medium of each group was replaced with fresh medium. Each group was subjected to the WST-1 assay two days after transfection ($n=3$, $P<0.05$).

5.3.14. Statistical analysis

Viability assay results are given as the mean ± SD for the indicated number of wells. Statistical analysis and one-way ANOVA were performed using OriginPro 2018 software (Originlab Corporation, Massachusetts, USA). A minimum of three to five samples were analyzed. Differences were considered statistically significant at $P < 0.05$).

5.4 Results

5.4.1. Fabrication of sericin nanoparticles (SNPs) and PEI-conjugated sericin nanoparticles (PEIS)

The sericin nanoparticles were prepared as previously described and dispersed in the same initial volume of 10 mM NaCl aqueous solution (pH 8.2) each time after purification. Purified nanoparticles showed a dark brown color after lyophilization and retained dispersity after being dissolved in DW again.

PEI-conjugated sericin nanoparticles (PEIS) were also prepared as previously described, dialyzed, and lyophilized. The PEIS showed flake-like morphology after lyophilization. The PEIS completely dissolved in DW after lyophilization.

5.4.2. Direct Laser Scattering (DLS)

The size, PDI, and zeta potential results of the SNPs and PEIS before and after complexation with DNA are depicted in Table 1. The average size of the SNPs was 156.65±22.48, with a zeta potential of -7.57±3.69 before complexation and an average size of 99.52±20.06, with a zeta potential of -12.56±3.34 after complexation. The PEIS showed an average size of 502.95±13.9 and a zeta potential of -7.88±3.75 before complexation and an average size of 102.59±20.06 and a zeta potential of -10.92±6.2 after complexation. The size of the nanoparticles in DW slightly decreased after complexation, and the charge became more negative.

5.4.3. Transmission electron microscopy (TEM)

As shown in Figure 3, the nanoparticles were spherical, indicating that sericin nanoparticles were successfully fabricated. PEIS without DNA showed large, even-sized particles, while even-sized particles were observed in GFP-complexed samples.

5.4.4. Nuclear magnetic resonance (NMR) spectroscopy

NMR results showed that the peaks of the SNPs were not much different from those of the original sericin. However, the PEIS showed PEI-specific peaks in addition to sericin peaks in the 2.6 to 3.0 ppm region, indicating that PEI was successfully conjugated to sericin, as shown in Figure 5.2.

5.4.5. Fourier transform-infra red (FT-IR) spectroscopy

The FT-IR spectra showed raw sericin, SNPs, and PEIS with similar peaks, such as overlapping N-H stretching and O-H stretching at 3255 cm^{-1}, C=O symmetry stretching at 1650 cm^{-1}, and C=O stretching at 1650 cm^{-1}. While indicating that hydroxyl and amine groups were preserved after fabrication, the PEIS showed a PEI-specific peak at 1461 cm^{-1}, indicating successful conjugation.

5.4.6. Gel shift assay

Gel shift results showed that the band of DNA complexed with nanoparticles became less advanced as the concentration increased. In the SNPs, bands were completely trapped in the well when the concentration exceeded 20 µg/50 µl. In the PEIS, the band did not advance after the DNA to particle ratio exceeded 6 µg per 1 µg of DNA. From NMR data and gel shift data, the optimal NP (amine to phosphate) ratio of the nanoparticles was calculated: the SNP was 1:20 and the PEIS was 1:10, as shown in Figure 5.2.

5.4.7. Viability assay

Cell viability assay results on the A549 adenocarcinoma cell line indicated that 10 µg SNP, PEIS, and Fugene did not decrease viability much, but in the 20 µg SNP group, the viability was significantly decreased. These results indicate that nanoparticles could induce cell death at higher concentrations, as shown in Figure 5.3.

siRNA transfection results showed a significant decrease in the SNP 20 µg group compared to the PEI and positive control groups, while the 10 µg SNP and PEIS groups induced a greater decrease in cell viability than the PEI and blank groups.

5.4.8. Quantitative real time PCR (qPCR)

Although there was no statistically significant difference, qPCR results of A549 cells treated with SHMT1 siRNA showed that -ΔΔCt values of SHMT1 largely decreased in the 20 µg SNP and PEIS groups, indicating inhibition. The -ΔΔCt values of p53 genes showed that every treated group enhanced the expression of p53, while the expression of the SNP 10 µg group was largest, followed by the

SNP 20, PEI and PEIS groups. Together with the TUNEL assay results, the qPCR results suggest that the viability decrease in the RNAi samples was induced by RNAi but not by the cytotoxicity of the nanoparticle itself, indicating that the siRNA transfection ability of the nanoparticles was functioning correctly. It is remarkable that SNP 10 showed the highest p53 expression, but the decrease in cell viability by siRNA complexation was not very significant in Section 5.4.9. SNP 20 was the only group that showed a significant decrease in cell viability and showed low expression of SHMT1 compared to PEIS. The decrease in viability by siRNA complexation of nanoparticles is estimated to affect the regulation of SHMT1, followed by enhanced expression of p53.

5.4.9. Reporter gene transfection

Images of tGFP DNA transfection by nanoparticles showed bright green fluorescence distributed throughout the well in SNP 20, as shown in Figure 5.4. While fewer fluorescent cells were observed, the green fluorescence itself was visible in the PEIS group. The PEI and control (nontreated) group did not show green fluorescence.

5.4.10. RNA interference (RNAi) assay

In the RNA transfection, the cells treated with SNPs and PEIS showed decreased viability compared to the control and PEI groups, while groups treated with SNPs had a statistically significant decrease in viability compared to the blank. Although having some toxicity depending on the concentration, SNPs successfully induced cell death by RNAi. While not significantly different, NP 10 and PEIS 20 also showed a tendency of decreasing viability when compared to the PEI and control group.

5.4.11. Terminal deoxynucleotidyl transferase dUTP nick end labeling assay (TUNEL)

TUNEL assay results of A549 cells showed dark colored morphologies when viewed under microscope in the NP 20, PEIS 20, and positive control groups. The dark-colored group was observed mostly in the positive control, followed by NP 20 and PEIS 20. The PEI and control groups (without any treatment) did not show any

prominent signs of apoptosis in the images.

5.4.12. RNAi of SHMT1 on the biochip platform and *in vitro*

In vitro groups treated with SNP 20+SHMT1 siRNA all showed a significant decrease in viability except for the AC (A549 cultured with CSC) group. In contrast, cells cultured in biochips showed no significant decrease in viability after treatment, while each group showed a trend of decreasing viability. When siRNA-treated viability to control was presented as a percentage, the *in vitro* and biochip cultured groups did not show significant differences between each other. This result is remarkable since cells cultured *in vitro* showed a significant decrease in viability compared to the biochip group when treated with doxorubicin. Thus, RNAi by SNPs could be an effective anticancer strategy because it can also decrease the viability of biochip-cultured cells, showing no significant difference from *in vitro* groups.

5.4.13. RNAi of SHMT1 by electrospray on a biochip platform and *in vitro*

Both the *in vitro* and biochip groups did not show significant differences before and after the treatment except for AHC *in vitro,* as shown in Figure 5.8.a. and 5.8.b. The trend was similar in percentage to the control (5.8.c.), while AHC *in vitro* had significantly lower viability than A, AH, AC, and biochip-cultured AC.

5.5. Discussion

Sericin nanoparticles were formed successfully, which was confirmed by TEM imaging, DLS, and NMR data. The particles were round, and the size was distributed in the 150-250 nm diameter range, while the charge was slightly negative.

Even though the nanoparticles were fabricated by desolvation and crosslinking with possibly cytotoxic materials (such as glutaraldehyde and PEI), they exhibited no significant toxicity to cells, in the case of the PEIS. This indicates that the nanoparticles have no significant toxicity to the cells, and the impurities and residual chemicals used in the process, such as EDC, NHS, and glutaraldehyde, were completely purified from the nanoparticles.

The PEIS showed similar peaks as the SNPs in the NMR data, but some regions

were different from the SNPs. This is mainly due to PEI conjugation because the PEIS showed a slightly higher zeta potential than the SNPs. Thus, conjugation of PEI to sericin can be considered as causing both change in structure and the electric charge of the micelle. Gel shift assays showed that DNA is completely complexed when the SNP concentration is over 20 μg, and the concentration of the PEIS is over 6 μg in a 50 μl solution, thus showing that the PEIS were more effective in forming nucleic acid to polymer complexes.

Upon transfection of reporter genes, both the SNP and PEIS groups showed green fluorescence, while the PEI and blank groups did not show prominent expression of GFP, but SNP 20 showed stronger expression of GFP than the PEIS. This trend also led to differences in the WST-1 results of RNAi-treated samples. Although SNP had some toxicity when compared to the nontreated group, it also showed a significant decrease in viability in RNAi-treated samples. Together, the DLS data suggest that the early inhibition of cancer cell viability by RNAi is largely affected by the vector size rather than the surface charge, as the diameter of nucleic acid-complexed SNPs is smaller than that of DNA-complexed PEIS. This is notable since it is believed that the positive surface charge of vectors is better than that of negatively charged vectors in gene transfection because nucleic acids (DNA, RNA) are negatively charged.

The TUNEL assay results showed dark stained areas, which are considered signs of apoptosis in the SNP and PEIS groups, similar to the DNAse-treated positive control groups. The PEI and control (nontreated) groups did not show or showed only small dark areas compared to the SNP, PEIS, and positive control groups. In particular, when comparing PEI to PEIS, 1,200 kDa PEI itself does not have gene transfection ability or cytotoxicity, and it shows cell death by RNAi while being not as cytotoxic as SNP 20.

Although qPCR results on RNAi-treated cells did not show a significant difference between the nontreated and each treatment group in SHMT1, the SNP 20 group showed the most prominent regression trends of SHMT1 genes and significant regression compared to the PEIS group. Enhancement of the p53 gene was largest in the SNP 10 group, while every treated group showed significant enhancement of p53 expression compared to the control. This may suggest that the expression of P53 is largely increased due to knockdown of SHMT1 when SHMT1 siRNA is

added to the cells, inducing an apoptotic reaction in the cells that can be seen in the TUNEL assay results. Even though SNP 10 showed more expression of p53, it is not significant result since it did not show significant viability decrease to control in 5.4.9.

When applied to the biochip platform developed in Chapter 4, SHMT1 siRNA applied with SNP 20 showed a significant decrease *in vitro* in most groups after treatment and no significant difference in the percentage of viability compared to the control. However, there was no significant difference after the same treatment by electrospray. This may be because the nucleic acid binds with the nanoparticle to form a complex, and the voltage applied in electrospray may have disrupted these interactions. SNPs alone showed different results than doxorubicin applied to chips in Chapter 4, showing that the application of siRNA by SNP 20 to biochips had a rather similar effect *in vitro* when considering the percentage data.

5.6. Conclusion

In this chapter, sericin nanoparticle for gene and drug delivery was fabricated. Two variations of Sericin nanoparticle were fabricated by desolvation method by adding ethanol to sericin solution and crosslinking and conjugating the sericin with PEI by EDC-NHS reaction, each called SNP and PEIS.

SNP and PEIS was checked with the morphology, size, zeta potential and polydispersity index, viability, actual gene transfection ability test by reporter genes. Both particles were round when complexed to DNA (Nucleic acid). SNP was slightly negative charged and small when compared to PEIS, due to existence of conjugated PEI and the micelle form in the solution as suggested by NMR results.

SNP showed cytotoxicity when dose was 0.4 μg/μl (SNP 20) group, while PEIS did not show significant cytotoxicity when compared to SNP 20. This seems to be caused by absolute mass of sericin was high in SNP 20. While reporter gene expression showed bright green fluorescence in both groups, SNP groups showed more bright and well distributed fluorescence compared to PEIS and others. This trend was also same in cytotoxicity results in RNAi treated samples and TUNEL assay, which showed cell viability decrease and sign of apoptosis possibly by RNAi. The expression of SHMT1 was regulated largely in SNP 20, to PEIS while

significance to other groups were not observed. Expression of p53 gene was significantly high in every treated group to control, SNP 20 following SNP 10. These results may suggest that apoptosis inducing effect of RNAi is mainly caused by regulation of SHMT1, followed by the expression of p53. This is clearer when SNP 10 showed largest p53 expression but did not show significant decrease of viability in RNAi assay or signs of apoptosis in TUNEL assay. Therefore, SHMT1 regression ability is more important in inducing apoptosis of cancer cells.

The difference in siRNA transfection capability of SNP and PEIS could be explained by functional group. As previously scribed, functional groups enhance clathrin-mediated intake of substrates regardless of surface charge. PEIS was fabricated by conjugating PEI by EDC-NHS method, which conjugated carboxyl group in sericin with amine group in PEI. Eventually PEIS would have less hydroxyl groups to SNP, because hydroxyl groups in sericin (including carboxyl groups) were involved in conjugation and changed to other structure.

Even though the sericin nanoparticles need more research to applicated in clinical area, such as enhancing the target specific ability, lowering the cytotoxicity *in vitro*, this research first conjugated PEI to sericin for gene therapy purpose, determined RNAi ability and low toxicity of the particle. Further studies would compensate the transfection ability and target specific ability of the vectors, thus giving new perspective to the field about nanoparticle vector fabricated with natural polymer.

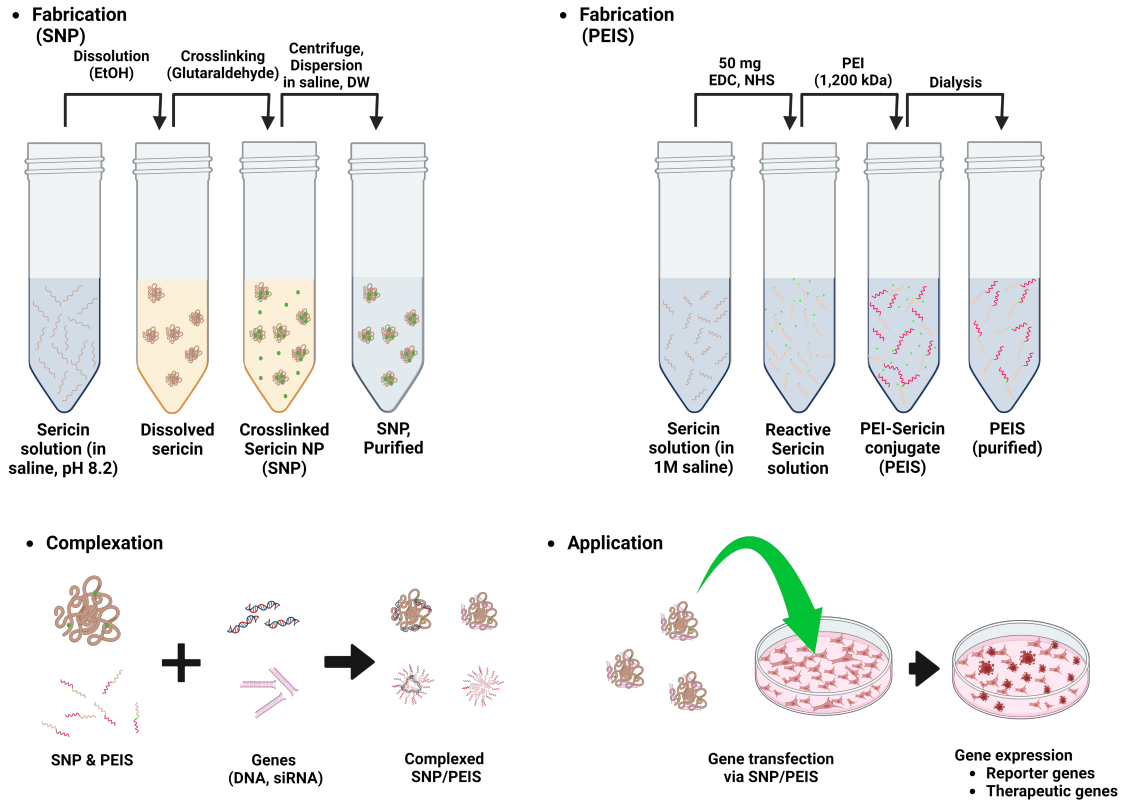

Figure 5.1. Schematic of sericin nanoparticle (SNP) and polyethylenimine conjugated sericin (PEIS) fabrication and its application. Images were fabricated on Biorender (Biorender.com).

A.

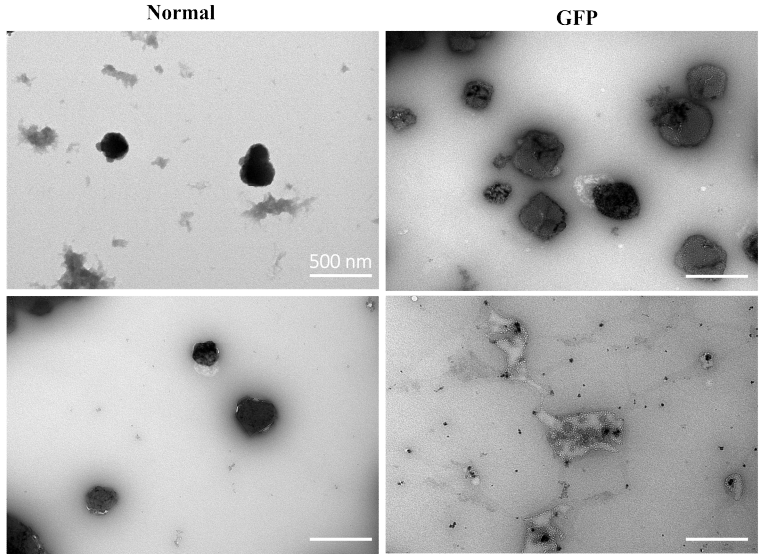

B.

Sample	Size	Zeta potential
SNP	156.65±22.48	-7.57±3.89
SNP GFP	99.52±20.06	-12.86±3.34
PEIS	502.95±13.9	-7.88±3.75
PEIS GFP	102.59±20.06	-10.92±6.2

Figure 5.2. Characteristics of particle properties. A. TEM image of SNPs and PEIS before and after DNA complexation. B. DLS data of SNP/PEIS before and after DNA complexation.

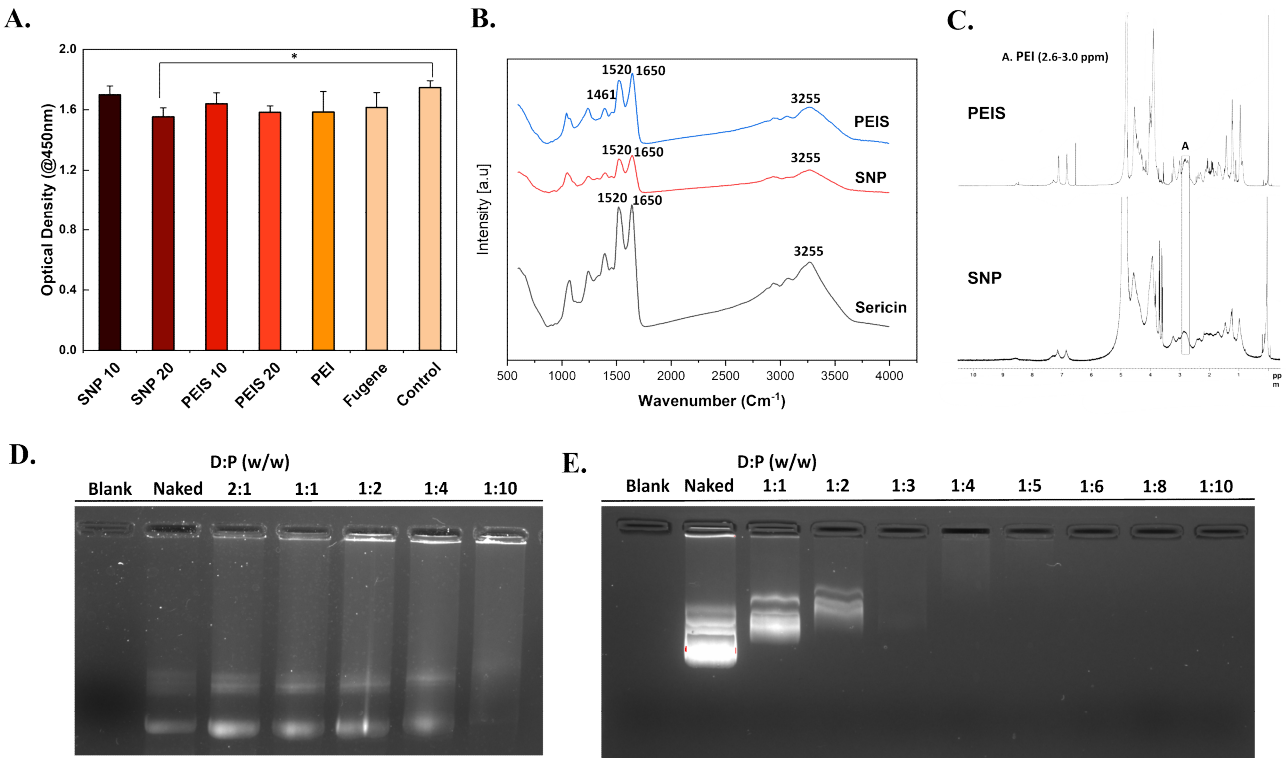

Figure 5.3. Cell viability, NMR, FT-IR and EMSA images of the nanoparticles. A. Cell viability of nanoparticles with control and commercial transfection reagent. B. NMR spectra of PEIS and SNPs. C. FT-IR spectra of PEIS and SNPs. D. EMSA results for SNPs. E. EMSA results for the PEIS (* indicates a significantly different value at $p<0.05$ (n=5).

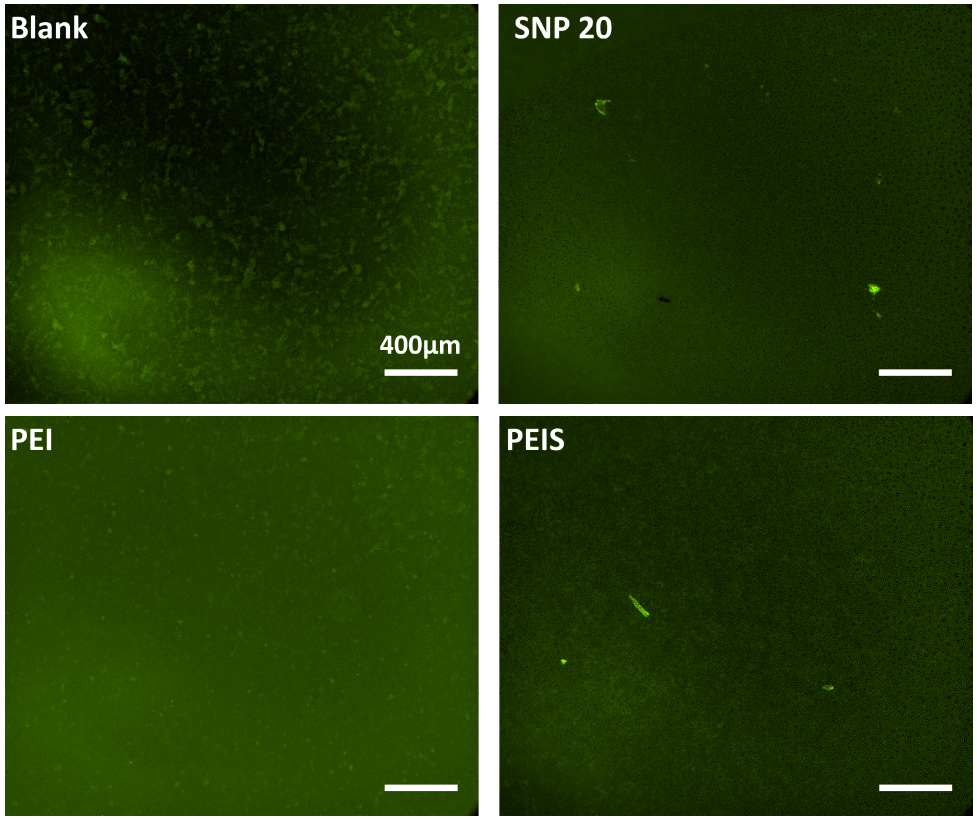

Figure 5.4. GFP transfection images of nanoparticles.

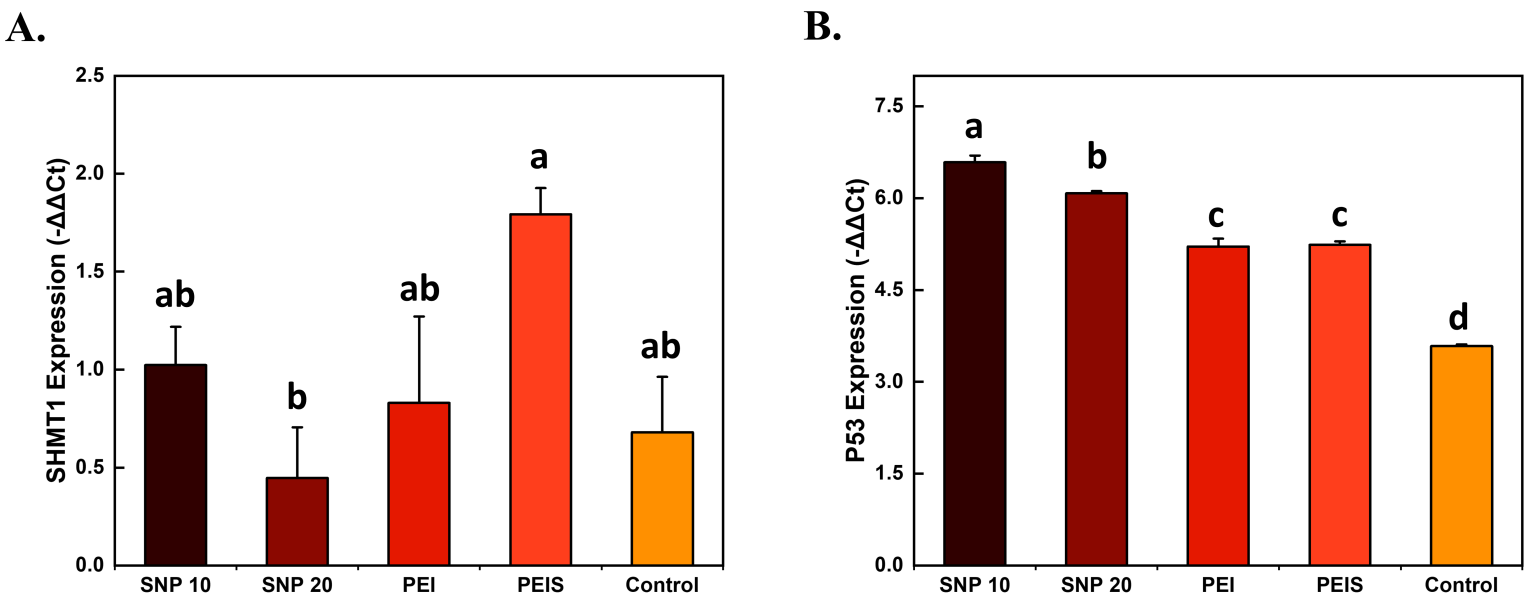

Figure 5.5. qPCR results of the A549 cells treated with RNAi by nanoparticle. A. SHMT1 expression of cells by -ΔΔCt. B. P53 expression of cells by -ΔΔCt. (* indicates a significantly different value at $p<0.05$ (n=3).

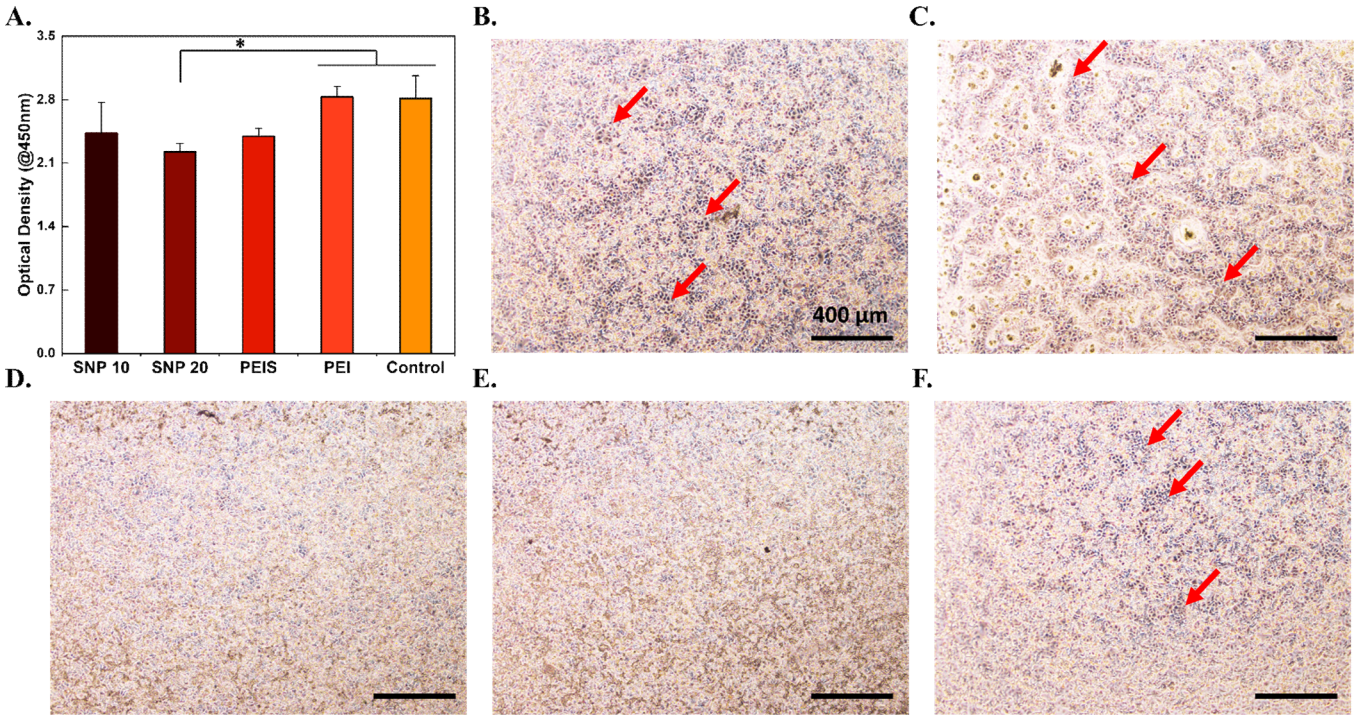

Figure 5.6. Cell viability and TUNEL assay images of the nanoparticles. A. Cell viability of nanoparticles. A. Cell viability of SHMT1 siRNA-treated A549 cells. B. TUNEL image of SNP 20 µg. C. TUNEL image of PEIS. D. TUNEL image of PEI. E. TUNEL image of control (nontreated). F. TUNEL image of the positive control (DNAse treated). The red arrow on the image indicates TUNEL-stained cells. Scale bar on the image indicates 400 µm (* indicates significantly different value at $p<0.05$ (n=5)).

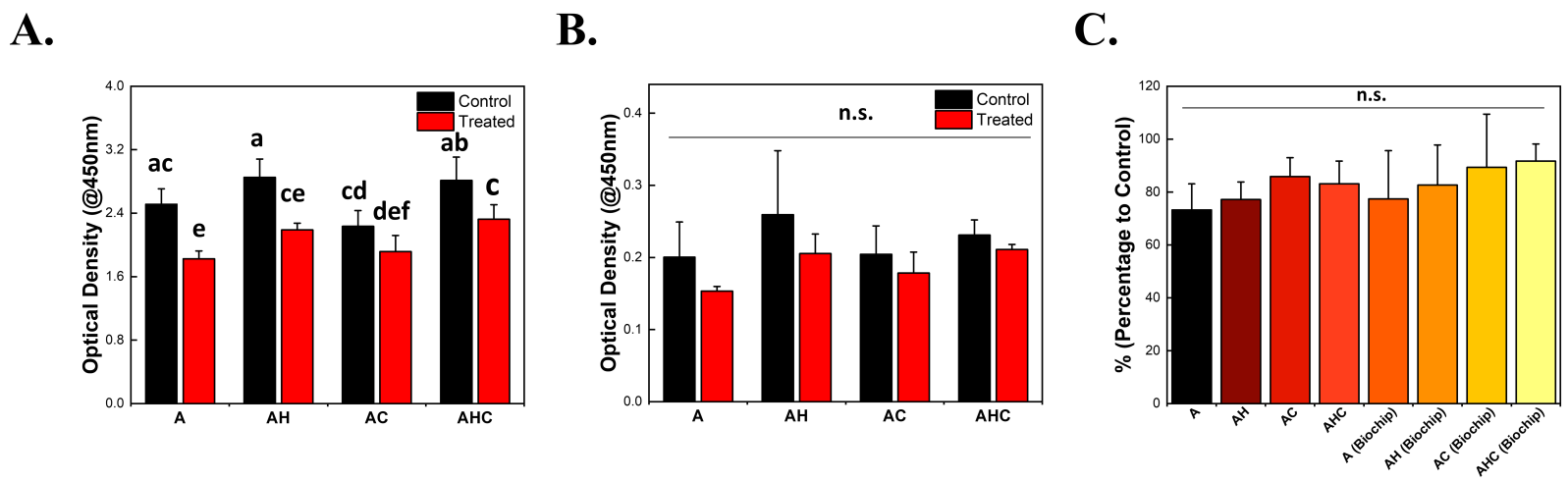

Figure 5.7. Comparison of cell viability *in vitro* and on the biochip before and after siRNA transfection by nanoparticles. A. WST-1 results of *in vitro* cultured cells treated with RNAi. B. WST-1 results of biochip-cultured cells treated with RNAi. C. Percentage of control to RNAi-treated groups in each sample (Abbreviations: A: A549 only, AH: A549+HUVEC, AC: A549+CSC, AHC: A549+HUVEC+AHC. Different letters indicate significantly different values at $p<0.05$ (n=3)).

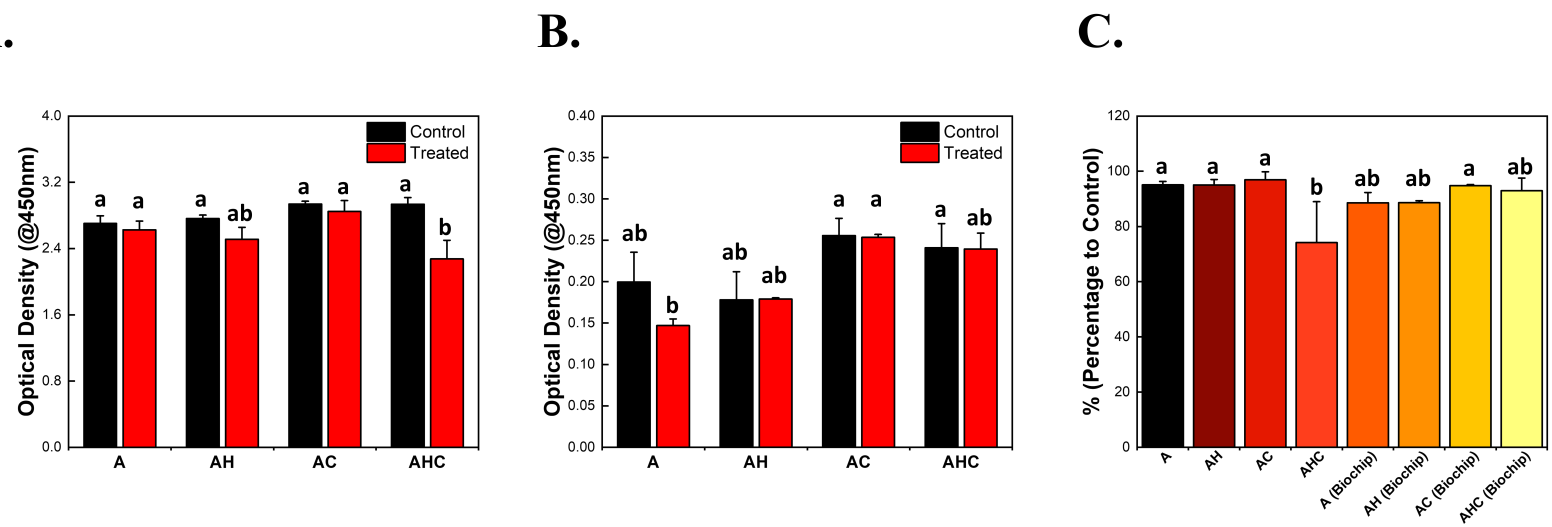

Figure 5.8. Comparison of cell viability *in vitro* and on a biochip before and after siRNA transfection by nanoparticles with electrospray. A. WST-1 results of *in vitro* cultured cells treated with RNAi-complexed nanoparticles by electrospray. B. WST-1 results of biochip-cultured cells treated with RNAi-complexed nanoparticles by electrospray. C. Percentage of control to RNAi-complexed nanoparticle by electrospray treated groups in each sample (Abbreviations: A: A549 only, AH: A549+HUVEC, AC: A549+CSC, AHC: A549+HUVEC+AHC. Different letters indicate significantly different values at $p<0.05$ (n=3)).

Table 5.1. Primer sequence used in qPCR.

Gene	Primer sequence (5'→ 3')	Size (bp)
GAPDH	F: CATGAGAAGTATGACAACAGCCT	113
(Housekeeping gene)	R: AGTCCTTCCACGAACCAAAGT	
SHMT1	F: AGGAAAGGAGTGAAAAGTGTGGAT	121
	R: ACACCAGTGTCGCTCTGGATCTG	
P53	F: TAACAGTTCCTGCAT GGGCGGC	110
	R: AGGACAGGCACAAACACGCACC	

6. Conclusion

In this dissertation, gene transfection vector with sericin was developed, starting from CDES drug delivery system. Sericin nanoparticles were fabricated for gene transfection, and spheroid-on-a-chip platform for therapy screening was established, and optimized culture condition was also developed.

In CDES drug delivery section, 6 kV of the voltage was proved suitable for electrospray induced cisplatin delivery. The 6 kV electrospray alone did not induce cytotoxicity, but increased permeability of the cell membrane.

In spheroid culture platform section, we introduced passive pumping induced by surface tension while culturing variation of cells into spheroids. Spheroids were less affected by anticancer drug when compared to *in vitro* cultured cells. Even more, spheroids mostly expressed stemness genes (nanog, Oct-4) stronger than *in vitro* cultured cells. In the biochip cultured cells, A549 cultured with HUVEC showed large fold of stemness gene expression in day 3. However, at day 5, A549 cultured with CSC and HUVEC showed the strongest stemness gene expression compared to others, presenting existence of co-cultured cells are important in promoting stemness. If the percentage of cells are modified on further research, it would be able to be applied in other cancers, and the pump itself can be applied or modified to give constant shear stress to the spheroids, such as circulating cell culture media inside the platform.

In sericin nanoparticle section, SNP and PEIS were fabricated successfully with size mostly distributed under 100 to 250 nm. Although sericin was used in some research before, our study first conjugated sericin to PEI by EDC-NHS method first time. DLS, NMR, WST-1 on nanoparticle itself and nanoparticle-RNAi treated samples, TUNEL, qPCR results showed that vector diameter was small in SNP, while surface charge was slightly positive in PEIS. This difference led to cytotoxic but inducing more apoptosis SNP, and PEIS expressing stronger regression of SHMT1, enhancement of p53 in gene level. This shows that it may seem to be SNP is more advantageous as vector for RNAi, but PEIS can possibly induce more apoptosis if long-term study is performed. Although only sericin and PEI was used to fabricate the nanoparticle in this study, antibody or peptides could be conjugated to the platform enabling more target specific transfection, reducing off-target

effects further.

Also, by combination of these two platforms, the gene transfection ability of sericin nanoparticles were confirmed on cancer spheroid culture platform. It would be able to apply these platforms together or separately to cancer therapy research and help current cancer research area as more easy and reliable way compared to conventional research method.

국문 초록

폐선암은 가장 생존률이 낮은 암 중 하나로, 현재 치료법이 효과적이지 않아 예후 역시 나쁜 편이다. 진행 정도에 따라 기본 요법인 방사선 요법, 화학 요법, 그리고 면역 요법은 이를 완전히 치료할 수 없고, 따라서 유전자 요법을 이용한 유전자 편집 기술을 이용할 필요가 있다. 그러나 유전자 전달체 중 바이러스성 전달체는 각각 발암성과 세포 독성이 있고, 다중양이온(Polycation) 고분자 비바이러스성 전달체의 경우에도 독성이 있는 등의 한계가 있다. 따라서 독성이 낮고 전달 효율이 높은 생분해성 비바이러스성 벡터를 제작할 필요가 있다. 실크 기반 단백질인 세리신은 다른 단백질처럼 풍부한 작용기를 가지고 있으며, 창상피복재나 무혈청 배지의 보충제로 들어갈 정도로 생체적합성 역시 뛰어나다.

치료법 연구에서, 동물 모델은 단일 층으로 배양된 세포에 대한 시험관 내 (*In vitro*) 시험법에 비해 더 신뢰성이 있고 나은 결과를 얻을 수 있다. 시험관 내 시험법에서 확실해 보이던 결과도 동물 모델을 이용한 생체 내에서의 결과와 상이해지는 경우가 빈번하다. 그러나 동물 모델의 개발은 윤리적 문제나 비용 문제, 그리고 동물의 생존성 문제 때문에 어려울 수 있다. 스페로이드(Spheroid)라고 불리는, 3D 배양된 암세포의 경우 미세유체 기술 기반 바이오칩에 배양될 경우 해법이 될 수 있다. 미세유체 장치 내부의 스피로이드는 생체 내의 종양과 유사하게 보다 정확한 미세환경을 모사할 수 있다. 따라서 이는 시험관 내 시험법을 통해 화학요법을 시행하는 것보다 더욱 신뢰성이 높다. 그러나 미세유체 장치의 운용은 어려울 수 있는데, 이는 펌프나 튜브, 그리고 원하는 결과를 내기 위해서 충분한 숙달을 필요로 하기 때문이다.

이 연구에서는 종양 스페로이드를 배양할 수 있는 미세유체 바이오칩을 개발하고 약물 전달용 세리신 기반 나노입자의 효율성을 확인하였다. 나노입자는 성공적으로 제작되었으며, 양성 대조군인 폴리에틸렌이민(Polyethyleneimine, PEI)에 비해 리포터 유전자의 발현이 보다 뛰어났다. 바이오칩에서 배양된 종양 스페로이드는 세포 활성이 뛰어났으며, 바이오칩 내부의 스페로이드에 siRNA와 결합한 세리신 기반 나노입자를 투여했을 경우 세포 사멸의 징후를 보였다. 이 연구는 3D 배양 기반 암 유전자치료 연구에 이후 기여할 수 있을 것이다.

키워드 : 바이오칩, 암, 세리신, 유전자 전달, 나노입자, 스페로이드
학번 : 2018-32443

Bibliography

1. Siegel, R. L., Miller, K. D., & Jemal, A. (2019). Cancer statistics, 2019. *CA: A Cancer Journal for Clinicians*, *69*(1), 7–34. https://doi.org/10.3322/caac.21551, MacDonagh, L., Gray, S. G., Breen, E., Cuffe, S., Finn, S. P., O'Byrne, K. J., & Barr, M. P. (2016). Lung cancer stem cells: The root of resistance. *Cancer Letters*, *372*(2), 147–156. https://doi.org/10.1016/j.canlet.2016.01.012
2. Vogelstein, B., & Kinzler, K. W. (2004). Cancer genes and the pathways they control. Nature Medicine, 10(8), 789–799. https://doi.org/10.1038/nm1087 (Oncogene (2017) 36, 1461–1473
3. Mujić, M. (2009). he role of the Hedgehog signaling pathway in cancer: A comprehensive review. *Bosnian Journal of Basic Medical Sciences / Udruženje Basičnih Mediciniskih Znanosti = Association of Basic Medical Sciences*, *9*(3), 173.
4. Borggrefe, T., & Oswald, F. (2009). The Notch signaling pathway: Transcriptional regulation at Notch target genes. *Cellular and Molecular Life Sciences*, *66*(10), 1631–1646. https://doi.org/10.1007/s00018-009-8668-7
5. Rabinowits, G., Gerçel-Taylor, C., Day, J. M., Taylor, D. D., & Kloecker, G. H. (2009). Exosomal microRNA: A diagnostic marker for lung cancer. Clinical Lung Cancer, 10(1), 42–46. https://doi.org/10.3816/CLC.2009.n.006
6. Bepler, G., Blum, M. G., Chang, A., Cheney, R. T., Chirieac, L. R., Amico, T. A. D., Demmy, T. L., Ganti, A. K. P., Govindan, R., Grannis, F. W., Kris, M. G., Krug, L. M., Le, Q., Lennes, I. T., Martins, R., Malley, J. O., Osarogiagbon, R. U., Otterson, G. A., Patel, J. D., … Yang, S. C. (2010). Non-small Cell Lung Cancer. J Natl Compr Canc, 8(7), 740–801.
7. Hirsch, F. R., Scagliotti, G. V., Mulshine, J. L., Kwon, R., Curran, W. J., Wu, Y. L., & Paz-Ares, L. (2017). Lung cancer: current therapies and new targeted treatments. The Lancet, 389(10066), 299–311. https://doi.org/10.1016/S0140-6736(16)30958-8

8. Hecht, S. S. (2011). Tobacco smoke carcinogens and lung cancer. Current Cancer Research, 6(14), 53–74. https://doi.org/10.1007/978-1-61737-995-6_3
9. Doll, R. (1993). Mortality from lung cancer in asbestos workers. Occupational and Environmental Medicine, 50(6), 484–484. https://doi.org/10.1136/oem.50.6.484
10. Pope III, C. A., Burnett, R. T., Thun, M. J., Calle, E. E., Krewski, D., & Thurston, G. D. (2002). Lung cancer, cardiopulmonary mortality, and long-term exposure to fine particulate air pollution. The Journal of the American Medical Association, 287(9), 1132–1141. https://doi.org/10.1001/jama.287.9.1132
11. H. Schliephake: Prognostic relevance ofmolecular markers oforal cancer—A review. Int. J. Oral Maxillofac. Surg. 2003; 32: 233–245. 0 2003 International Association of Oral and Maxillofacial Surgeons
12. Unoki, M., Daigo, Y., Koinuma, J., Tsuchiya, E., Hamamoto, R., & Nakamura, Y. (2010). UHRF1 is a novel diagnostic marker of lung cancer. British Journal of Cancer, 103(2), 217–222. https://doi.org/10.1038/sj.bjc.6605717
13. Lu, C. H., Yeh, D. W., Lai, C. Y., Liu, Y. L., Huang, L. R., Lee, A. Y. L., Jin, S. L. C., & Chuang, T. H. (2018). USP17 mediates macrophage-promoted inflammation and stemness in lung cancer cells by regulating TRAF2/TRAF3 complex formation. Oncogene, 37(49), 6327–6340. https://doi.org/10.1038/s41388-018-0411-0
14. Li, K., Guo, W., Li, Z., Wang, Y., Sun, B., Xu, D., Ling, J., Song, H., Liao, Y., Wang, T., Jing, B., Hu, M., Kuang, Y., Wang, Q., Yao, F., Sun, A., Zhu, L., Wang, L., & Deng, J. (2019). ALDH2 Repression Promotes Lung Tumor Progression via Accumulated Acetaldehyde and DNA Damage. Neoplasia (United States), 21(6), 602–614. https://doi.org/10.1016/j.neo.2019.03.008
15. Visus, C., Wang, Y., Lozano-Leon, A., Ferris, R. L., Silver, S., Szczepanski, M. J., Brand, R. E., Ferrone, C. R., Whiteside, T. L., Ferrone, S., DeLeo, A. B., & Wang, X. (2011). Targeting ALDH bright human carcinoma-initiating cells with ALDH1A1-specific CD8 + T cells. Clinical Cancer

Research, 17(19), 6174–6184. https://doi.org/10.1158/1078-0432.CCR-11-1111

16. Paone, A., Marani, M., Fiascarelli, A., Rinaldo, S., Giardina, G., Contestabile, R., Paiardini, A., & Cutruzzolà, F. (2014). SHMT1 knockdown induces apoptosis in lung cancer cells by causing uracil misincorporation. Cell Death and Disease, 5(11), 1–11. https://doi.org/10.1038/cddis.2014.482;
17. Hong, I. S., Jang, G. B., Lee, H. Y., & Nam, J. S. (2015). Targeting cancer stem cells by using the nanoparticles. International Journal of Nanomedicine, 10, 251–260. https://doi.org/10.2147/IJN.S88310
18. Pützer, B. M., Solanki, M., & Herchenröder, O. (2017). Advances in cancer stem cell targeting: How to strike the evil at its root. Advanced Drug Delivery Reviews, 120, 89–107. https://doi.org/10.1016/j.addr.2017.07.013
19. Ramamoorth, M., & Narvekar, A. (2015). Non viral vectors in gene therapy - An overview. Journal of Clinical and Diagnostic Research, 9(1), GE01–GE06. https://doi.org/10.7860/JCDR/2015/10443.5394
20. Dunbar, C. E., High, K. A., Joung, J. K., Kohn, D. B., Ozawa, K., & Sadelain, M. (2018). Gene therapy comes of age. Science, 359(6372). https://doi.org/10.1126/science.aan4672
21. Somia, N. V., Miyoshi, H., Schmitt, M. J., & Verma, I. M. (2000). Retroviral Vector Targeting to Human Immunodeficiency Virus Type 1-Infected Cells by Receptor Pseudotyping. Journal of Virology, 74(9), 4420–4424. https://doi.org/10.1128/jvi.74.9.4420-4424.2000
22. Cong, L., Ran, F. A., Cox, D., Lin, S., Barretto, R., Habib, N., Hsu, P. D., Wu, X., Jiang, W., Marraffini, L. A., & Zhang, F. (2013). Multiplex Genome Engineering Using CRISPR/Cas Systems. Science, 339(February), 819–824.
23. Carroll, D. (2008). Progress and prospects: Zinc-finger nucleases as gene therapy agents. Gene Therapy, 15(22), 1463–1468. https://doi.org/10.1038/gt.2008.145
24. Zhang, S., Chen, H., & Wang, J. (2019). Generate TALE/TALEN as Easily and Rapidly as Generating CRISPR. Molecular Therapy - Methods and

Clinical Development, 13(June), 310–320. https://doi.org/10.1016/j.omtm.2019.02.004

25. Hsu, P. D., Lander, E. S., & Zhang, F. (2014). Development and applications of CRISPR-Cas9 for genome engineering. Cell, 157(6), 1262–1278. https://doi.org/10.1016/j.cell.2014.05.010
26. Napoli, C., Lemieux, C., & Jorgensen, R. (1990). Introduction of a chimeric chalcone synthase gene into petunia results in reversible co-suppression of homologous genes in trans. Plant Cell, 2(4), 279–289. https://doi.org/10.2307/3869076
27. Fire, A., Xu, S., Montgomery, M. K., Kostas, S. A., Driver, S. E., & Mello, C. C. (1998). Potent andspecific genetic interferenceby double-strandedRNA in Caenorhabditiselegans. Nature, 391(February), 806–811. https://www.nature.com/articles/35888.pdf
28. Kamath, R. S., Martinez-Campos, M., Zipperlen, P., Fraser, A. G., & Ahringer, J. (2001). Effectiveness of specific RNA-mediated interference through ingested double-stranded RNA in Caenorhabditis elegans. Genome Biology, 2(1), 1–10.
29. Sledz, C. A., Holko, M., De Veer, M. J., Silverman, R. H., & Williams, B. R. G. (2003). Activation of the interferon system by short-interfering RNAs. Nature Cell Biology, 5(9), 834–839. https://doi.org/10.1038/ncb1038
30. Rubinson, D. A., Dillon, C. P., Kwiatkowski, A. V., Sievers, C., Yang, L., Kopinja, J., Zhang, M., McManus, M. T., Gertler, F. B., Scott, M. L., & Van Parijs, L. (2003). A lentivirus-based system to functionally silence genes in primary mammalian cells, stem cells and transgenic mice by RNA interference. Nature Genetics, 33(3), 401–406. https://doi.org/10.1038/ng1117
31. Konnikova, L., Kotecki, M., Kruger, M. M., & Cochran, B. H. (2003). Knockdown of STAT3 expression by RNAi induces apoptosis in astrocytoma cells. BMC Cancer, 3, 7–13. https://doi.org/10.1186/1471-2407-3-23
32. Aagaard, L., & Rossi, J. J. (2007). RNAi therapeutics: Principles, prospects and challenges. *Advanced Drug Delivery Reviews*, *59*(2–3), 75–86.

https://doi.org/10.1016/j.addr.2007.03.005

33. Kim, D. H., & Rossi, J. J. (2008). RNAi mechanisms and applications. *BioTechniques*, *44*(5), 613–616. https://doi.org/10.2144/000112792
34. Kara, G., Calin, G. A., & Ozpolat, B. (2022). RNAi-based therapeutics and tumor targeted delivery in cancer. *Advanced Drug Delivery Reviews*, *182*, 114113. https://doi.org/10.1016/j.addr.2022.114113
35. Guo, X., & Huang, L. (2012). Recent advances in nonviral vectors for gene delivery. *Accounts of Chemical Research*, *45*(7), 971–979. https://doi.org/10.1021/ar200151m
36. Terry, S. C., Herman, J. H., & Angell, J. B. (1979). A Gas Chromatographic Air Analyzer Fabricated on a Silicon Wafer. *IEEE Transactions on Electron Devices*, *26*(12), 1880–1886. https://doi.org/10.1109/T-ED.1979.19791
37. Esashi, M., Shoji, S., & Nakano, A. (1989). Normally Closed Microvalve and Micropump Fabricated on a Silicon Wafe. Sensors and Actuators A: Physical, 20, 163–169.
38. van Lintel, H. T. G., van De Pol, F. C. M., & Bouwstra, S. (1988). A piezoelectric micropump based on micromachining of silicon. Sensors and Actuators, 15(2), 153–167. https://doi.org/10.1016/0250-6874(88)87005-7
39. A. Manz, N. Graber, and H. áM Widmer, “Miniaturized total chemical analysis systems: a novel concept for chemical sensing,” Sensors actuators B Chem., vol. 1, no. 1–6, pp. 244–248, 1990
40. Harrison, D. J., Manz, A., Fan, Z., & Widmer, H. M. (1992). Capillary Electrophoresis and Sample Injection Systems Integrated on a Planar Glass Chip. *Anal. Chem.*, *18*, 1926–1932
41. Singhvi, R., Kumar, A., Lopez, G. P., Stephanopoulos, G. N., Wang, D. I. C., Whitesides, G. M., & Ingber, D. E. (1994). Engineering cell shape and function. Science, 264(5159), 696–698. https://doi.org/10.1126/science.8171320
42. Duffy, D. C., McDonald, J. C., Schueller, O. J. A., & Whitesides, G. M. (1998). Rapid prototyping of microfluidic systems in

poly(dimethylsiloxane). Analytical Chemistry, 70(23), 4974–4984. https://doi.org/10.1021/ac980656z

43. Takayama, S., Ostuni, E., LeDuc, P., Naruse, K., Ingber, D. E., & Whitesides, G. M. (2001). Subcellular positioning of small molecules. Nature, 411(6841), 1016. https://doi.org/10.1038/35082637
44. Huh, D. (2010). Reconstituting Organ-Level Lung. Science, June, 1662–1668.Kim, H. J., Huh, D., Hamilton, G. and Ingber, D. E. (2012). Human Gut-on-a-Chip inhabited by microbial flora that experiences intestinal peristalsis-like motions and flow. Lab. Chip 12, 2165-2174
45. Kim, H. J., Huh, D., Hamilton, G. and Ingber, D. E. (2012). Human Gut-on-a-Chip inhabited by microbial flora that experiences intestinal peristalsis-like motions and flow. Lab. Chip 12, 2165-2174.
46. Musah, S., Mammoto, A., Ferrente, T. C., Jeanty, S. S. F., Hirano-Kobayashi, M., Mammoto, T., Roberts, K., Chung, S., Novak, R., Ingram, M. et al. (2017)
47. Salmon, I., Grebenyuk, S., Abdel Fattah, A. R., Rustandi, G., Pilkington, T., Verfaillie, C., & Ranga, A. (2022). Engineering neurovascular organoids with 3D printed microfluidic chips. Lab on a Chip, 22(8), 1615–1629. https://doi.org/10.1039/d1lc00535a)
48. (Li, B. B., Scott, E. Y., Olafsen, N. E., Matthews, J., & Wheeler, A. R. (2022). Analysis of the effects of aryl hydrocarbon receptor expression on cancer cell invasion via three-dimensional microfluidic invasion assays. Lab on a Chip, 22(2), 313–325. https://doi.org/10.1039/d1lc00854d
49. Kameda, Y., Chuaychob, S., Tanaka, M., Liu, Y., Okada, R., Fujimoto, K., Nakamura, T., & Yokokawa, R. (2022). Three-dimensional tissue model in direct contact with an on-chip vascular bed enabled by removable membranes. Lab on a Chip, 22(3), 641–651. https://doi.org/10.1039/d1lc00751c
50. Goreke, U., Bode, A., Yaman, S., Gurkan, U. A., & Durmus, N. G. (2022). Size and density measurements of single sickle red blood cells using microfluidic magnetic levitation. Lab on a Chip, 22(4), 683–696. https://doi.org/10.1039/d1lc00686j

51. Moshksayan, K., Kashaninejad, N., Warkiani, M. E., Lock, J. G., Moghadas, H., Firoozabadi, B., Saidi, M. S., & Nguyen, N. T. (2018). Spheroids-on-a-chip: Recent advances and design considerations in microfluidic platforms for spheroid formation and culture. *Sensors and Actuators, B: Chemical*, *263*, 151–176. https://doi.org/10.1016/j.snb.2018.01.223
52. G. Mehta, A.Y. Hsiao, M. Ingram, G.D. Luker, S. Takayama, Opportunities and challenges for use of tumor spheroids as models to test drug delivery and efficacy, J. Controlled Release 164 (2012) 192–204
53. K. Ziółkowska, A. Stelmachowska, R. Kwapiszewski, M. Chudy, A. Dybko, Z. Brzózka, Long-term three-dimensional cell culture and anticancer drug activity evaluation in a microfluidic chip, Biosens. Bioelectron. 40 (2013) 68–74.
54. V.E. Santo, M.F. Estrada, S.P. Rebelo, S. Abreu, I. Silva, C. Pinto, et al., Adaptable stirred-tank culture strategies for large scale production of multicellular spheroid-based tumor cell models, J. Biotechnol. 221 (2016) 118–129.
55. J. Friedrich, R. Ebner, L.A. Kunz-Schughart, Experimental anti-tumor therapy in 3-D: spheroids-old hat or new challenge? Int. J. Radiat. Biol. 83 (2007) 849–871.
56. F. Hirschhaeuser, H. Menne, C. Dittfeld, J. West, W. Mueller-Klieser, L.A. Kunz-Schughart, Multicellular tumor spheroids: an underestimated tool is catching up again, J. Biotechnol. 148 (2010) 3–15
57. J. Ruppen, L. Cortes-Dericks, E. Marconi, G. Karoubi, R.A. Schmid, R. Peng, et al., A microfluidic platform for chemoresistive testing of multicellular pleural cancer spheroids, Lab Chip 14 (2014) 1198–1205
58. E. Curcio, S. Salerno, G. Barbieri, L. De Bartolo, E. Drioli, A. Bader, Mass transfer and metabolic reactions in hepatocyte spheroids cultured in rotating wall gas-permeable membrane system, Biomaterials 28 (2007) 5487–5497
59. J.M. Kelm, N.E. Timmins, C.J. Brown, M. Fussenegger, L.K. Nielsen, Method for generation of homogeneous multicellular tumor spheroids applicable to a wide variety of cell types, Biotechnol. Bioeng. 83 (2003)

173–180.

60. R. Sutherland, R. Durand, Growth and Cellular Characteristics of Multicell Spheroids, Spheroids in Cancer Research, Springer, 1984, pp. 24–49.
61. L.A. KUNZ-SCHUGHART, M. Kreutz, R. Knuechel,;1 Multicellular spheroids: a three-dimensional in vitro culture system to study tumour biology, Int. J. Exp. Pathol. 79 (1998) 1–23
62. Sutherland, R. M., Mccredie, J. A., & Inch, R. W. (1971). Growth of Multicell Spheroids in Tissue. *J Natl Cancer Inst.*, *46(1)*, 113–120
63. Yuhas, J. M., Li, A. P., Martinez, A. O., & Ladman, A. J. (1977). A Simplified Method for Production and Growth of Multicellular Tumor Spheroids. *Cancer Research*, *37*(10), 3639–3643.
64. Fukuda, J., & Nakazawa, K. (2005). Orderly arrangement of hepatocyte spheroids on a microfabricated chip. *Tissue Engineering*, *11*(7–8), 1254–1262. https://doi.org/10.1089/ten.2005.11.1254
65. Wu, L. Y., Di Carlo, D., & Lee, L. P. (2008). Microfluidic self-assembly of tumor spheroids for anticancer drug discovery. *Biomedical Microdevices*, *10*(2), 197–202. https://doi.org/10.1007/s10544-007-9125-8
66. Torisawa, Y. S., Mosadegh, B., Luker, G. D., Morell, M., O'Shea, K. S., & Takayama, S. (2009). Microfluidic hydrodynamic cellular patterning for systematic formation of co-culture spheroids. *Integrative Biology*, *1*(11–12), 649–654. https://doi.org/10.1039/b915965g
67. Liu, T., Lin, B., & Qin, J. (2010). Carcinoma-associated fibroblasts promoted tumor spheroid invasion on a microfluidic 3D co-culture device. *Lab on a Chip*, *10*(13), 1671–1677. https://doi.org/10.1039/c000022a
68. Ziółkowska, K., Kwapiszewski, R., Stelmachowska, A., Chudy, M., Dybko, A., & Brzózka, Z. (2012). Development of a three-dimensional microfluidic system for long-term tumor spheroid culture. *Sensors and Actuators, B: Chemical*, *173*, 908–913. https://doi.org/10.1016/j.snb.2012.07.045
69. Zuchowska, A., Jastrzebska, E., Chudy, M., Dybko, A., & Brzozka, Z. (2017). 3D lung spheroid cultures for evaluation of photodynamic therapy (PDT) procedures in microfluidic Lab-on-a-Chip system. *Analytica*

Chimica Acta, *990*, 110–120. https://doi.org/10.1016/j.aca.2017.07.009

70. Alexander, F., Eggert, S., & Wiest, J. (2018). A novel lab-on-a-chip platform for spheroid metabolism monitoring. *Cytotechnology*, *70*(1), 375–386. https://doi.org/10.1007/s10616-017-0152-x
71. Petreus, T., Cadogan, E., Hughes, G., Smith, A., Pilla Reddy, V., Lau, A., O'Connor, M. J., Critchlow, S., Ashford, M., & Oplustil O'Connor, L. (2021). Tumour-on-chip microfluidic platform for assessment of drug pharmacokinetics and treatment response. *Communications Biology*, *4*(1), 1–11. https://doi.org/10.1038/s42003-021-02526-y
72. Yildiz-Ozturk, E., Saglam-Metiner, P., & Yesil-Celiktas, O. (2021). Lung carcinoma spheroids embedded in a microfluidic platform. *Cytotechnology*, *73*(3), 457–471. https://doi.org/10.1007/s10616-021-00470-7
73. Couvreur, P. (2013). Nanoparticles in drug delivery: Past, present and future. *Advanced Drug Delivery Reviews*, *65*(1), 21–23. https://doi.org/10.1016/j.addr.2012.04.010
74. Kreuter, J. (2007). Nanoparticles-a historical perspective. *International Journal of Pharmaceutics*, *331*(1), 1–10. https://doi.org/10.1016/j.ijpharm.2006.10.021
75. Tipplook, M., Pornaroontham, P., Watthanaphanit, A., & Saito, N. (2020). Liquid-Phase Plasma-Assisted in Situ Synthesis of Amino-Rich Nanocarbon for Transition Metal Ion Adsorption. *ACS Applied Nano Materials*, *3*(1), 218–228. https://doi.org/10.1021/acsanm.9b01915
76. Robatjazi, H., Bao, J. L., Zhang, M., Zhou, L., Christopher, P., Carter, E. A., Nordlander, P., & Halas, N. J. (2020). Plasmon-driven carbon–fluorine (C(sp 3)–F) bond activation with mechanistic insights into hot-carrier-mediated pathways. *Nature Catalysis*, *3*(7), 564–573. https://doi.org/10.1038/s41929-020-0466-5
77. Sikdar, D., Pendry, J. B., & Kornyshev, A. A. (2020). Nanoparticle meta-grid for enhanced light extraction from light-emitting devices. *Light: Science and Applications*, *9*(1), 1–11.
78. Boebinger, M. G., Yarema, O., Yarema, M., Unocic, K. A., Unocic, R. R., Wood, V., & McDowell, M. T. (2020). Spontaneous and reversible hollowing of alloy anode nanocrystals for stable battery cycling. *Nature*

Nanotechnology, *15*(6), 475–481. https://doi.org/10.1038/s41565-020-0690-9

79. Birrenbach, G., & Speiser, P. P. (1976). Polymerized micelles and their use as adjuvants in immunology. *Journal of Pharmaceutical Sciences*, *65*(12), 1763–1766. https://doi.org/10.1002/jps.2600651217
80. Jokerst, J. V., Lobovkina, T., Zare, R. N., & Gambhir, S. S. (2011). Nanoparticle PEGylation for imaging and therapy. *Nanomedicine*, *6*(4), 715–728. https://doi.org/10.2217/nnm.11.19
81. Li, J., Rao, J., & Pu, K. (2018). Recent progress on semiconducting polymer nanoparticles for molecular imaging and cancer phototherapy. *Biomaterials*, *155*, 217–235.
82. Tian, H., Chen, J., & Chen, X. (2013). Nanoparticles for gene delivery. *Small*, *9*(12), 2034–2044. https://doi.org/10.1002/smll.201202485
83. Chithrani, B. D., & Chan, W. C. W. (2007). Elucidating the mechanism of cellular uptake and removal of protein-coated gold nanoparticles of different sizes and shapes. *Nano Letters*, *7*(6), 1542–1550. https://doi.org/10.1021/nl070363y
84. Harush-Frenkel, O., Debotton, N., Benita, S., & Altschuler, Y. (2007). Targeting of nanoparticles to the clathrin-mediated endocytic pathway. *Biochemical and Biophysical Research Communications*, *353*(1), 26–32. https://doi.org/10.1016/j.bbrc.2006.11.135
85. Tiwari, G.; Tiwari, R.; Bannerjee, S.K.; Bhati, L.; Pandey, S.; Pandey, P.; Sriwastawa, B. Drug delivery systems: An updated review. Int. J. Pharm. Investig. 2012, 2, 2–11.
86. Patra, J.K.; Das, G.; Fraceto, L.F.; Campos, E.V.R.; del Pilar Rodriguez-Torres, M.; Acosta-Torres, L.S.; Diaz-Torres, L.A.; Grillo, R.; Swamy, M.K.; Sharma, S.; et al. Nano based drug delivery systems: Recent developments and future prospects. J. Nanobiotechnol. 2018, 16, 71
87. Hua, S.; De Matos, M.B.C.; Metselaar, J.M.; Storm, G. Current Trends and Challenges in the Clinical Translation of Nanoparticulate Nanomedicines: Pathways for Translational Development and Commercialization. Front. Pharmacol. 2018, 9, 790.
88. Lakshmanan, S.; Gupta, G.K.; Avci, P.; Chandran, R.; Sadasivam, M.;

Jorge, A.E.S.; Hamblin, M.R. Physical energy for drug delivery; poration, concentration and activation. Adv. Drug Deliv. Rev. 2014, 71, 98–114.

89. Swierczewska, M.; Han, H.; Kim, K.; Park, J.; Lee, S. Polysaccharide-based nanoparticles for theranostic nanomedicine. Adv. Drug Deliv. Rev. 2016, 99, 70–84.
90. Tran, S.; DeGiovanni, P.; Piel, B.; Rai, P. Cancer nanomedicine: A review of recent success in drug delivery. Clin. Transl. Med. 2017, 6, 44.
91. Qi, L.; Luo, Q.; Zhang, Y.; Jia, F.; Zhao, Y.; Wang, F. Advances in Toxicological Research of the Anticancer Drug Cisplatin. Chem. Res. Toxicol. 2019, 32, 1469–1486
92. Senapati, S.; Mahanta, A.K.; Kumar, S.; Maiti, P. Controlled drug delivery vehicles for cancer treatment and their performance. Signal Transduct. Target. Ther. 2018, 3, 7.
93. Vargo, J.A.; Moiseenko, V.; Grimm, J.; Caudell, J.; Clump, D.A.; Yorke, E.; Xue, J.; Vinogradskiy, Y.; Moros, E.G.; Mavroidis, P.; et al. Head and Neck Tumor Control Probability: Radiation Dose–Volume Effects in Stereotactic Body Radiation Therapy for Locally Recurrent Previously-Irradiated Head and Neck Cancer: Report of the AAPMWorking Group. Int. J. Radiat. Oncol. 2018, 18, S0360–S3016.
94. Li, Y.; Gao, Y.; Zhang, X.; Guo, H.; Gao, H. Nanoparticles in precision medicine for ovarian cancer: From chemotherapy to immunotherapy. Int. J. Pharm. 2020, 591, 119986.
95. Wang, Y.; Luo, Y.-L.; Chen, Y.-F.; Lu, Z.-D.; Wang, Y.; Czarna, A.; Shen, S.; Xu, C.-F.; Wang, J. Dually regulating the proliferation and the immune microenvironment of melanoma via nanoparticle-delivered siRNA targeting onco-immunologic CD155. Biomater. Sci. 2020, 8, 6683–6694.
96. Chen, J.; Ma, Y.; Du, W.; Dai, T.; Wang, Y.; Jiang, W.; Wan, Y.; Wang, Y.; Liang, G.; Wang, G. Furin-Instructed Intracellular Gold Nanoparticle Aggregation for Tumor Photothermal Therapy. Adv. Funct. Mater. 2020, 30, 2001566.
97. Kumar, M.; Nagpal, R.; Hemalatha, R.; Verma, V.; Kumar, A.; Singh, S.; Marotta, F.; Jain, S.; Yadav, H. Targeted cancer therapies: The future of cancer treatment. Acta Bio-Med. Atenei Parm. 2012, 83, 220–233.

98. Wolinsky, J.B.; Colson, Y.L.; Grinstaff, M.W. Local drug delivery strategies for cancer treatment: Gels, nanoparticles, polymeric films, rods, and wafers. J. Control. Release 2012, 159, 14–26.
99. Browning, R.J.; Reardon, P.J.T.; Parhizkar, M.; Pedley, R.B.; Edirisinghe, M.; Knowles, J.C.; Stride, E. Drug Delivery Strategies for Platinum-Based Chemotherapy. ACS Nano 2017, 11, 8560–8578.
100. Oh, G.-S.; Kim, H.-J.; Shen, A.; Bin Lee, S.; Khadka, D.; Pandit, A.; So, H.-S. Cisplatin-induced Kidney Dysfunction and Perspectives on Improving Treatment Strategies. Electrolytes Blood Press. 2014, 12, 55–65.
101. Ramesh, G.; Reeves, W.B. Salicylate reduces cisplatin nephrotoxicity by inhibition of tumor necrosis factor-α. Kidney Int. 2004, 65, 490–498.
102. Peng, X.-H.; Wang, Y.; Huang, D.; Wang, Y.; Shin, H.J.; Chen, Z.; Spewak, M.B.; Mao, H.; Wang, X.; Wang, Y.; et al. Targeted delivery of cisplatin to lung cancer using ScFvEGFR-heparin-cisplatin nanoparticles. ACS Nano 2011, 5, 9480–9493.
103. He, Z.; Huang, J.; Xu, Y.; Zhang, X.; Teng, Y.; Huang, C.; Wu, Y.; Zhang, X.; Zhang, H.; Sun, W. Co-delivery of cisplatin and paclitaxel by folic acid conjugated amphiphilic PEG-PLGA copolymer nanoparticles for the treatment of non-small lung cancer. Oncotarget 2015, 6, 42150–42168.
104. Chen, D.; Tang, Q.; Xue, W.; Xiang, J.; Zhang, L.; Wang, X. The preparation and characterization of folate-conjugated human serum albumin magnetic cisplatin nanoparticles. J. Biomed. Res. 2010, 24, 26–32.
105. Mandriota, G.; Di Corato, R.; Benedetti, M.; De Castro, F.; Fanizzi, F.P.; Rinaldi, R. Design and Application of Cisplatin-Loaded Magnetic Nanoparticle Clusters for Smart Chemotherapy. ACS Appl. Mater. Interfaces 2019, 11, 1864–1875.
106. Xie, H.; Goins, B.; Bao, A.; Wang, Z.J.; Phillips, W.T. Effect of intratumoral administration on biodistribution of 64Cu-labeled nanoshells. Int. J. Nanomed. 2012, 7, 2227–2238.
107. Celikoglu, S.I.; Karayel, T.; Demirci, S.; Celikoglu, F.; Cagatay, T. Direct injection of anti-cancer drugs into endobronchial tumours for palliation of major airway obstruction. Postgrad. Med. J. 1997, 73, 159–162.
108. Marmor, J.B. Interactions of hyperthermia and chemotherapy in animals.

Cancer Res. 1979, 39, 2269–2276. [PubMed] 25. Seynhaeve, A.L.B.; Amin, M.; Haemmerich, D.; Van Rhoon, G.C.; Ten Hagen, T.L.M. Hyperthermia and smart drug delivery systems for solid tumor therapy. Adv. Drug Deliv. Rev. 2020, 163–164, 125–144.

109. Miklavˇciˇc, D.; Mali, B.; Kos, B.; Heller, R.; Serša, G. Electrochemotherapy: From the drawing board into medical practice. Biomed. Eng. Online 2014, 13, 29.
110. Tafuto, S.; Von Arx, C.; De Divitiis, C.; Maura, C.T.; Palaia, R.; Albino, V.; Fusco, R.; Membrini, M.; Petrillo, A.; Granata, V.; et al. Electrochemotherapy as a new approach on pancreatic cancer and on liver metastases. Int. J. Surg. 2015, 21, S78–S82.
111. Calvet, C.Y.; Mir, L.M. The promising alliance of anti-cancer electrochemotherapy with immunotherapy. Cancer Metastasis Rev. 2016, 35, 165–177.
112. Sersa, G.; Stabuc, B.; Cemazar, M.; Miklavcic, D.; Rudolf, Z. Electrochemotherapy with cisplatin: Clinical experience in malignant melanoma patients. Clin. Cancer Res. 2000, 6, 863–867.
113. Gulfam, M.; Kim, J.-E.; Lee, J.M.; Ku, B.; Chung, B.H. Anticancer Drug-Loaded Gliadin Nanoparticles Induce Apoptosis in Breast Cancer Cells. Langmuir 2012, 28, 8216–8223.
114. Wu, Y.; Mackay, J.A.; McDaniel, J.R.; Chilkoti, A.; Clark, R.L. Fabrication of Elastin-Like Polypeptide Nanoparticles for Drug Delivery by Electrospraying. Biomacromolecules 2008, 10, 19–24.
115. Xu, Y.; Skotak, M.; Hanna, M. Electrospray encapsulation of water-soluble protein with polylactide. I. Effects of formulations and process on morphology and particle size. J. Microencapsul. 2006, 23, 69–78.
116. Duong, A.D.; Sharma, S.; Peine, K.J.; Gupta, G.; Satoskar, A.R.; Bachelder, E.M.; Wyslouzil, B.E.; Ainslie, K.M. Electrospray encapsulation of toll-like receptor agonist resiquimod in polymer microparticles for the treatment of visceral leishmaniasis. Mol. Pharm. 2013, 10, 1045–1055.
117. Okubo, Y.; Ikemoto, K.; Koike, K.; Tsutsui, C.; Sakata, I.; Takei, O.; Adachi, A.; Sakai, T. DNA Introduction into Living Cells by Water Droplet

Impact with an Electrospray Process. Angew. Chem. Int. Ed. 2008, 47, 1429–1431.

118. Ikemoto, K.; Sakata, I.; Sakai, T. Collision of millimetre droplets induces DNA and protein transfection into cells. Sci. Rep. 2012, 2, 289.
119. Boehringer, S.; Ruzgys, P.; Tamò, L.; Šatkauskas, S.; Geiser, T.; Gazdhar, A.; Hradetzky, D. A new electrospray method for targeted gene delivery. Sci. Rep. 2018, 8, 4031.
120. Lee, M.C.; Seonwoo, H.; Garg, P.; Jang, K.J.; Pandey, S.; Kim, H.B.; Park, S.B.; Ku, J.B.; Kim, J.H.; Lim, K.T.; et al. Development of a bio-electrospray system for cell and non-viral gene delivery. RSC Adv. 2018, 8, 6452–6459.
121. Campos-Xolalpa, N.; Alonso-Castro, Á.J.; Sánchez-Mendoza, E.; Zavala-Sánchez, M.Á.; Pérez-Gutiérrez, S. Cytotoxic activity of the chloroform extract and four diterpenes isolated from Salvia ballotiflora. Rev. Bras. Farm. 2017, 27, 302–305.
122. Effenhauser, C. S., Harttig, H., & Krämer, P. (2002). An evaporation-based disposable micropump concept for continuous monitoring applications. Biomedical Microdevices, 4(1), 27–32. https://doi.org/10.1023/A:1014215728074
123. Randall, G. C., & Doyle, P. S. (2005). Permeation-driven flow in poly(dimethylsiloxane) microfluidic devices. Proceedings of the National Academy of Sciences of the United States of America, 102(31), 10813–10818. https://doi.org/10.1073/pnas.0503287102
124. Park, J. Y., Hwang, C. M., Lee, S. H., & Lee, S. H. (2007). Gradient generation by an osmotic pump and the behavior of human mesenchymal stem cells under the fetal bovine serum concentration gradient. Lab on a Chip, 7(12), 1673–1680. https://doi.org/10.1039/b710777c
125. Walker, G. M., & Beebe, D. J. (2002). A passive pumping method for microfluidic devices. Lab on a Chip, 2(3), 131–134. https://doi.org/10.1039/b204381e
126. Meyvantsson, I., Warrick, J. W., Hayes, S., Skoien, A., & Beebe, D. J. (2008). Automated cell culture in high density tubeless microfluidic device arrays. Lab on a Chip, 8(5), 717–724. https://doi.org/10.1039/b715375a

127. Yang, Y.; Xiang, Y.; Xu, M. From red to green: The propidium iodide-permeable membrane of Shewanella decolorationis S12 is repairable. Sci. Rep. 2015, 5, 18583.
128. Umebayashi, Y.; Miyamoto, Y.; Wakita, M.; Kobayashi, A.; Nishisaka, T. Elevation of Plasma Membrane Permeability on Laser Irradiation of Extracellular Latex Particles. J. Biochem. 2003, 134, 219–224.
129. W. Zhao, Y. Li, X. Zhang, Stemness-Related Markers in Cancer, Cancer Transl Med 2017;3(3):87–95 doi: 10.4103/ctm.ctm_69_16
130. Robertson, F. M., Ogasawara, M. A., Zaiming Ye, Chu, K., Pickei, R., Debeb, B. G., Woodward, W. A., Hittelman, W. N., Cristofanilli, M., & Barsky, S. H. (2010). Imaging and analysis of 3D tumor spheroids enriched for a cancer stem cell phenotype. *Journal of Biomolecular Screening*, *15*(7), 820–829. https://doi.org/10.1177/1087057110376541
131. Barisam, M., Niavol, F. R., Kinj, M. A., Saidi, M. S., Ghanbarian, H., & Kashaninejad, N. (2022). Enrichment of cancer stem-like cells by controlling oxygen, glucose and fluid shear stress in a microfluidic spheroid culture device. *Journal of Science: Advanced Materials and Devices*, *7*(2), 100439. https://doi.org/10.1016/j.jsamd.2022.100439
132. Ozpolat, B., Sood, A. K., & Lopez-Berestein, G. (2014). Liposomal siRNA nanocarriers for cancer therapy. *Advanced Drug Delivery Reviews*, *66*, 110–116. https://doi.org/10.1016/j.addr.2013.12.008
133. Huang, J., Bu, L., Xie, J., Chen, K., Cheng, Z., Li, X., & Chen, X. (2010). Effects of nanoparticle size on cellular uptake and liver MRI with polyvinylpyrrolidone-coated iron oxide nanoparticles. *ACS Nano*, *4*(12), 7151–7160. https://doi.org/10.1021/nn101643u
134. Das, S. K., Dey, T., & Kundu, S. C. (2014). Fabrication of sericin nanoparticles for controlled gene delivery. *RSC Advances*, *4*(5), 2137–2142. https://doi.org/10.1039/c3ra44990d
135. J.C.Celed´on,L.J.Palmer, X. Xu,B.Wang, Z. Fang,and S. T. Weiss, "Sensitization to silk and childhood asthma in rural China," Pediatrics, vol. 107, no. 5, p. E80, 2001.
136. H.K.Soong andK.R.Kenyon, "Adverse reactions to virgin silk sutures in

cataract surgery," Ophthalmology,vol.91, no.5,pp. 479–483, 1984.

137. W. Zaoming, R. Codina, E. Fern´andez-Caldas, and R. F. Lockey, "Partial characterization of the silk allergens in mulberry silk extract," Journal of Investigational Allergology and Clinical Immunology,vol.6,no. 4, pp.237–241,1996.
138. L. Lamboni, M. Gauthier, G. Yang, and Q. Wang, "Silk sericin: a versatile material for tissue engineering and drug delivery," Biotechnology Advances,vol.33, no.8,pp. 1855–1867, 2015.
139. J. M. Anderson, A. Rodriguez, and D. T. Chang, "Foreign body reaction to biomaterials," Seminars in Immunology,vol.20, no. 2, pp. 86–100, 2008engineering, vol. 100, no. 6, pp. 667–671, 2005
140. Jiao, Z., Song, Y., Jin, Y., Zhang, C., Peng, D., Chen, Z., Chang, P., Kundu, S. C., Wang, G., Wang, Z., & Wang, L. (2017). In Vivo Characterizations of the Immune Properties of Sericin: An Ancient Material with Emerging Value in Biomedical Applications. Macromolecular Bioscience, 17(12), 1–6. https://doi.org/10.1002/mabi.201700229
141. G. H. Altman, F. Diaz, C. Jakuba et al., "Silk-based biomaterials," Biomaterials, vol. 24, no. 3, pp. 401–416, 2003
142. P.Aramwit,S.Kanokpanont,W.De-Eknamkul,and Trichana,"Monitoring of inflammatory mediators induced by silk sericin," Journal of Bioscience and Bioengineering,vol.107,no. 5, pp.556–561,2009.
143. S. Terada, T. Nishimura, M. Sasaki, H. Yamada, and M. Miki, "Sericin, a protein derived from silkworms, accelerates the proliferation of several mammalian cell lines including a hybridoma," Cytotechnology,vol.40, no.1–3,pp. 3–12,2003
144. Tung, Y. C., Hsiao, A. Y., Allen, S. G., Torisawa, Y. S., Ho, M., & Takayama, S. (2011). High-throughput 3D spheroid culture and drug testing using a 384 hanging drop array. *Analyst*, *136*(3), 473–478. https://doi.org/10.1039/c0an00609b
145. Lee, M. C., Pandey, S., Lim, J. W., Park, S., Kim, J. E., Son, H., Han, J., Seonwoo, H., Garg, P., & Chung, J. H. (2021). Induction of apoptosis of cancer cells using the cisplatin delivery based electrospray (CDES) system. Applied Sciences (Switzerland), 11(7).

https://doi.org/10.3390/app11073203

146. Hail, N., Chen, P., & Wempe, M. F. (2010). The hydroxyl functional group of N-(4-hydroxyphenyl)retinamide mediates cellular uptake and cytotoxicity in premalignant and malignant human epithelial cells. Free Radical Biology and Medicine, 49(12), 2001–2009. https://doi.org/10.1016/j.freeradbiomed.2010.09.032

147. Wang, S., Li, Z., Aispuro, D., Guevara, N., Van Valkenburgh, J., Chen, B., Zhou, X., McCarroll, M. N., Ji, F., Cong, X., Sarkar, P., Chaudhuri, R., Guo, Z., Perkins, N. P., Shao, S., Sello, J. K., Chen, K., & Xue, M. (2022). Hydroxyl-Rich Hydrophilic Endocytosis-Promoting Peptide with No Positive Charge. Journal of the American Chemical Society, 144(44), 20288–20297. https://doi.org/10.1021/jacs.2c07420

148. Pardal, R., Clarke, M. F., & Morrison, S. J. (2003). Applying the principles of stem-cell biology to cancer. *Nature Reviews Cancer*, *3*(12), 895–902. https://doi.org/10.1038/nrc1232

149. Reya, T., Morrison, S. J., Clarke, M. F., & Weissman, I. L. (2001). Stem cells and cancer stem cells. *Nature*, *414*(6859), 105–111. https://doi.org/doi: 10.1038/35102167

150. Koren, E., & Fuchs, Y. (2016). The bad seed: Cancer stem cells in tumor development and resistance. *Drug Resistance Updates*, *28*, 1–12. https://doi.org/10.1016/j.drup.2016.06.006

151. Adorno-Cruz, V., Kibria, G., Liu, X., Doherty, M., Junk, D. J., Guan, D., Hubert, C., Venere, M., Mulkearns-Hubert, E., Sinyuk, M., Alvarado, A., Caplan, A. I., Rich, J., Gerson, S. L., Lathia, J., & Liu, H. (2015). Cancer stem cells: Targeting the roots of cancer, seeds of metastasis, and sources of therapy resistance. *Cancer Research*, *75*(6), 924–929. https://doi.org/10.1158/0008-5472.CAN-14-3225

152. Perona, R., López-Ayllón, B. D., De Castro Carpeño, J., & Belda-Iniesta, C. (2011). A role for cancer stem cells in drug resistance and metastasis in non-small-cell lung cancer. *Clinical and Translational Oncology*, *13*(5), 289–293. https://doi.org/10.1007/s12094-011-0656-3

153. Alguacil-Núñez, C., Ferrer-Ortiz, I., García-Verdú, E., López-Pirez, P., Llorente-Cortijo, I. M., & Sainz, B. (2018). Current perspectives on the crosstalk between lung cancer stem cells and cancer-associated fibroblasts. *Critical Reviews in Oncology/Hematology*, *125*(February), 102–110. https://doi.org/10.1016/j.critrevonc.2018.02.015

154. Maiuthed, A., Chantarawong, W., & Chanvorachote, P. (2018). Lung cancer stem cells and cancer stem cell-targeting natural compounds.

Anticancer Research, *38*(7), 3797–3810. https://doi.org/10.21873/anticanres.12663

155. Heng, W. Sen, Gosens, R., & Kruyt, F. A. E. (2019). Lung cancer stem cells: origin, features, maintenance mechanisms and therapeutic targeting. *Biochemical Pharmacology*, *160*(December 2018), 121–133. https://doi.org/10.1016/j.bcp.2018.12.010

156. Cianciosi, D., Varela-Lopez, A., Forbes-Hernandez, T. Y., Gasparrini, M., Afrin, S., Reboredo-Rodriguez, P., Zhang, J. J., Quiles, J. L., Nabavi, S. F., Battino, M., & Giampieri, F. (2018). Targeting molecular pathways in cancer stem cells by natural bioactive compounds. *Pharmacological Research*, *135*(August), 150–165. https://doi.org/10.1016/j.phrs.2018.08.006

157. Kim, T., Im, J. H., Choi, H. S., Yang, S. J., Kim, S. W., & Park, C. R. (2011). Preparation and photoluminescence (PL) performance of a nanoweb of P3HT nanofibers with diameters below 100 nm. *Journal of Materials Chemistry*, *21*(37), 14231–14239. https://doi.org/10.1039/c1jm10396b

158. Leon, G., MacDonagh, L., Finn, S. P., Cuffe, S., & Barr, M. P. (2016). Cancer stem cells in drug resistant lung cancer: Targeting cell surface markers and signaling pathways. *Pharmacology and Therapeutics*, *158*, 71–90. https://doi.org/10.1016/j.pharmthera.2015.12.001

159. Eramo, A., Haas, T. L., & De Maria, R. (2010). Lung cancer stem cells: Tools and targets to fight lung cancer. *Oncogene*, *29*(33), 4625–4635. https://doi.org/10.1038/onc.2010.207

160. Ranji, P., Salmani Kesejini, T., Saeedikhoo, S., & Alizadeh, A. M. (2016). Targeting cancer stem cell-specific markers and/or associated signaling pathways for overcoming cancer drug resistance. *Tumor Biology*, *37*(10), 13059–13075. https://doi.org/10.1007/s13277-016-5294-5

161. Teng, Y., Wang, X., Wang, Y., & Ma, D. (2010). Wnt/β-catenin signaling regulates cancer stem cells in lung cancer A549 cells. *Biochemical and Biophysical Research Communications*, *392*(3), 373–379. https://doi.org/10.1016/j.bbrc.2010.01.028

162. Yang, J., Chen, J., He, J., Li, J., Shi, J., Cho, W. C., & Liu, X. (2016). Wnt signaling as potential therapeutic target in lung cancer. *Expert Opinion on Therapeutic Targets*, *20*(8), 999–1015. https://doi.org/10.1517/14728222.2016.1154945

163. Takebe, N., & Percy Ivy, S. (2010). Controversies in cancer stem cells: Targeting embryonic signaling pathways. *Clinical Cancer Research*, *16*(12), 3106–3112. https://doi.org/10.1158/1078-0432.CCR-09-2934

164. Wiznerowicz, M., & Trono, D. (2003). Conditional Suppression of Cellular Genes: Lentivirus Vector-Mediated Drug-Inducible RNA Interference.

Journal of Virology, *77*(16), 8957–8951. https://doi.org/10.1128/jvi.77.16.8957-8951.2003

165. Brouns, S. J. J., Jore, M. M., Lundgren, M., Westra, E. R., Slijkhuis, R. J. H., Snijders, A. P. L., Dickman, M. J., Makarova, K. S., Koonin, E. V., & van der Oost, J. (2008). Small CRISPR RNAs Guide Antiviral Defense in Prokaryotes. *Science*, *321*(August 2008), 960–965.

166. van der Oost, J., Jore, M. M., Westra, E. R., Lundgren, M., & Brouns, S. J. J. (2009). CRISPR-based adaptive and heritable immunity in prokaryotes. *Trends in Biochemical Sciences*, *34*(8), 401–407. https://doi.org/10.1016/j.tibs.2009.05.002

167. David, R. M., & Doherty, A. T. (2017). Viral Vectors: The road to reducing genotoxicity. *Toxicological Sciences*, *155*(2), 315–325. https://doi.org/10.1093/toxsci/kfw220

168. Verhoeyen, E., & Cosset, F. L. (2004). Surface-engineering of lentiviral vectors. *Journal of Gene Medicine*, *6*(SUPPL. 1). https://doi.org/10.1002/jgm.494

169. Chen, X., Nomani, A., Patel, N., Nouri, F. S., & Hatefi, A. (2018). Bioengineering a non-genotoxic vector for genetic modification of mesenchymal stem cells. *Biomaterials*, *152*, 1–14. https://doi.org/10.1016/j.biomaterials.2017.10.028

170. Hardee, C. L., Arévalo-Soliz, L. M., Hornstein, B. D., & Zechiedrich, L. (2017). Advances in non-viral DNA vectors for gene therapy. *Genes*, *8*(2). https://doi.org/10.3390/genes8020065

171. Wang, M., Lu, P., Wu, B., Tucker, J. D., Cloer, C., & Lu, Q. (2012). High efficiency and low toxicity of polyethyleneimine modified Pluronics (PEI-Pluronic) as gene delivery carriers in cell culture and dystrophic mdx mice. *Journal of Materials Chemistry*, *22*(13), 6038–6046. https://doi.org/10.1039/c2jm15625c

172. Jiang, H. L., Islam, M. A., Xing, L., Firdous, J., Cao, W., He, Y. J., Zhu, Y., Cho, K. H., Li, H. S., & Cho, C. S. (2017). Degradable Polyethylenimine-Based Gene Carriers for Cancer Therapy. *Topics in Current Chemistry*, *375*(2), 1–36. https://doi.org/10.1007/s41061-017-0124-9

173. Katt, M. E., Placone, A. L., Wong, A. D., Xu, Z. S., & Searson, P. C. (2016). In vitro tumor models: Advantages, disadvantages, variables, and selecting the right platform. *Frontiers in Bioengineering and Biotechnology*, *4*(FEB). https://doi.org/10.3389/fbioe.2016.00012

174. Loisel, S., Ohresser, M., Pallardy, M., Daydé, D., Berthou, C., Cartron, G., & Watier, H. (2007). Relevance, advantages and limitations of animal models used in the development of monoclonal antibodies for cancer treatment. *Critical Reviews in Oncology/Hematology*, *62*(1), 34–42.

https://doi.org/10.1016/j.critrevonc.2006.11.010

175. García, Y., & Díaz-Castro, J. (2013). Advantages and disadvantages of the animal models v. in vitro studies in iron metabolism: A review. *Animal*, *7*(10), 1651–1658. https://doi.org/10.1017/S1751731113001134

176. Carvalho, M. R., Lima, D., Reis, R. L., Correlo, V. M., & Oliveira, J. M. (2015). Evaluating Biomaterial- and Microfluidic-Based 3D Tumor Models. *Trends in Biotechnology*, *33*(11), 667–678. https://doi.org/10.1016/j.tibtech.2015.09.009

177. Lee, F., Iliescu, C., Yu, F., & Yu, H. (2018). Constrained spheroids/organoids in perfusion culture. In *Methods in Cell Biology* (1st ed., Vol. 146). Elsevier Inc. https://doi.org/10.1016/bs.mcb.2018.05.003

178. Sung, K. E., & Beebe, D. J. (2014). Microfluidic 3D models of cancer. *Advanced Drug Delivery Reviews*, *79*, 68–78. https://doi.org/10.1016/j.addr.2014.07.002

179. Dela Cruz, C. S., Tanoue, L. T., & Matthay, R. A. (2011). Lung Cancer: Epidemiology, Etiology, and Prevention. *Clinics in Chest Medicine*, *32*(4), 605–644. https://doi.org/10.1016/j.ccm.2011.09.001

180. Travis, W. D. (2011). Pathology of Lung Cancer. *Clinics in Chest Medicine*, *32*(4), 669–692. https://doi.org/10.1016/j.ccm.2011.08.005

181. Wheless, L., Brashears, J., & Alberg, A. J. (2013). Epidemiology of lung cancer. *Lung Cancer Imaging*, *123*(1), 1–15. https://doi.org/10.1007/978-1-60761-620-7_1

182. Minna, J. D., Roth, J. A., & Gazdar, A. F. (2002). Focus on lung cancer. *Cancer Cell*, *1*(1), 49–52. https://doi.org/10.1016/S1535-6108(02)00027-2

183. Alberg, A. J., Brock, M. V., & Samet, J. M. (2005). Epidemiology of lung cancer: Looking to the future. *Journal of Clinical Oncology*, *23*(14), 3175–3185. https://doi.org/10.1200/JCO.2005.10.462

184. Meng, X., Li, M., Wang, X., Wang, Y., & Ma, D. (2009). Both CD133+ and CD133- subpopulations of A549 and H446 cells contain cancer-initiating cells. *Cancer Science*, *100*(6), 1040–1046. https://doi.org/10.1111/j.1349-7006.2009.01144.x

185. Roudi, R., Korourian, A., Shariftabrizi, A., & Madjd, Z. (2015). Differential expression of cancer stem cell markers ALDH1 and CD133 in various lung cancer subtypes. *Cancer Investigation*, *33*(7), 294–302. https://doi.org/10.3109/07357907.2015.1034869

186. Niidome, T., & Huang, L. (2002). Gene therapy progress and prospects: Nonviral vectors. *Gene Therapy*, *9*(24), 1647–1652. https://doi.org/10.1038/sj.gt.3301923

187. Scheller, E. L., & Krebsbach, P. H. (2009). Gene therapy: Design and prospects for craniofacial regeneration. *Journal of Dental Research*, *88*(7), 585–596. https://doi.org/10.1177/0022034509337480

188. Ghosh, S., Brown, A. M., Jenkins, C., & Campbell, K. (2020). Viral Vector Systems for Gene Therapy: A Comprehensive Literature Review of Progress and Biosafety Challenges. *Applied Biosafety*, *25*(1), 7–18. https://doi.org/10.1177/1535676019899502

189. Shirley, J. L., de Jong, Y. P., Terhorst, C., & Herzog, R. W. (2020). Immune Responses to Viral Gene Therapy Vectors. *Molecular Therapy*, *28*(3), 709–722. https://doi.org/10.1016/j.ymthe.2020.01.001

190. Wang, Y., Bruggeman, K. F., Franks, S., Gautam, V., Hodgetts, S. I., Harvey, A. R., Williams, R. J., & Nisbet, D. R. (2020). Is Viral Vector Gene Delivery More Effective Using Biomaterials? *Advanced Healthcare Materials*, *2001238*, 1–25. https://doi.org/10.1002/adhm.202001238

191. Garcia-Guerra, A., Dunwell, T. L., & Trigueros, S. (2018). Nano-Scale Gene Delivery Systems: Current Technology, Obstacles, and Future Directions. *Current Medicinal Chemistry*, *25*(21), 2448–2464. https://doi.org/10.2174/0929867325666180108100723

192. Shan, Y., Luo, T., Peng, C., Sheng, R., Cao, A., Cao, X., Shen, M., Guo, R., Tomás, H., & Shi, X. (2012). Gene delivery using dendrimer-entrapped gold nanoparticles as nonviral vectors. *Biomaterials*, *33*(10), 3025–3035. https://doi.org/10.1016/j.biomaterials.2011.12.045

193. Zhang, Y., Satterlee, A., & Huang, L. (2012). In vivo gene delivery by nonviral vectors: Overcoming hurdles. *Molecular Therapy*, *20*(7), 1298–1304. https://doi.org/10.1038/mt.2012.79